New methods for multimodal MS imaging of histological tissue sections

The work described in this thesis was performed at the FOM Institute for Atomic and Molecular Physics, Science Park 104, 1098 XG Amsterdam, The Netherlands.

ISBN/EAN: 978-90-77209-56-1

New methods for multimodal MS imaging of histological tissue sections

Erika R. Amstalden van Hove

New methods for multimodal MS imaging of histological tissue sections

Nieuwe methodes voor multimodale MS imaging van weefsels

(met een samenvatting in het Nederlands)

Proefschrift

ter verkrijging van de graad van doctor aan de Universiteit Utrecht
op gezag van de rector magnificus, prof.dr. G.J. van der Zwaan, ingevolge het besluit van het college voor promoties in het openbaar te verdedigen op maandag 21 november 2011 des middags te 12.45 uur

door

Erika Regina Amstalden van Hove

geboren op 8 juni 1975

te Indaiatuba, Brazilië

Promotor: Prof. dr. R.M.A. Heeren

This work is part of the research program of the “Stichting voor Fundamenteel Onderzoek der Materie (FOM)", which is financially supported by the "Nederlandse organisatie voor Wetenschappelijk Onderzoek (NWO)". This work was in part supported by The Netherlands Proteomics Centre, the Virtual Laboratory for e-Science (VLe), the Computis Program, 6th European Framework Program for Research and Technological Development (FP6) and by Janssen Pharmaceutical Research & Development.

Table of Contents

Chapter 1

1. Introduction

Mass Spectrometry (MS) imaging is a technique which combines spectral analysis and spatial information. The application and importance of MS imaging is rapidly growing, with further developments focusing on current needs. This thesis addresses the need for better methods of sample preparation and their application, as well as other quantification challenges.

One of the areas in which MS imaging is proving its value is the study of disease-related biomolecules. Other techniques that are conventionally applied in these types of studies, such as mass spectrometry based "-omics" (e.g. proteomics, lipidomics, metabolomics) [1-9] combined with separation methods such as electrophoresis, lasercapture microdissection (LMD), allow regional selectivity but lack spatial information.

Besides MS imaging other imaging techniques are available and in use. Magnetic resonance spectroscopy imaging (MRSI), positron emission tomography (PET), immunostaining and fluorescence based techniques for instance are being used to determine the spatial localization of molecules in clinical studies [10-15]. *In-vivo* techniques, such as MRI and PET, target specific classes of molecules but with low specificity within the class. *Ex-vivo* techniques (e.g fluorescence and immunostaining) are highly specific within the class, but allow the visualization of tagged proteins only, and with a limited number of detectable analytes per section. Whole-body autoradioluminography (WBA) is commonly used in drug distribution studies, but requires the use of labels and needs complementary data to distinguish metabolites from the intact compound, e.g. the analysis of plasma, urine and feces material [16].

The strength of MS imaging lies in its ability to combine both mass spectrometric mass resolving power and to provide the direct correlation of molecules with their spatial localization. In addition, MS imaging can be applied to a wide detection range, from single elements to macromolecules [17] and is a label-free technique. MS imaging is suitable for

qualitative and (semi-)quantitative studies, and can be combined with traditional imaging and "-omics" techniques. MS imaging also provides a high spatial resolution (ranging from 5 to 100 μm) which depends on the ion source. For example, secondary ion mass spectrometry (SIMS) can achieve sub-micrometer spatial resolution [18], while matrix assisted laser desorption/ionization (MALDI) can reach pixel sizes of 500 nm and image resolving power of 4 μm [19, 20].

The increasing importance of MS imaging is demonstrated by its application in multiple areas such as disease studies, e.g. neurodegenerative diseases [21, 22] and cancer cell type discrimination [23], drug distribution studies [24] , and forensics [25, 26].

1.1 Challenges in MS imaging

Sample preparation is a key factor in the detection of molecules of interest in MS imaging techniques. Different sample preparation methods can be applied in order to improve analyte detection. Examples of sample preparation methods are sample washing to enhance peptide or protein detection [19, 21, 27-31], on-tissue digestion [32-36], and surface deposition of metal (e.g. gold) [37] or ionic matrix [27, 30, 34, 38-46]. Improper sample handling may cause diffusion of substances through the sample surface, loss of molecules of interest from the sample and physical surface changes. Also, fragile tissue sections can be damaged by conventional washing methods, such as immersion and pipette washing.

In order to wash such fragile tissue sections as well as to perform localized tissue washing, a new method was developed that uses a common laboratory wipe (KimWipe) wetted with washing solvent. This method consists of direct application of the wetted paper on top of the tissue of interest for a short time (30-60s). Comparative analysis between paper wash and conventional washing methods showed similar results. In addition, the paper wash method allowed surface washing of fragile tissues that could not be treated by conventional washing.

An additional challenge in MS imaging is the direct quantitation of analytes from a tissue surface. With the development of MS imaging from qualitative to quantitative analysis, its scope will be broadened. One of the challenges encountered in the application of MS imaging for quantitative purposes, is the ion suppression effect [47-51], a common problem in MS imaging studies. In pharmaceutical studies the most widespread method for quantification with MS imaging consists of the deposition of standards on un-dosed (or healthy) organ sections. This process however does not fully mimic the interaction of drugs with cell contents and it can be used merely as an indication. Chemical and physical properties of the tissue surface also interfere with the detection of molecules [52, 53] and may cause different ion suppression effects. In other words, the drug-organ interaction in the cells may be significantly different from the interaction when a drug is applied on the surface of a tissue section, and therefore the ion suppression effect will also be different than calculated with standards deposition on organs. In order to investigate the impact of cellular composition and sample preparation in drug quantitation by both contact (drug standards on top of homogenates) and interaction between drug and cell contents (mixed in-vitro), a complex experimental set-up was developed. In a study with risperidone, a psychotropic agent, and five different organs (brain, lung, liver, kidney and testis), homogenized organs replaced tissue sections, allowing the evaluation of tissue-specific effects on drug quantitation by MS imaging. The results of this study confirmed that drug ionization response is affected by sample preparation (applied on top or mixed with organ homogenates), and is also organ dependent. Calibration curves created by application of drugs on top of tissue could lead to over or under-representation of the drug amount, depending on the organ analyzed.

1.2 Application of MS imaging in cancer studies

In the study of disease-related molecules, MS imaging provided a broader view of the role of several molecules involved in breast cancer growth and malignancy. MS

imaging performed on tumor sections of MDA-MB-231, a highly metastatic human mammary epithelial cancer cell line, and MCF-7, a non-metastatic, estrogen-sensitive (estrogen-dependent) line, permitted the determination of spatial distributions of phosphocholine (PC), choline (Cho), and glycerophosphocholine (GPC), as well as sodium (Na^+) and potassium (K^+), among many others. The results obtained strongly confirmed the hypothesis that increased PC levels can be linked with tumor malignancy, showing that PC and Cho intensity were increased in viable regions compared to necrotic regions of MDA-MB-231 tumors, but relatively homogeneously distributed in MCF-7 tumors. Such behavior may be related to the role of PC and PC-related enzymes, such as choline kinase, choline transporters and others in malignant tumor growth. At the same time, MS imaging provided information on other pathways, due to the –unexpected- opposite behavior of Na^+ and K^+ in the highly aggressive and less aggressive tumor types: Na^+ and K^+ being co-localized in the necrotic tumor areas of aggressive tumors, whereas in non-metastatic tumors Na^+ was detected in necrotic and K^+ in viable tumor regions. This behavior may be attributed to differential Na^+/K^+ pump functions and K^+ channel expressions[54, 55]. MS imaging also reaches such a high spatial resolution (~1-5μm) that Na^+ and K^+ could be observed in hematoxylin-positive bodies (intracellular space) in necrotic regions of metastatic tumors, which likely originated from dead or dying cells. In the viable region, however, both ions were so homogeneously distributed that no distinction could be made between intra and extracellular space based on MS imaging only. Additionally, principal component analysis of the MS imaging data clearly identified different tumor micro-environmental regions by their distinct molecular signatures. The information obtained by MS imaging could thus provide distinction of tumor micro-environments, confirmation of the importance of PC in tumor malignancy, and differentiation between tumor types based on their molecular signature and the possible differential Na^+/K^+ pump functions and K^+ channel expressions in the different tumor types.

The application of new surface treatment methods as well as quantitative and qualitative analyzes by MS imaging on fields such as disease and pharmaceutical research

makes MS imaging a versatile technique, which provides valuable spatial and molecular information of substances, as will be demonstrated in the following chapters of this thesis.

1.3 Scope of the thesis

Chapter two provides an introduction to the reader of MS imaging techniques, their principles, application, advantages and disadvantages.

Chapter three describes a method developed for selective surface cleaning in order to minimize diffusion, allow surface cleaning of fragile samples and samples attached to tapes, and surface treatment of regions of interest.

Chapter four comprises studying ion suppression effects in a drug study,, using a combination of MS imaging techniques and different sample preparations that are suited for quantitative analysis.

Chapter five shows how the use of mass spectrometry imaging techniques combined with magnetic resonance and optical techniques allowed for the confirmation of the role played by choline, phosphocholine and other molecules in cancer growth and malignancy, as well as the cellular distribution of analytes directly from tissue sections.

Chapter 2

2. A Concise Review of Mass Spectrometry Imaging*

Mass spectrometric (MS) imaging allows for the investigation of the spatial distribution of molecules at complex surfaces. The combination of molecular speciation with local analysis renders a chemical microscope that can be used for the direct biomolecular characterization of histological tissue surfaces. MS imaging advantageously allows label-free detection and mapping of a wide-range of biological compounds whose presence or absence can be the direct result of disease pathology. Successful detection of analytes of interest at the desired spatial resolution requires careful attention to several steps in the MS imaging protocol. This chapter will describe and discuss a selected number of crucial developments in ionization, instrumentation, and application of this innovative technology. The focus of this review is on the latest developments in MS imaging. Selected biological applications are employed to illustrate some of the novel features discussed. Two commonly used MS imaging techniques, secondary ion mass spectrometric (SIMS) imaging and matrix assisted laser desorption ionization (MALDI) mass spectrometric imaging, center this review. New instrumental developments are discussed that extend spatial resolution, mass resolving power, mass accuracy, tandem MS capabilities, and offer new gas phase separation capabilities for both imaging techniques. It will be shown how the success of MS imaging is crucially dependent on sample preparation protocols as they dictate the nature and mass range of detected biomolecules that can be imaged. Finally, developments in data analysis strategies for large imaging datasets will be discussed briefly.

* Based on: Erika R. Amstalden van Hove, Donald F. Smith and Ron M.A. Heeren, *Journal of Chromatography A*, 2010, **1217** (25), 3946-54.

2.1 Introduction

Mass spectrometric imaging, the combination of molecular mass analysis and spatial information, provides visualization of molecules on complex surfaces. The inception of MALDI-time-of-flight (MALDI-TOF) based MS imaging techniques in 1997 [56] has led to a surge in methodological and instrumental developments and subsequent applications of mass spectrometry imaging. In addition, the biological applications of time-of-flight SIMS (TOF-SIMS) have increased, due to the high spatial resolution offered by SIMS. Multi-modal MS imaging strategies, as well as the adaption of proteomics protocols, have made MS imaging a powerful tool for spatial localization and identification of elements, pharmaceuticals, metabolites, lipids, peptides and proteins in biological tissues. Figure 1 shows the number of publications per year from an ISI Web of Science search of the topics "imaging mass spectrometry" and "mass spectrometry imaging". Here, we will refer to "mass spectrometry imaging", MSI, or simply "MS imaging" to avoid the confusion of "imaging mass spectrometry", IMS, with "ion mobility separation".

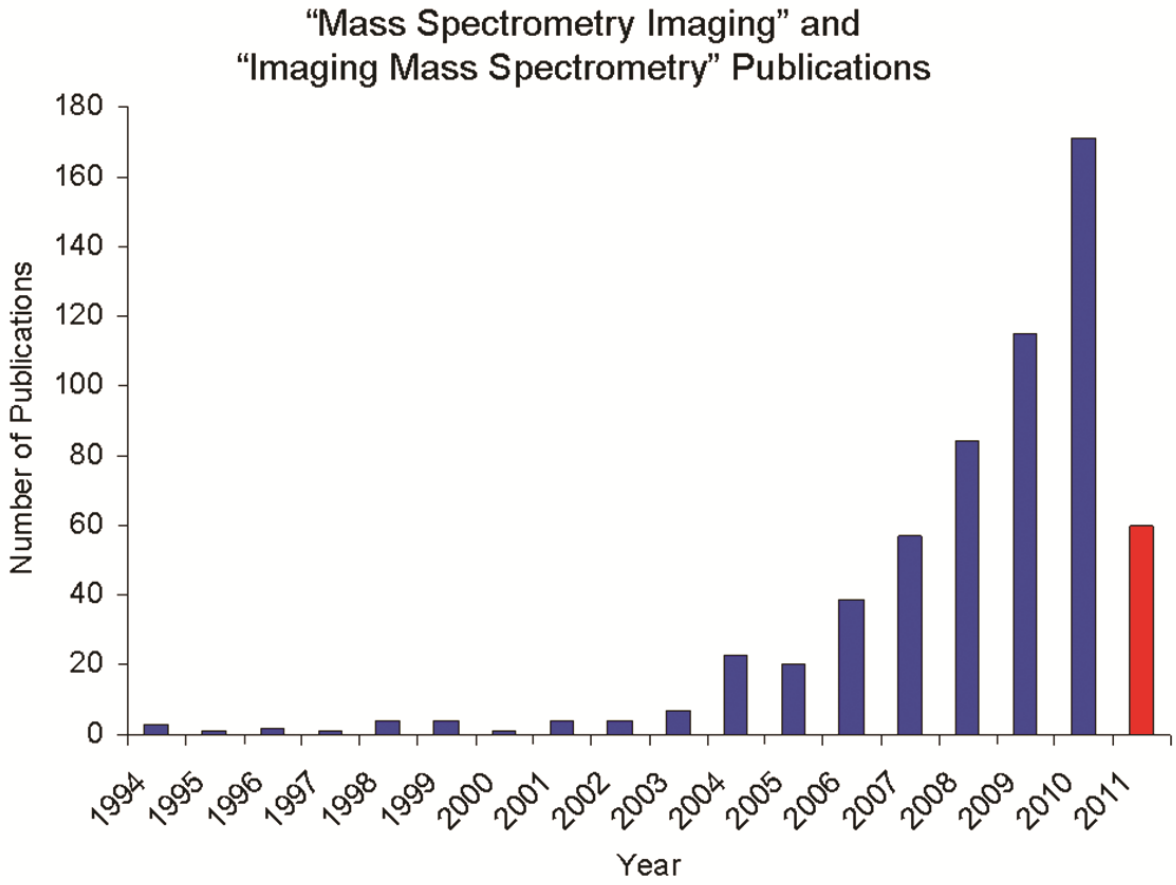

***Figure 1**: Number of publications per year from an ISI Web of Science search of the topics "imaging mass spectrometry" and "mass spectrometry imaging".*

Mass spectrometry based "-omics" technologies have become routine for the analysis of biomolecules related to various diseases [1-4]. With high-throughput methods combining mass spectrometry and separation techniques, such as liquid-chromatography and electrophoresis, numerous biomarkers have been identified for diseases in bulk bodily fluids [5-7]. Biomolecules isolated from cell-lysates or tissue homogenates offer a more selective approach, also analyzed by MS based proteomics [3]. Laser capture microdissection (LMD) offers the highest regional selectivity and can be used for single cell analyses [8, 9]. This approach is time consuming and requires a high number of cells in order to detect low abundance molecules. Voxelization and subsequent LC-MS of a mouse brain tissue section

has been used for spatial mapping and quantitation of over 800 proteins, but at the cost of low spatial resolution (1 mm^3) and extensive sample preparation [35].

Clinical imaging methods, such as magnetic resonance spectroscopy imaging (MRI), positron emission tomography (PET), immunostaining and fluorescent based techniques are used for the spatial localization of substances in biomedical studies [10-15]. Immunostaining is highly specific and allows the visualization of one analyte per histological section at high spatial resolution. Similarly, fluorescence tags allow for highly specific visualization of proteins with high spatial resolution [15]. In both cases the spatial resolution is limited by classical diffraction theory (~200nm). *In vivo* techniques, such as MRI and PET, target specific classes of molecules but with low specificity within the class. The spatial resolution of MRI varies from $1cm^3$ [57] to $1mm^3$ and new PET instrumentation designs been developed to achieve less than $1mm^3$ isotropic volume resolution [58]. MS imaging allows for label-free discovery of multiple classes of biomolecules directly from a tissue surface, and can be combined with traditional imaging and proteomic methods.

MS imaging has been combined with MRI for complementary localization of proteins in mouse brain [59, 60] as well as choline, phosphocholine and other molecules in breat tumors[61]. Biomedical applications range from neurodegenerative diseases [22] including spatial localization of amyloid beta peptides, related to Alzheimer's disease, on brain sections form transgenic mice [21], to protein detection on breast tumor xenograft and human formalin-fixed paraffin-embedded breast cancer [32], and cancer cell type discrimination [23]. The distribution of pharmaceuticals and their metabolites can be followed in whole-body sections [24, 62, 63], as well as in specific organs [64, 65]. Figure 2 shows whole-body sections of a rat after compound administration comparing wholebody autoradioluminography (WBA) with mass spectrometry imaging (MSI). The results are comparable, while MS imaging precludes the need for compound labeling [66]. Also, TOF-SIMS has shown accumulation of several lipid classes as well as the depletion of vitamin E in non-alcoholic fatty liver [67]. Desorption electrospray ionization (DESI) allows ambient sampling of tissue sections and has been used to map lipids in human liver

adenocarcinoma, rat brain and several other tissue types [68]. These applications combined demonstrate the power of mass spectrometry imaging as a tool for drug discovery, proteomics and metabolomics research.

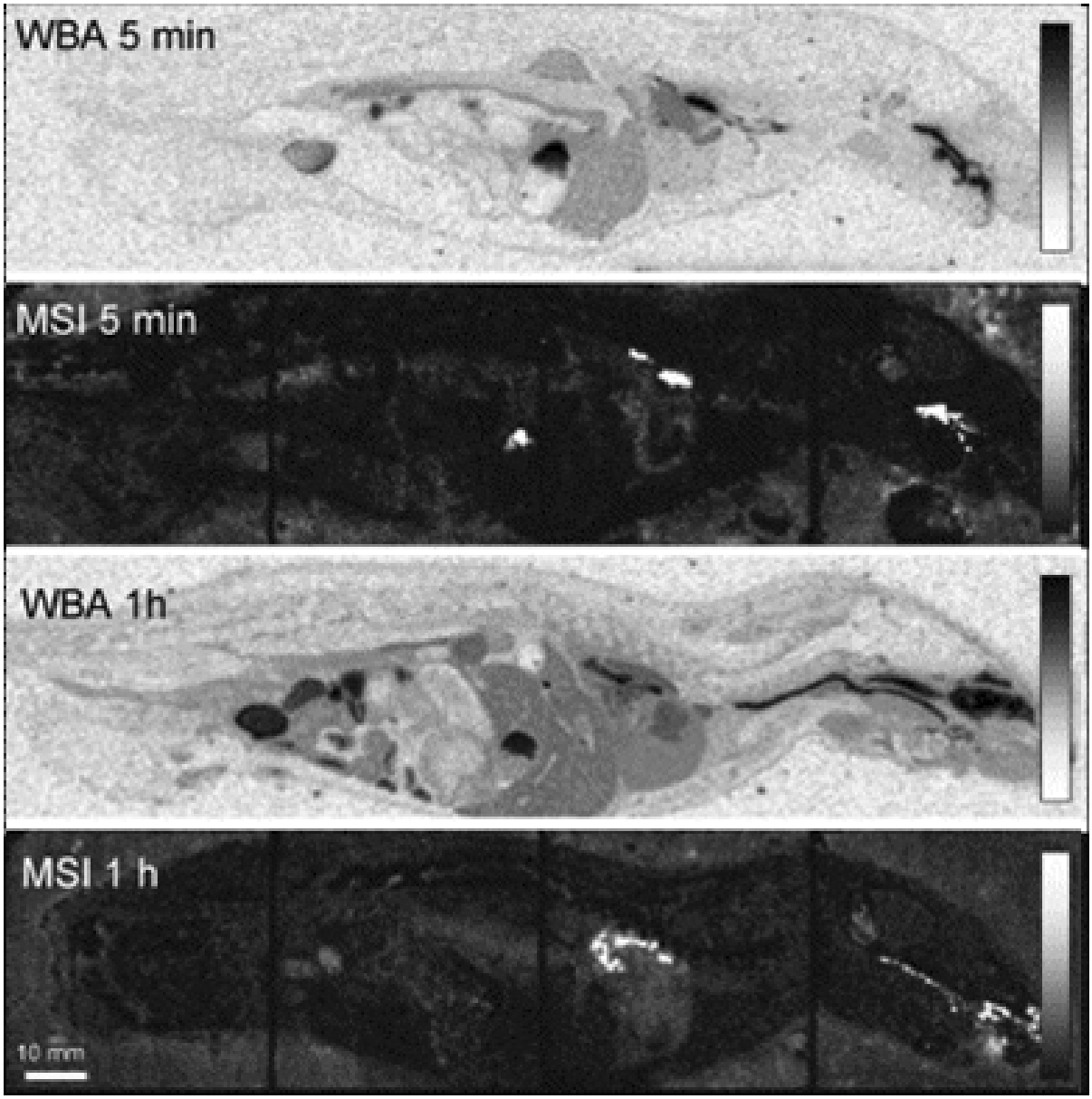

***Figure 2**: Comparison of Mass Spectrometry Imaging (MSI) with Whole-Body Autoradioluminography (WBA) using whole-body sections after intra-tracheal administration of a compound (0.5 mg/kg) to rats. The two corresponding sections are from the same animal, but from different positions. The comparison of the methods shows*

remarkable similarity in the results: High levels are detected in the trachea, the lung and the stomach and lower levels in blood.[66*]

MS imaging studies began with laser microprobe mass spectrometry (LMMS) and laser microprobe mass analysis (LAMMA), commercially available in the late 1970s [69]. LMMS is used in the analysis of biological samples as well as inorganic samples. A focused UV laser pulse is used to desorb and ionize solid samples without matrix and different mass analyzers having been implemented (e.g. TOF and Fourier transform ion cyclotron resonance (FT-ICR))[70-72]. In LAMMA, the laser beam is used to generate light pulses and ionizes the analytes which are accelerated into the mass spectrometer. This technique is used for the analysis of powdered samples, were the molecules are excited to an ionized state by a focused laser beam [73, 74]. In addition, the development of static SIMS in the late 1960s, combined with the high sensitivity of TOF instruments, have made TOF-SIMS a powerful tool for MS imaging [75].

A TOF-MS is the mass analyzer of choice for both MALDI and SIMS mass spectrometry imaging. Speed, sensitivity and broad mass range detection (m/z ~1 – 100,000) make it attractive for imaging purposes. Recently, there have been a number of instrumental developments for MS imaging to increase throughput, mass resolving power, mass accuracy, MS/MS capabilities and spatial resolution. Traveling-wave ion-mobility TOF adds a gas-phase separation step prior to analysis that aids analysis of complex samples to recover spatial information caused by unresolved peaks. In addition, the ion-mobility cell (or quadrupole in QTOF systems) can be used for improved MS/MS. The development of MALDI mass spectrometry imaging sources for high mass resolution and high mass accuracy mass analyzers, such as FT-ICR and FT-Orbitrap (FT-MS), allows for the separation of ions with the same nominal mass and confident assignment of elemental

[*] Reprinted from International Journal of Mass Spectrometry, 260, (2-3), Stoeckli, M.; Staab, D.; Schweitzer, Compound and metabolite distribution measured by MALDI mass spectrometric imaging in whole-body tissue sections, **2007,** 195-202A., Copyright (2011), with permission from Elsevier.

formulas for small molecules and lipids. Furthermore, various MS/MS techniques are available for FT-MS systems. The development of scanning microprobe MALDI for imaging can provide spatial resolution as low as 8 μm with the high-sensitivity ionization of biomolecules by MALDI [76].

Sample preparation is crucial for successful detection of desired molecules [29, 31]. Recent advances in method development have increased both chemical and spatial information from imaging experiments. Washing protocols for tissue sections have proven useful for enhanced ionization of specific molecules in both SIMS and MALDI, likely due to the minimization of ion suppression due to the presence of salts and other undesired analytes [30, 31, 77]. Metal-enhanced and matrix-assisted SIMS allow for the detection of a broader range of analytes than unmodified surfaces [37]. In addition, the choice for a MALDI matrix dictates the molecular weight range observed. Moreover, careful MALDI matrix deposition must ensure adequate sample extraction without surface diffusion. The stretched-sample method [78] and dry matrix application[79] have proven useful for reducing surface diffusion of analytes.

In this chapter, a discussion is presented on the current state and recent advances in MS imaging instrumentation and method development. The focus will be on improvements for spatial and chemical resolving power, and increased sample throughput, with selected applications highlighting specific advances. Also, the advances in mass spectrometry imaging require new data treatment approaches for large imaging datasets, which will be briefly discussed. Finally, perspectives for mass spectrometry imaging will be discussed.

2.2 Ionization methodologies for imaging MS

2.2.1 *Secondary Ion Mass Spectrometry (SIMS)*

SIMS uses high-energy primary ions (e.g., Ar^+, Ga^+, In^+) to strike the sample surface. The primary ion penetrates the sample surface and induces a collision cascade with atoms and molecules in the surface region. Secondary ions are released from the surface when their kinetic energy is increased above the binding energy to the substrate. This typically occurs at a depth of 10 Å and is size independent. The detailed fundamentals on cascade theory and aspects of organic and inorganic SIMS are reviewed in detail elsewhere [80-82].

SIMS typically desorbs and ionizes elements and small molecules. The practical mass range is limited to ~m/z 1000 as a result of extensive surface fragmentation [75]. The use of a matrix in matrix-enhanced (ME)-SIMS can overcome this limit through the use of an organic MALDI matrix. This approach improves detection of higher mass species.

In SIMS, a distinction is made between the static mode or dynamic mode. Each technique has a different extent of surface damage and is used for different purposes. Static SIMS uses a primary dose lower than 10^{12} ions/cm^2, which minimizes the interaction of primary ions to the top monolayer of molecules. Each primary ion strikes an undisturbed region and the interaction between primary ion beam and atoms and molecules is limited to less than 1% [83-85].

Dynamic SIMS is more destructive as a larger primary ion dose is used, which results in interactions with deeper sample surface layers. The differences between static and dynamic SIMS have a direct effect on their applications; static SIMS is largely used for qualitative imaging [86] while dynamic SIMS application consists primarily of quantitative elemental imaging [87-89]. The details of dynamic and static SIMS can be found elsewhere [75].

2.2.2 *MALDI*

The mechanism of ion formation in MALDI is a complex phenomenon. The desorption process and ion formation mechanisms have been intensively reviewed [90, 91]. The addition of a matrix to sample surface serves several purposes: extraction of analytes from the sample surface and the formation of analyte-doped crystals, and absorption of laser energy for soft-ionization of sample molecules.

2.2.3 *DESI*

Desorption electrospray ionization (DESI) is performed by the interaction of electrospray generated charged droplets with the sample surface. The impact of the droplets with the surface produces a second generation of charged droplets with dissolved surface molecules. These secondary droplets proceed through an electrospray-type mechanism to form gaseous ions which are directed into an atmospheric inlet of the mass spectrometer [92, 93]. The angle of the secondary electrospray plume and the MS inlet must be optimized to allow the maximum ion volume to enter the mass spectrometer. The ions measured directly from tissue surfaces by DESI are mainly singly charged lipids [64, 68, 92, 94-97]. DESI allows ambient surface sampling without sample pretreatment, albeit with lower spatial resolution than SIMS and MALDI.

Table 1 summarizes important aspects of the common desorption/ionization methods used for mass spectrometry imaging.

***Table 1**: Desorption and Ionization Methods*

Source	Examples	Environment	Energy	Spot Size (d)	Surface Current	MW Range (m/z)
Liquid Metal Ion Gun	Ga^+, In^+, Au^+ Au^{2+}, Au^{3+}	UHV*	>25 eV	> 1 µm	1-10 nA	2 000†
Solid-State Cs^+ Gun	UHV	10 keV	2-3 µm	< 10 nA		3 000
C_{60}^+ Cluster Source		C_{60}^+	UHV	5 eV – 40 k eV	200 nm - 200 µm	
MALDI	Nd:YAG, N_2 Nd:YLF	UHV, HV‡ Ambient	100-200 µJ/	5-300 µm pulse	n/a	500k
DESI	Solvent	Ambient	n/a	>150 µm	0.5-50 nA[98]	66k

2.3 Instrumentation

Recent instrumental developments aim to increase the throughput, mass resolving power, mass accuracy, tandem MS capabilities and spatial resolution for MS imaging. McDonnell *et al.* have constructed a sample handling system for automatic introduction of sample slides from an environment controlled sample chamber to the mass spectrometer, for more time-efficient mass spectrometer use[99]. The Caprioli group has constructed two MALDI-TOF systems which operate in the continuous scanning mode with a 5 kHz laser, which show significant improvements in speed (> 2x) over commercially available MALDI-TOF instruments[100].

* UHV: Ultra high vaccum, with pressure lower than 10^{-9} torr
† no surface treatment: ~1000; ME-SIMS: ~2000 (see Section 4.1)
‡ HV: High vacuum, with pressure between 10^{-3} and 10^{-8} torr

While TOF-MS offers great throughput for MALDI MS imaging experiments, its lack of mass resolving power can result in the loss of important chemical and spatial information. New technologies for MS imaging are under investigation and being implemented to overcome this limitation. Among these new technologies are ion-mobility based MS imaging, MALDI FT-ICR MS and MALDI FT-Orbitrap. Ion-mobility separation offers a gas-phase separation dimension, based on the ions' collisional cross-section, which allows separation of ions at the same nominal mass, originating from the tissue surface or matrix clusters [101, 102]. The combination of ion-mobility separation with MS imaging has been shown to improve the spatial mapping of the anti-cancer drug vinblastine, by the removal of an interfering endogenous lipid [24]. High performance MS methods, such as FT-ICR MS and FT-Orbitrap, offer high mass resolving power and high-mass accuracy, and FT-ICR MS been shown to resolve and identify ions at a single nominal mass that are commonly present in MALDI imaging mass spectra [97, 103, 104]. In addition, the high mass accuracy of FT-ICR has been used for high confidence identification of olanzapine and it's metabolites from rat kidney (< 1 ppm across the entire dataset) [60]. Figure 3 shows MALDI FT-ICR MS spectra and mass selected images of hydroxymethyl olazapine and three ions at the same nominal mass from a dosed rat kidney. Further, the tandem-MS capabilities of FT-ICR MS have been shown for the identification of drugs and molecules directly from biological tissues [60, 104, 105].

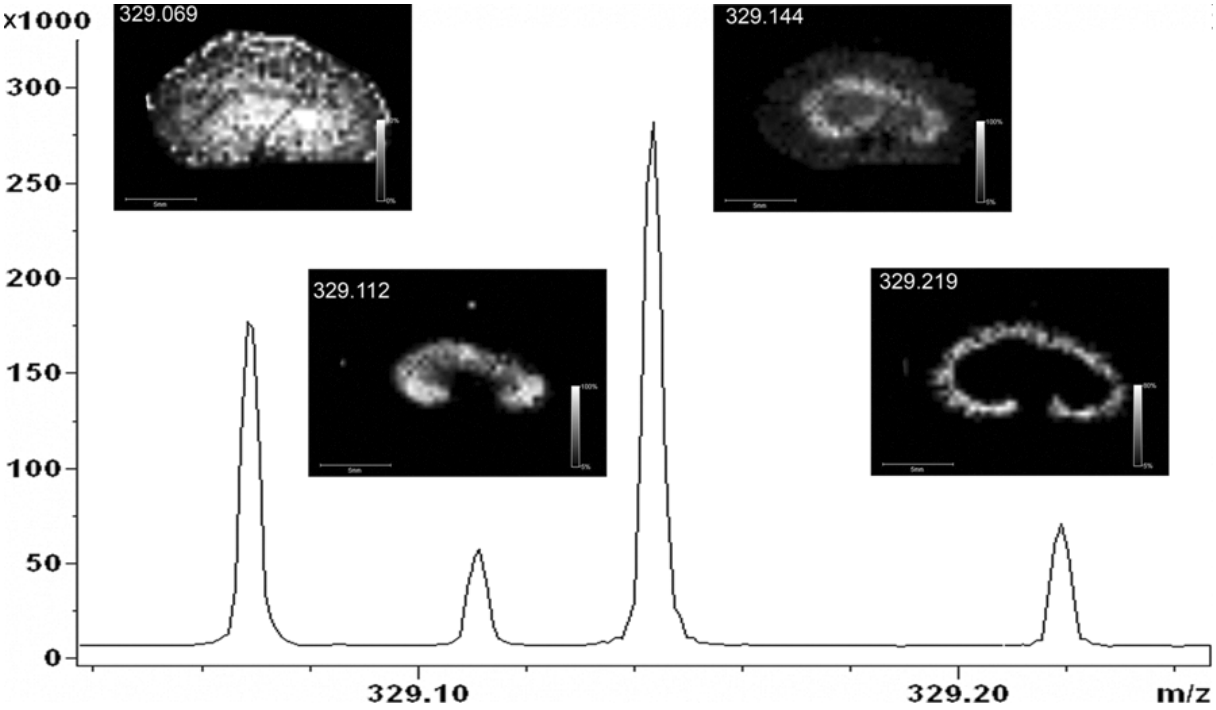

***Figure 3**: FT-ICR MS images of hydroxymethyl OLZ and three other ions at m/z 329.2.*[103*]

Tandem-MS has traditionally not been available for static-SIMS imaging instruments, due to the need to retain the spatial distribution of ions from the surface to the detector. However, the improvement of cluster beam sources has improved the sensitivity, mass range and lateral resolution for biological SIMS [106]. The Winograd group has developed a C_{60} SIMS hybrid-quadrupole orthogonal-TOF MS with tandem-MS capabilities [107]. This instrument has been employed to directly map gramicidin S (m/z 1141) under a copper grid at spatial resolution of 25-30 µm in both MS and MS/MS modes. Similarly, the Vickerman group has constructed a TOF-based instrument which employs a C_{60} ion source, operated in direct-current mode, with a secondary-ion buncher, a collision-cell for MS/MS and a reflectron-TOF analyzer [108].

[*] Reprinted from Analytical Chemistry, 80 (14), 260, (2-3), Cornett, D. S.; Frappier, S. L.; Caprioli, R. M., MALDI-FTICR imaging mass spectrometry of drugs and metabolites in tissue, **2008,** 5648-5653, Copyright (2011), with permission from ACS Publications.

The increase of spatial resolution in MS imaging experiments is pursued through efforts to decrease the spot size of the laser or ion beam. A coaxial objective has been employed in MALDI decreasing the laser spot size to 1 micrometer or better [76]. However, fluence considerations limit the applicability of this approach. An alternative approach to increase the spatial resolution is the use of the microscope mode imaging technology [20]. This approach decouples the attainable spatial resolution from the desorption and ionization spot size. The spatial resolution is determined by the quality of the image forming ion optics and the quality of the position (X-Y) and time detector used. We have coupled a C_{60} SIMS approach with a delay-line detector for microscope mode high-spatial resolution (3-4 μm) TOF-SIMS imaging. The position-sensitive delay-line-detector allows the C_{60} source to be operated at full current and without the need for cluster-beam focusing [109].

2.4 Sample preparation

Several factors for MS imaging sample preparation must be considered, from sample collection to surface treatment prior to analysis. The proper and immediate treatment of tissue after surgical removal is essential to avoid degradation and spatial rearrangement of molecules [29]. A common protocol for multi-modal MS imaging at AMOLF is shown in Figure 4.

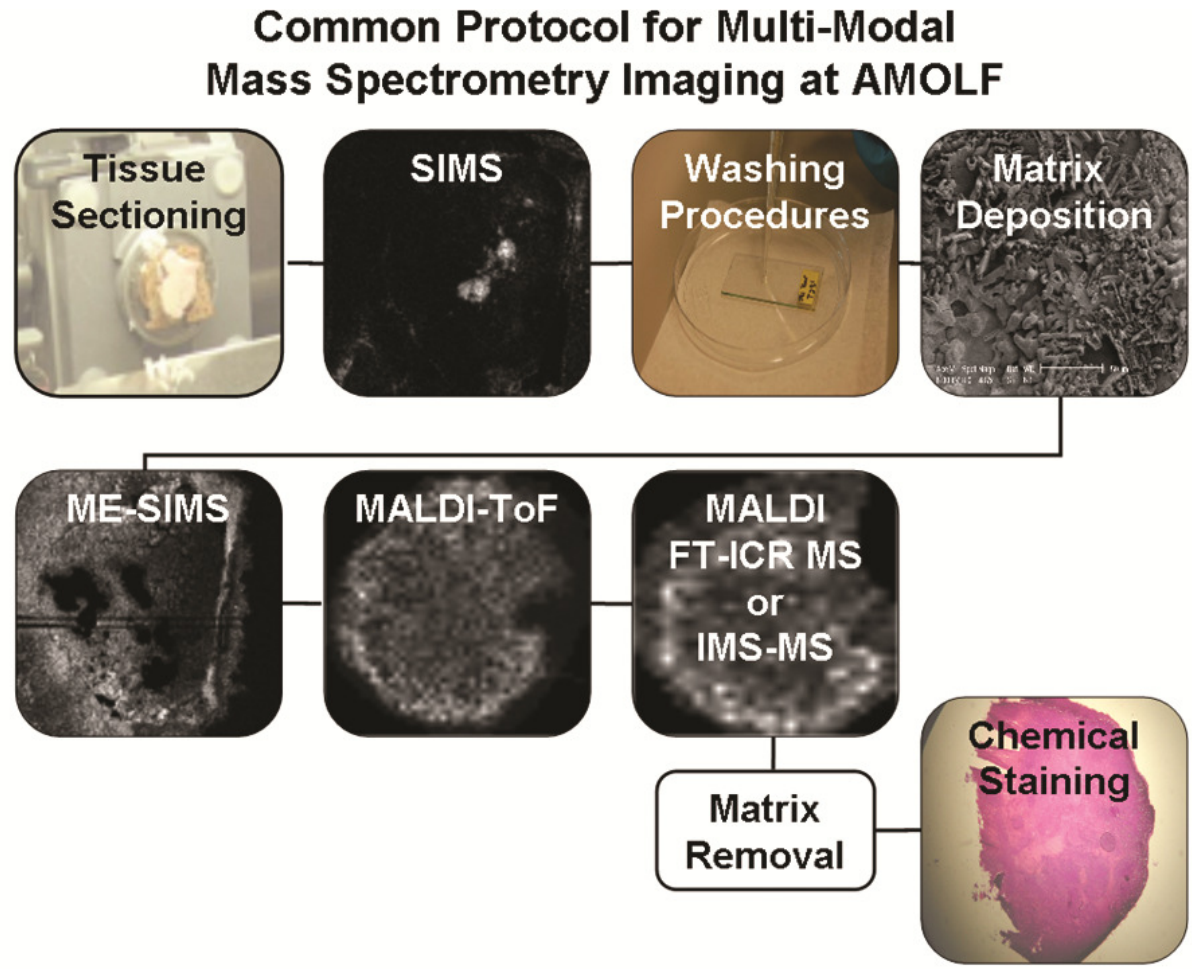

***Figure 4**: A common multi-modal MS imaging protocol used at the FOM Institute AMOLF.*

Thin, flat surfaces are required for MS imaging analysis. Samples are typically prepared by cryo-sectioning on a microtome, where the temperature of sectioning depends on the type of tissue (e.g. fatty tissue requires lower temperatures than more water based tissues). The sectioned tissue slice can be directly applied on a conductive surface (e.g. metal MALDI target or indium tin oxide (ITO)-coated glass slide) for full tissue imaging. An alternate approach is the sample stretching method. Here, the tissue slice is deposited onto glass beads embedded in parafilm and stretched homogeneously in two dimensions with the parafilm attached to a glass slide for stability. The stretching method allows increased spatial resolution and improved analyte extraction without diffusion concerns [78, 110].

In both methods, the sample may require further sample preparation after the tissue section has been mounted onto a target. Washing steps, enzymatic digestion and matrix deposition can all be utilized depending on the mass analyzer, ionization method and desired molecule type. Several procedures and applications have been reviewed in past few years and frequently used protocols will be discussed here [19, 29-31, 33, 37].

No washing steps are recommended if the molecules of interest are salts or lipids, as they are often removed with common washing solvents. One or more wash steps are recommended prior to matrix deposition for peptides or proteins [31]. The most commonly used washing procedure for the removal of surface lipids or salts is 70-80% cold ethanol, (4ºC) [19, 29]. The removal of salts, which may react with the matrix, allows homogeneous crystallization of the matrix, which increases the ionization efficiency of peptides and proteins. Salts and lipids are readily ionized, and may cause ion suppression and saturation of the detector. A more severe washing procedure with organic solvents such as chloroform, hexane or acetone can improve peptide and protein detection on older tissues sections [27]. Harsh washing procedures, however, may damage the sample and remove peptides of analytical interest. It is recommend to optimize matrix and washing procedures on adjacent slices, in order to evaluate the best sample preparation protocol to be used in each sample type. For DESI, there is typically no sample pretreatment.

On-tissue enzymatic digestion (e.g. tryptic digestion) can be performed to improve protein detection and identification capabilities. This method is always preceded by washing steps to prevent denaturation or deactivation of the proteolytic enzymes used [32-36]. On-tissue digestion protocols are typically accompanied by analysis of an adjacent slide for intact protein identification.

2.4.1 *Surface Treatment for SIMS*

The upper mass limit in SIMS can be partially overcome by dedicated surface treatments. Here, we will briefly describe two surface modification techniques that are

commonly used in biomedical imaging studies; metal assisted SIMS (MetA-SIMS) and matrix enhanced SIMS (ME-SIMS).

For MetA-SIMS, a thin layer (1-5 nm) of metal (e.g. gold) is coated on top of the sample. MetA-SIMS enhances the ionization of several species, including cholesterol and lipids [37]. The metal layer can be quickly and reproducibly applied using plasma sputter coaters.

ME-SIMS uses an organic MALDI matrix (e.g. α-cyanno-4-hydroxycinnamic acid or 2,5-dihydroxybenzoic acid) deposited on the surface of the sample. ME-SIMS can increase the mass range to m/z ~2000 and peptides not detectable in normal SIMS preparations can be observed. Matrix deposition is the critical step for ME-SIMS, since the crystal size determines the spatial resolution for this method. Remarkably, ME-SIMS yields spectra similar to MALDI. Static mode ME-SIMS consumes a significantly lower amount of surface material than MALDI. Thus, the same tissue can subsequently be used for other desorption/ionization methods that require a matrix.

2.4.2 *Matrix selection and deposition for MALDI and ME-SIMS*

Matrix deposition for both MALDI and ME-SIMS is another crucial step in the sample preparation protocol for MS imaging. Matrix deposition must be homogeneous, reproducible, provide sufficient sensitivity and should be easy to use. In addition, the size of the matrix crystals determines the maximum spatial resolution attainable. Matrix deposition may be performed with or without previous wash steps for biological samples (e.g. tissue from biopsy) [31]. Below, a number of matrix deposition considerations for MS imaging is discussed.

The successful detection of analyte molecules depends on the correct choice of the MALDI matrix. The matrix must not react with the analytes in the tissue section and should posses a low sublimation rate. The latter is important since most MS imaging studies are conducted under HV or UHV conditions, but not for ambient desorption

methods that employ a matrix. In addition, the type and molecular weight of the analytes of interest must be considered when choosing a MALDI matrix. Table 2 lists common MALDI matrices and their applications for biological MS imaging.

Table 2: *Matrix Selection for MALDI-MS*

Matrix	**Applications**
2,5-dihydroxybenzoic acid (DHB, gentisic acid)[38-40]	Lipids, small peptides, carbohydrates, nucleotides, glycopeptides, glycoproteins and small proteins
α-cyano-4- hydroxycinnamic acid (HCCA)[40, 41]	peptides, glycopeptides, small proteins, glycoproteins, and oligonucleotides
3,5-dimethoxy-4-hydroxycinnamic acid (SA, sinapinic acid)[40, 42, 43]	Proteins with MW>10kDa, especially glycoproteins and hydrophobic proteins
,4,6-Trihydroxyacetophenone (THAP)[40]	Oligonucleotides
3-Hydroxypicolinic acid (3-HPA) [40, 44]	Oligonucleotides, peptides and glycoproteins
2,6-Dihydroxyacetophenone (DHA) [30, 40, 45]	Phospholipids
2,4-Dinitrophenylhydrazine (2,4-DNPH) [34]	Peptides, proteins (also for FFPE)
HCCA/aniline [46]	Peptides
HCCA/N,N-dimethylaniline [46]	Peptides
HCCA/2-amino-4-methyl-5-nitropyridine [46]	Peptides

The matrix deposition method for MALDI and ME-SIMS MS imaging should also be carefully considered. The matrix layer should be as homogeneous as possible, in order to avoid local variations in desorption and ionization. The environmental conditions (e.g. humidity, presence of oxygen) during matrix deposition are also important, since they may result in poor interaction between matrix and analytes. For example, if the matrix reaches the surface already or almost dry there is little opportunity for extraction of surface analytes

into the matrix. Conversely, a film of matrix solution can lead to surface diffusion [111, 112]. The principal methods for matrix deposition for MS imaging are briefly described below. A more in-depth review of this subject matter can be found elsewhere [31].

Dried-droplet method:

The matrix solution is applied on the sample manually with a pipette. This method is simple and fast and ideal for profiling, but it is not recommended for imaging purposes. Diffusion may occur inside the matrix spot, the size of the spot is typically large and there may be irregular distribution of matrix crystals.

Pneumatic nebulization:

The matrix solution is sprayed onto the sample with a hand-held Thin Layer Chromatography sprayer or airbrush [29, 37]. A gentle spray allows the formation of a homogeneous crystal layer on the sample surface. The spray has to be optimized previous to each application, thus reproducibility may be an issue. This method can also be automated in a controlled environment such as shown by Stoeckli et al.[113].

Chemical inkjet printer:

Small droplets of matrix solution are applied with a piezoelectric droplet printing device. This technique allows the deposition of small volumes per spot (100 pL) per cycle. Each single matrix spot has a diameter of 150μm or smaller, dependent on the total amount of solution applied per cycle. Examples of devices are the chemical inkjet printer (ChIP) [114, 115] of Shimadzu, the acoustic reagent multi-spotter of Labcyte [116] and the acoustic matrix deposition method developed by Aerni *et al.* [116]. The deposition is precise, highly reproducible and the droplets are uniform. Due to the droplet size, it is more suitable for lower spatial resolution MSI. Several home build devices using inkjet printing technology have also been reported in literature [117].

Automated vibrational spray coater (ImagePrep by Bruker Daltonics):

This commercial device is dedicated for MALDI imaging MS and produces a homogeneous matrix layer with small crystals and operates in a closed system. Control of droplet size limits surface diffusion and the interaction time between analytes and matrix can be optimized for maximum co-crystalization [28].

Matrix Sublimation:

Solid matrix is placed on the bottom section of a condenser and the sample is attached to the condenser with double sided thermally conductive tape facing the solid matrix. The sublimation occurs under low pressure and high temperature (approximately 125 °C) which allows the matrix to condense on the cold sample surface. This method provides enhanced purity of matrix applied to the sample, small crystal size, and uniformity of deposition [118].

Dry-Coating:

Finely ground solid matrix is filtered directly onto the tissue surface through a 20 µm sieve. This method is useful for fast and reproducible matrix application for analysis of lipids. Similar to the sublimation method, surface diffusion is limited due to the absence of solvents [79].

The choice of the matrix deposition is governed by the type of application pursued. Automated methods are better for large scale samples and high-throughput studies. The manual methods are favored when testing new protocols. Some of the matrix deposition devices, such as the Chip-1000, the ImagePrep and the Labcyte spotter are also suited for the deposition of proteolytic enzymes for on-tissue digestion. Matrix deposition technologies are being researched heavily, as they may prove to be the limiting factor for

future high throughput biomedical studies, as rapid and reproducible matrix deposition is currently difficult.

2.5 Data Analysis

A number of different software packages are available to generate images from position correlated mass spectra. These include Novartis' BioMap, Brukers' Flex software series and AMOLFs' "datacube" generator and viewer. The data generated by a MS imaging experiment can vary from > 100Mbytes in size up to a few Gbytes per sample, and is dependent on the spatial resolution and mass analyzer used. Thus, manual interpretation of the data often becomes very difficult and time consuming. To these ends, a number of statistical software based tools have been developed to aid in MS imaging data interpretation.

Principal component analysis (PCA) [119, 120] is a widely used multivariate data analysis method that is easily applied to MS imaging datasets. PCA is an unsupervised method that is used to identify groups of closely correlated variables; spatial coordinates and mass for MS imaging. Figure 5 shows the use of principal component analysis with AMOLF's ChemomeTricks toolbox for MATLAB version 7.0 (The MathWorks, Natick,MA) [86]. Here, components that are associated with areas outside the tissue are subtracted and yield improved correlations of the remaining components.

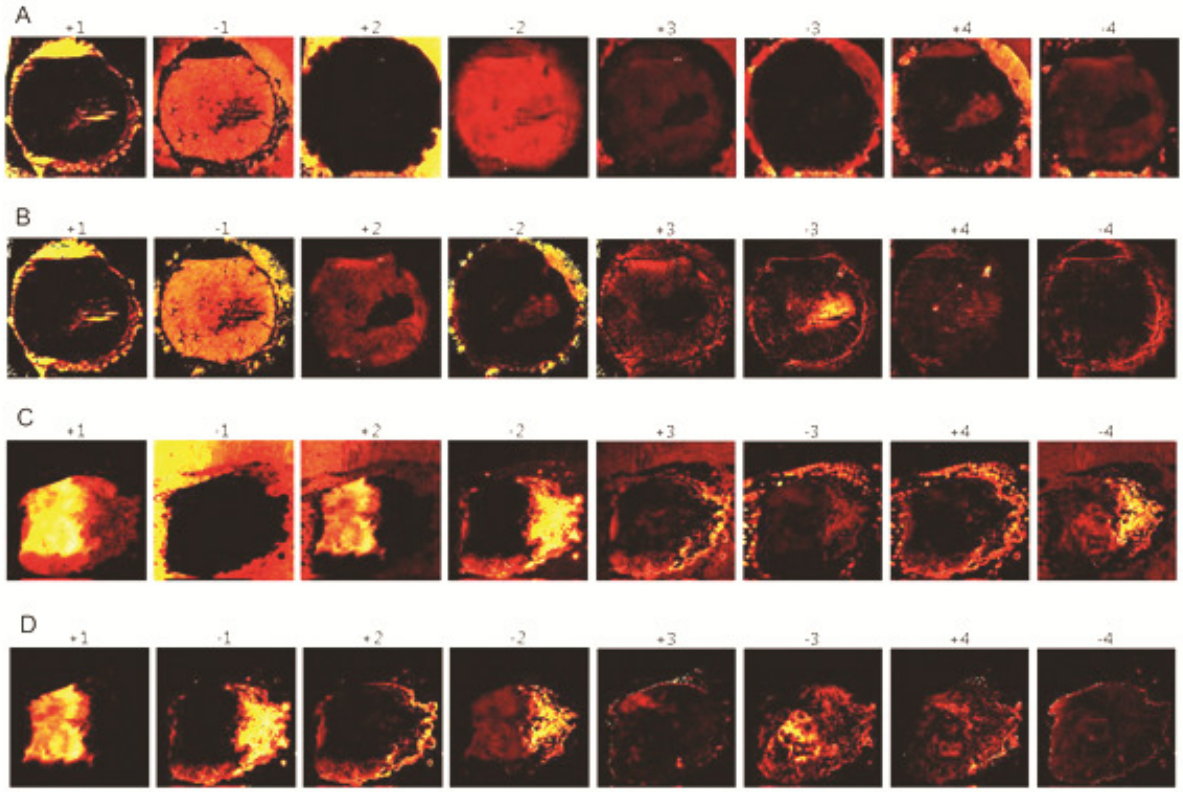

Figure 5: *PCA analysis of SIMS imaging dataset of (A) Xenograft human breast tumor MDA-MB-231 and (B) The data from section A after removal of component +2 (background removal); (C) Xenograft human breast tumor MCF-7 and (D) The data from section C after removal of component -1 (background removal).*[86]

Where PCA can have non-negative components, probabilistic latent semantic analysis (pLSA) results in non-negative components decomposition of imaging datasets that combine with noise reduction and automated tissue classification, also called digital staining [121, 122]. PCA combined with canonical correlation analysis (CCA) can be used to correlate MS imaging data obtained from different techniques. This approach correlates the spatial and spectral components from each dataset, and leads to improved individual results. Figure 6A shows PCA scores (top) for SIMS and MALDI MS imaging of human cerebellum, and correlation scores via CCA analysis are shown in Figure 6B. Correlation

of the results leads to marked improvement of component 2 +/- for both SIMS and MALDI datasets. Quantification of correlations between mass spectrometry images has also been described [123].

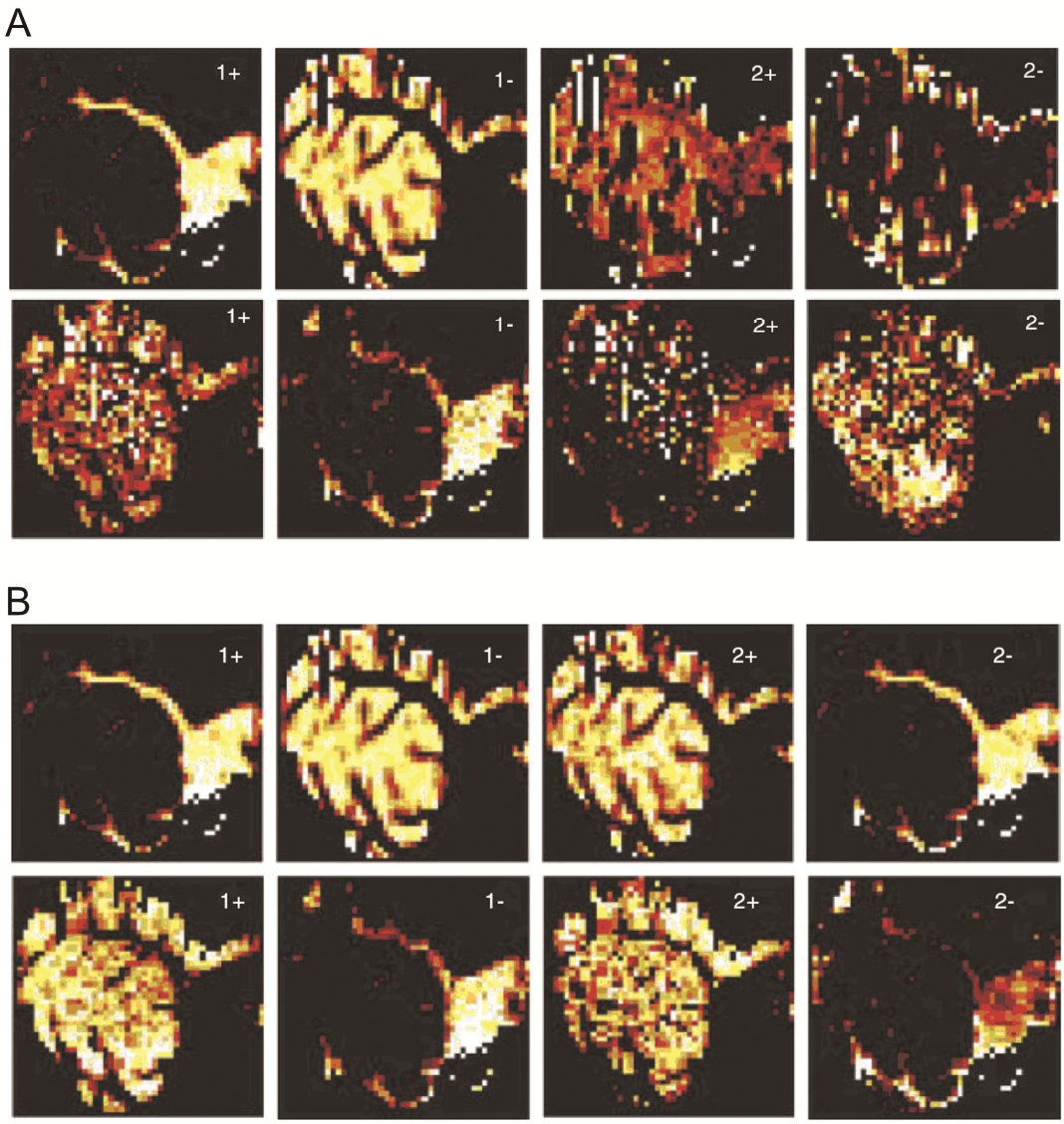

Figure 6: *Figure 6A: Principle Component Analysis score images for SIMS (top row) and MALDI (bottom row) data of human cerebellum tissue. Figure 6B: Conocal Correlation*

Analysis score images for SIMS (top row) and MALDI (bottom row) data of human cerebellum tissue.[86*]

2.6 Perspectives

Recent developments, from instrumentation to sample preparation, have improved the sensitivity, spatial resolution and identification capabilities for MS imaging by SIMS and MALDI. These improvements are broadening the application of MS imaging for lipid, peptide and protein biomarker identification, as well as drug and metabolite imaging. The combination of MS imaging, direct tissue MS/MS, and standard bioanalytical protocols (e.g. LC MS/MS and electrophoresis) will allow for confident identification of pathologically relevant compounds and their localization in cells and tissues. Efforts toward three-dimensional image construction will allow more global understanding of tumor environments and organ physiology. In addition, the integration of MS imaging with current clinical imaging techniques (e.g. MRI, PET and CT) promises chemically specific complimentary spatial information.

---

[*] Reprinted from International Surface and Interface Analysis, 41 (8), Eijkel, G. B.; Kaletas, B. K.; van der Wiel, I. M.; Kros, J. M.; Luider, T. M.; Heeren, R. M. A., Correlating MALDI and SIMS imaging mass spectrometric datasets of biological tissue surfaces **2009,** 675-685, Copyright (2011), with permission from John Wiley and Sons

Chapter 3

3. An alternative paper based tissue washing method for Mass Spectrometry Imaging: Localized Washing and Fragile Tissue Analysis*

Surface treatment of biological tissue sections improves detection of peptides and proteins for mass spectrometry imaging. However, liquid surface treatments can result in diffusion of surface analytes and fragile tissue sections can be easily damaged by typical washing solvents. Here, a new surface washing procedure is presented for mass spectrometry imaging, which allows localized tissue washing of fragile samples by established washing solutions. A wetted fiber free paper is applied directly onto the biological tissue surface and the washing solution is spatially contained by the paper structure, thus the formation of a liquid film on the tissue surface is avoided. Direct analysis of the paper used for washing shows blotting of salts onto the paper. This procedure enables local washing of tissue sections for mass spectrometry imaging and tissue profiling experiments. In addition, the method allows fragile tissues that cannot be treated by conventional washing techniques to be analyzed by MS imaging.

---

*Based on: Erika R. Amstalden van Hove, Donald F. Smith, Lara Fornai, Kristine Glunde, Ron M.A Heeren, *Journal of the American Society of Mass Spectrometry*, 2011, **22** (10), 1885-1890.

3.1 Introduction

The quality of MS imaging results depends heavily on the choice and execution of sample preparation methods. Specific molecular classes often require different sample preparation treatments, such as optimized washing steps and the correct choice of matrix for matrix assisted laser desorption ionization (MALDI). Several washing methods have been tested, optimized and have become standard elements in many MS imaging workflows[19, 27, 29-31]. Popular washing methods include immersion of the sample in washing solution or pipette application of the solution onto the sample and subsequent removal by pipette. However, such washing steps often lead to undesired diffusion of molecules over the tissue surface. Delicate biological sections can also be severely damaged when washed with harsh solvents.

Blotting techniques have been applied to transfer intact proteins from biological sections onto polyvinylidene difluoride (PVDF) membranes, which are then measured in an indirect imaging experiment [56, 124, 125]. The "molecular scanner" has been used to extract and digest proteins from 1D and 2D SDS-PAGE gels and from tissues onto capture membranes, while keeping their spatial organization [21, 126, 127]

In this chapter, a surface cleaning method is presented which also relies on the contact between biological material and a wetted fiber-free paper. Unlike the above-mentioned blotting techniques, here the biological tissue is directly analyzed with a MS imaging experiment. The solutions used in the surface cleaning are the same solutions already established for MS imaging sample preparation [27, 29-31, 85, 128]. The use of paper for surface cleaning allows its application on selected sample areas, enabling the simultaneous comparison of washed and unwashed areas on a single tissue sample. This gentle method allows surface cleaning of fragile biological samples, which cannot be washed by pipette or immersion methods.

3.2 Material and Methods

Rat heart and rat brain from male rats (type WU) and mouse brain from a female mouse (type 9CFW-1) were purchased from Harlan Laboratories. (Boxmeer, The Netherlands). A MDA-MB-231 clone developed at Johns Hopkins University School of Medicine, which was derived from the highly metastatic human mammary epithelial cancer cell line MDA-MB-231, was used for inoculation to generate breast tumor xenograft models in the upper left thoracic mammary fat pad of female severe combined immunodeficient (SCID) mice.[129] All experimental animal protocols were approved by the Institutional Animal Care and Use Committee of the Johns Hopkins University School of Medicine.

Rat heart and brain, and tumor xenografts were sectioned at 10 µm thickness on a cryo-microtome (Microm International, Walldorf, Germany) and thaw mounted on indium-tin-oxide coated glass slides (ITO, 4-8 Ω resistance; Delta Technologies, Stillwater, MN). Adjacent 12 µm thick mouse brain sections were collected for comparison of washing methods and thaw mounted on ITO slides. All samples were stored at -80 °C prior to use and dried in a vacuum dessicator for 30 minutes prior to washing, matrix coating and MS analysis.

In addition, two mouse brain sections (12 µm thick) were spotted with three different colors of permanent marker (Lumocolor permanent Red, Green and Blue; STAEDTLER Mars GmbH & Co. KG, Nuernberg, Germany, Article numbers 318-2, 318-5 and 318-3) in order to access surface diffusion of small molecules. One section was washed with the fiber free paper washing procedure and the other by the immersion method, with 70% ethanol (in H_2O) as the wash solvent.

Fiber Free Paper Washing Procedure

The fiber free paper washing procedure uses a common laboratory wipe (KIMTECH SCIENCE* Precision Wipes, Kimberly-Clark, Roswell, GA, USA), which is

wetted with the wash solvent of choice and carefully placed on top of the tissue section. Figure 1 documents the procedure photographically for a rat heart section. The paper is cut to a size slightly larger than the tissue section to allow for full coverage, or can be cut to any size for localized washing. Typically, a solvent volume of 100-200 µL is sufficient to completely wet the paper with a pipette. Alternatively, the papers can be soaked in the wash solvent before application, though care should be taken that the paper is not too saturated, as this can cause flooding of the tissue section. Contact time is typically 30-60 seconds, and depends on the washing type and solvent of choice. Unlike submersion and pipette washing methods, volatile washing solvents (such as alcohols) will evaporate from the paper, which does not allow extensive contact periods (> 60 seconds). Care should be taken when removing the wetted paper from the tissue section in order to reduce smearing effects from the application and lifting process.

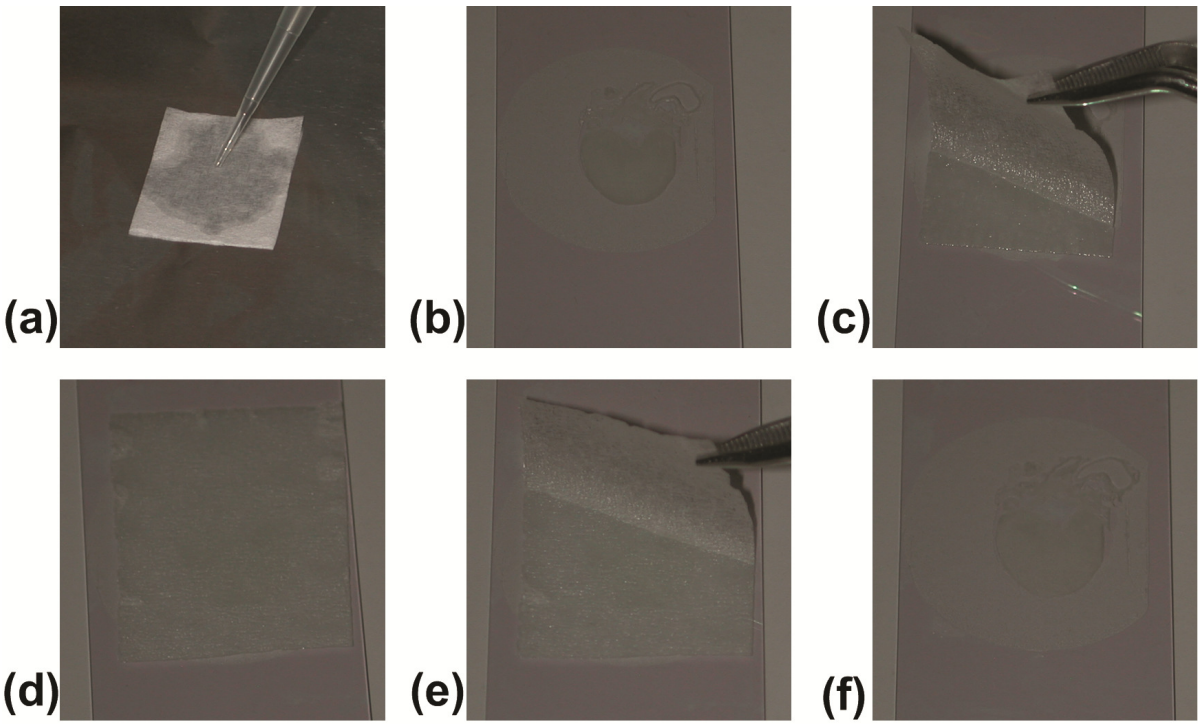

Figure 1: *Steps for wetted paper washing procedure: (a) paper wetting; (b) sample on ITO glass –dry and at room temperature; (c) application of wetted paper on top of the tissue; (d) incubation; (e) paper removal; (f) tissue after surface cleaning.*

Rat heart was washed twice with fiber free paper wetted with 70% cold ethanol, each for one minute. The paper used to wash the rat heart was saved and imaged by MetA-SIMS. A rat brain section was locally washed with paper strips wetted with 70% cold ethanol for one minute per strip. A mouse brain section was washed with isopropanol (70% and 95%, in H_2O; 30 seconds each) for comparison with conventional washing procedures for the enhancement of protein signals.

Fragile MDA-MB-231 breast tumor section was washed for protein enhancement with a paper wetted with 100% methanol (twice for 30 seconds each).

To compare diffusion of small molecules with an immersion wash, a mouse brain section spotted with permanent markers was washed with a paper wetted with 70% ethanol (in H_2O) for 60 seconds.

Immersion Washing Procedure

The immersion washing procedure was adapted from Seeley et al. [30] The ITO slide with the tissue section was immersed in a bath of the wash solvent of choice in a Petri dish (typically 50 mL solvent). No swirling or mixing was performed.

A mouse brain section was immersed in isopropanol (70% and 95%, in H_2O; 30 seconds each) for comparison with wetted paper and pipette washing. The fragile MDA-MB-231 breast tumor section was immersed in 100% methanol (once for 30 seconds), which completely destroyed the tissue (data not shown). A mouse brain section spotted with permanent markers was immersed in 70% ethanol (in H_2O) for 60 seconds to assess the degree of diffusion of small molecules.

Pipette Washing Procedure

The pipette washing procedure was adapted from Lemaire et al.[27] A volume of ~200 µL/ cm^2 was loaded into a pipette and rinsed over the tissue section while holding the

ITO slide at an angle to allow the solvent to efficiently drain. A mouse brain section was rinsed with isopropanol (70% and 95%, in H_2O; 200 µL each) for comparison with wetted paper and immersion washing. The fragile MDA-MB-231 breast tumor section was rinsed with 100% methanol (100 µL).

Metal deposition

For metal assisted secondary ion mass spectrometry (MetA-SIMS), a 1 nm gold layer was sputter coated onto the locally washed rat brain section and the paper used to wash the heart section. A Quorum Technologies (Newhaven, East Sussex, U.K.) SC7640 sputter coater equipped with a FT7607 quartz crystal microbalance stage and a FT7690 film thickness monitor was used.

Matrix deposition

Sinnapinic acid (25 mg/ml in 50% acetonitrile/0.1% trifluoroacetic acid) was used for protein MS imaging of the mouse brain sections washed with isoproanol. The matrix was applied using a vibrational spray coater (ImagePrep, Bruker Daltonics, Bremen, Germany). For the comparison of diffusion for small molecules on mouse brain tissues subjected to different washing procedures, α-Cyano-4-hydroxycinnamic acid (10 mg/mL in 50% acetonitrile/0.1% trifluoroacetic acid) was used and applied using a vibrational spray coater, as described above.

MS imaging

SIMS experiments were performed on a Physical Electronics (Eden Prairie, MN, USA) TRIFT II time-of-flight secondary ion mass spectrometer with an Au^{1+} primary ion beam. Experiments were performed with a primary ion beam current of 450 pA, a primary pulse length of 30 ns, a spot diameter of 500 nm, and a primary ion energy of 22 keV. Large areas were analyzed using a mosaic of 128x128 individual analysis tiles unless otherwise noted. The raster size (or FOV) used was 150 µm per tile, with resolution of

256x256 pixels per tile. The FOV is automatically calculated by the WinCadence 4.4.0.17 software (ULVAC-PHI Inc.) based on the maximum raster size defined by the user and the total measurement area. The acquisition time was one second per tile. Both FOV and acquisition time were constant throughout the experiment, which covered the entire sample surface. The data acquisition was performed by WinCadence 4.4.0.17 software, which can also be used for data visualization.

MALDI experiments were performed on an Ultraflex III time-of-flight mass spectrometer (Bruker Daltonik GmbH, Bremen, Germany), with an accumulation of 1,000 shots per position for proteins and 700 shots for small molecules with a raster size of 200 μm.

3.3 Results and Discussion

Tissue washing has been shown to improve the spectral wealth and quality for intact proteins, as well as improving peptide detection [19, 27, 29-31]. Most washing procedures target the removal of abundant lipids, which allows less abundant proteins and peptides to be ionized and detected. Conventional washing procedures, such as immersion of the tissue section in the wash solvent of choice or washing the tissue section with solvent applied by pipette, are used routinely to improve MS imaging experiments. Here, a new method is presented that uses a fiber free paper, wetted with the wash solvent of choice, which allows localized washing and presents a number unique advantages over conventional methods. Samples deposited on substrates that cannot be washed by conventional methods due to sample mounting (e.g. whole-body animal section deposited on double sided adhesive tape) can be washed with this method, as well as fragile sections that may be damaged by conventional washing procedures.

The use of wetted paper allows surface cleaning of selected areas of a tissue section. Thus, analytes detected with and without surface washing can be compared on one

tissue section. Paper strips wetted with 70% ethanol were applied on different parts of a rat brain and the section was measured by MetA-SIMS. Figure 2 shows the total ion image (Fig. 2a) and mass selected images of sodium (m/z 22.9) (Fig. 2b), potassium (m/z 38.9) (Fig. 2c) and phosphocholine (m/z 184) (Fig. 2d) from the localized washing experiment. The washed areas show a decrease in signal intensity for salt cations such as sodium and potassium, and an increase in signal intensity for small organic molecules such as phosphocholine (m/z 184).

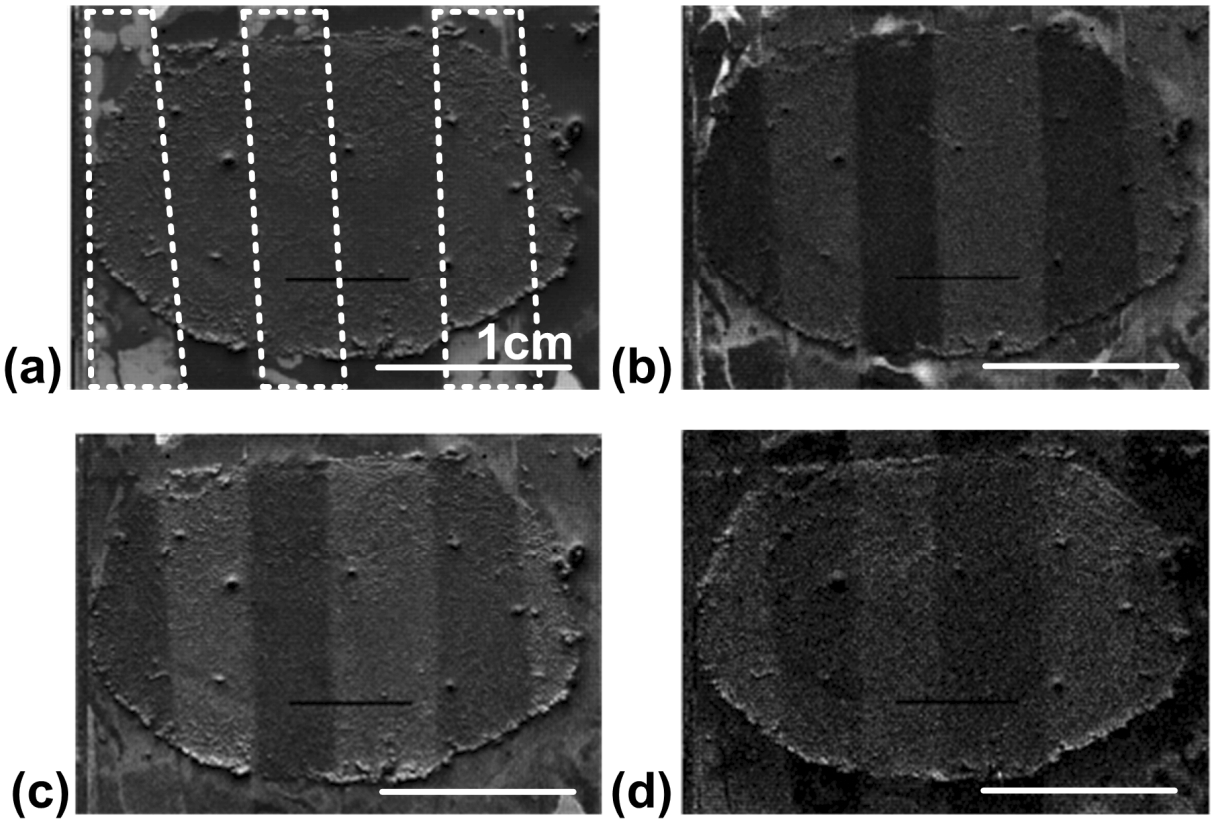

Figure 2*: MetA-SIMS MS imaging experiment of a selectively washed rat brain section. The areas enclosed by the dotted lines in (a) indicate the areas selectively washed by wetted strips of paper. (a) total ion image, (b) Na^+ (m/z 22.9) (c) K^+ (m/z 38.9) and (d) phosphocholine (m/z 184). Scale bar = 1cm.*

The decrease in relative abundance of (salt) cations is likely due to migration of these species from the tissue section into the wetted paper. Evidence of this migration is presented in Figure 3, where an entire rat heart section was cleaned once with wetted paper (cold 70% ethanol, 60 seconds). The analysis of the washing paper by MetA-SIMS shows that Na^+ and K^+ were blotted from the tissue section onto the paper (Fig. 3b). The signal enhancement of certain ions after this localized surface cleaning procedure is likely due to reduced ion suppression resulting from the removal of the easily ionized cations. The method does result in transfer of some organic molecules, such as cholesterol, to the washing paper. Principal component analysis (PCA) was performed on the MetA-SIMS data acquired from the paper used for surface cleaning as shown in Figure 3c and 3d. The first principal component identifies the region of the paper that was in contact with the rat heart tissue section (function +1), with the main species being sodium and potassium. In addition, silicone contaminates (m/z 73 and 147) [75], which can be detrimental to SIMS experiments, are removed with the paper washing procedure.

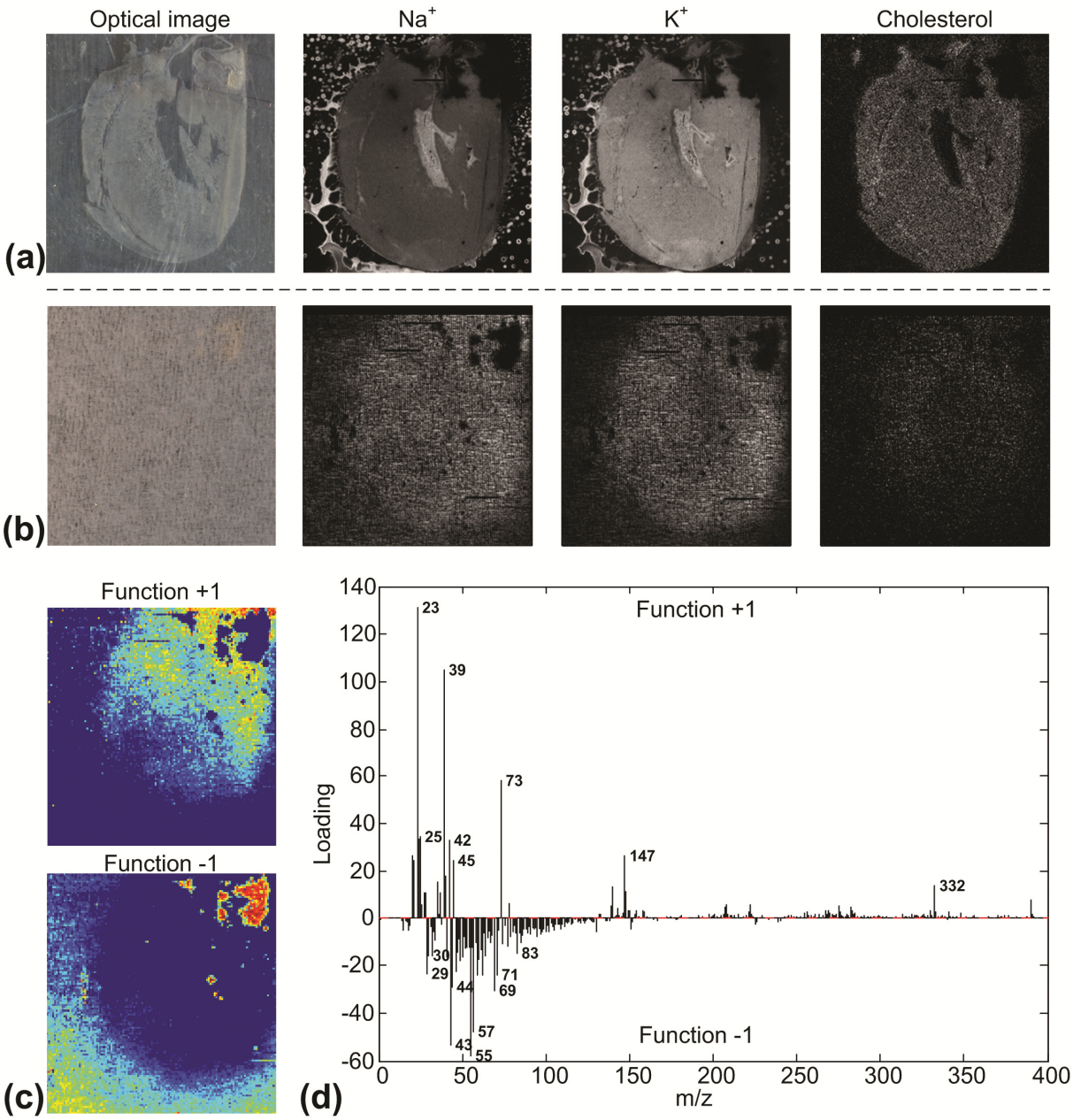

***Figure 3**: MetA-SIMS of a rat heart and the cleaning paper from a 70% ethanol treatment. (a) Mass selected images from the rat heart and (b) corresponding images of the same species from the washing paper. (c) Image of the first principal component of the MetA-SIMS spectra acquired from the paper used to wash the heart tissue and (d) the corresponding loading spectrum. Dominant species from the area in contact with the rat heart section show removal of salt cations, silicone contaminants such as*

polydimethylsiloxanes, m/z 73 ($C_3H_9Si^+$) and m/z 147 ($C_5H_{15}Osi_3^+$), and a mounting compound (Optimal Cutting Temerature compound) related peak at m/z 332.

The fiber free wetted paper method has been used to clean very fragile tissue sections which are not amenable to conventional washing protocols. Figure 4 shows the results of a methanol wash of a very fragile breast tumor xenograft section (MDA-MB-231 clone). Fig. 3a shows an unwashed section and Fig. 3b shows the section after two cycles of cleaning by the wetted paper method. An adjacent section washed by the conventional pipette washing method shows extensive damage as shown in Fig. 3c. Another section from the same tumor was washed with the immersion method, but the harshness of the method destroyed the tissue section completely. Thus, the conventional immersion and pipette washing left the tissue unusable for MALDI MS imaging experiments, whereas the wetted paper method is more gentle and allows for imaging analysis.

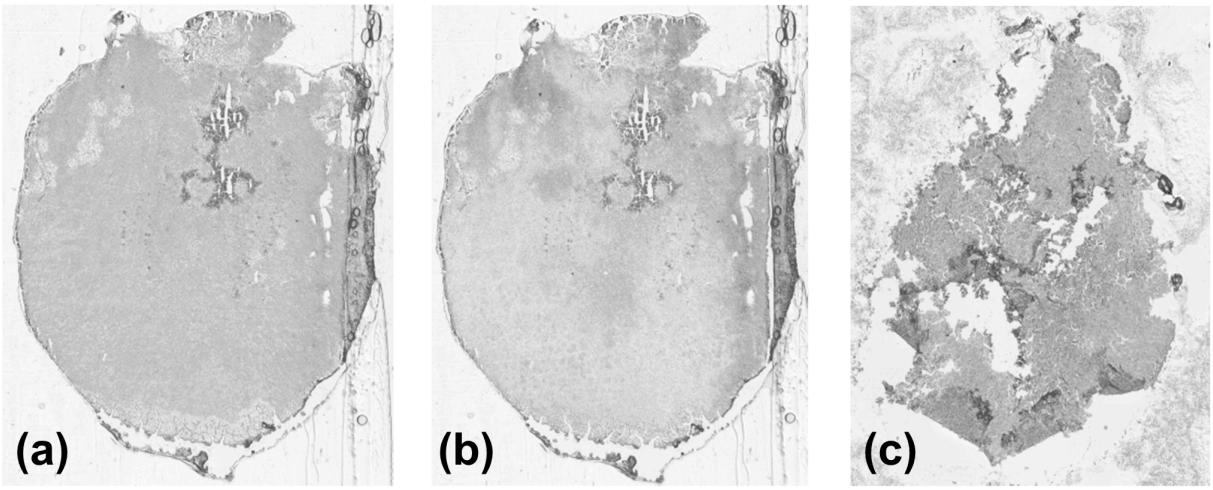

Figure 4: *Optical images of (a) unwashed t breast tumor xenograft MDA-MB-231 clone, (b) after surface cleaning with a wetted paper (100% methanol for 30 seconds, twice) and (c) after conventional pipette washing procedure with 100µL 100% methanol for 30 seconds.*

In order to compare washing methods, serial mouse brain sections were freshly prepared and submitted to three washing protocols with isopropanol (70% and 95% in

H_2O), coated with sinapinic acid MALDI matrix and imaged. Figure 5 shows the average, baseline subtracted, mass spectra from the MS imaging runs. As expected, a wash improves the spectral quality over no washing. Without a washing procedure (Fig. 5a), proteins are still detected from the tissue, but with less peaks observed. The fiber free wetted paper wash (Fig. 5b), immersion wash (Fig. 5c) and pipette wash (Fig. 5d) show an increase in the number of peaks observed, as well as increased intensities for ions that are observed with no washing procedure. The image insets in Fig. 5 show an overlay of three selected protein ions. With no wash, the ion at m/z 13,751 is not observed. However, all three washing procedures improve the detection of this ion, as well as retaining the spatial distribution of the intact proteins. Thus, the fiber free wetted paper method is comparable, both spectrally and spatially, to accepted standard washing procedures for proteins. Profile spectra were collected on each sample to assess the effectiveness of each method for the removal of surface active lipids.

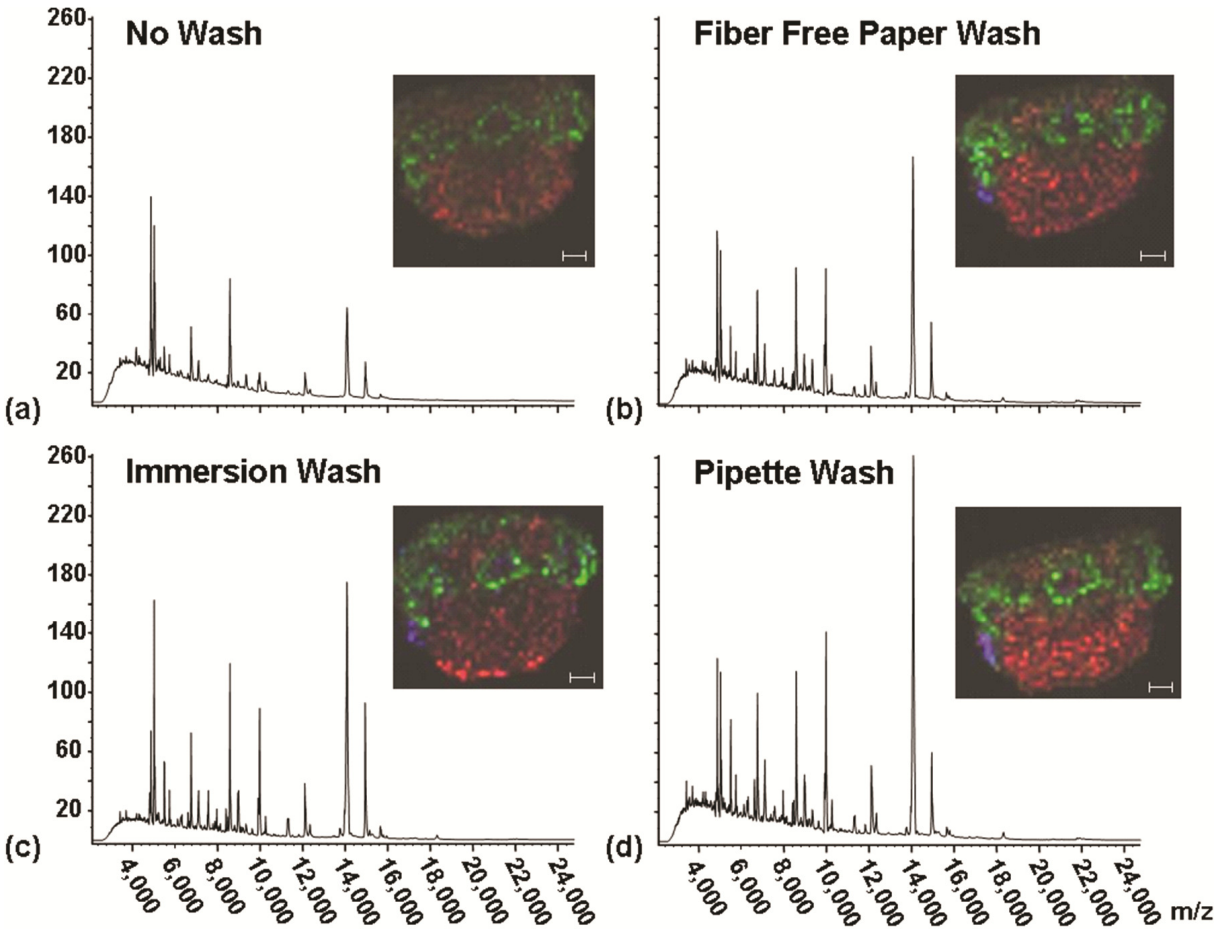

***Figure 5**: Spectral comparison of different washing methods of mouse brain sections using isopropanol (70% and 95% in H_2O, 30 seconds each, or 200 µL each by the pipette method)). The baseline subtracted, average mass spectra (over the entire image) are shown. (a) no washing step (b) wetted fiber free paper wash (c) immersion wash (d) pipette wash. Inset images show three selected protein ions (Blue: m/z 13,751 ±10, Green: m/z 6,755 ±10 and Red: m/z 7,093 ±10) which show that the spatial organization is retained by all washing methods. Scale bar = 1 mm.*

Figure 6 shows that all three washing methods reduce the lipid content on the tissue surface, with the immersion wash essentially eliminating all lipids, and the fiber free paper and pipette wash also reducing their intensity.

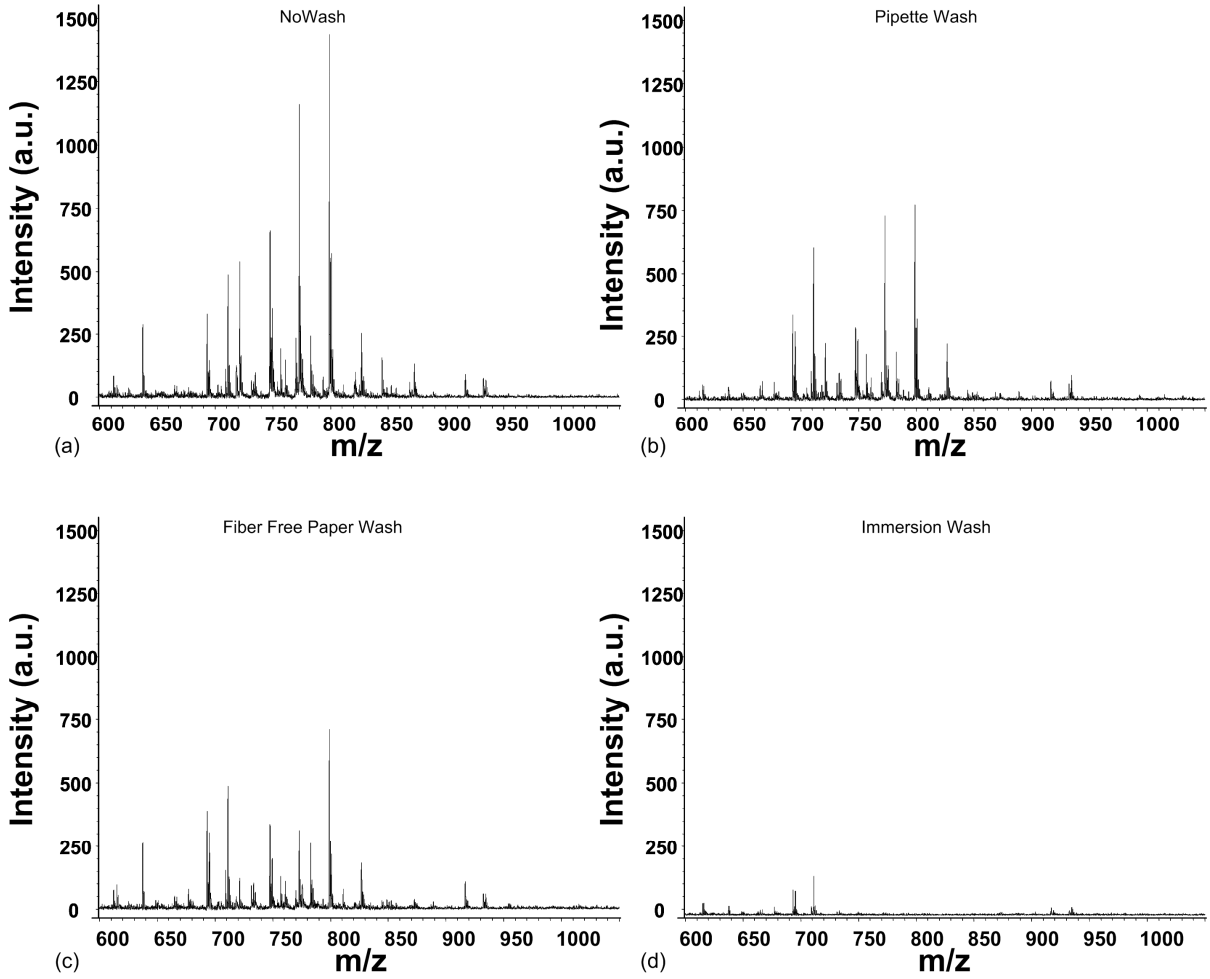

Figure 6: *Spectral comparison of lipids from mouse brain tissue after different washing methods using isopropanol (70% and 95% in H_2O, 30 seconds each, or 200 µL each by the pipette method)). The mass spectra were collected at the same position on each mouse brain (1,000 laser shots each) and are smoothed and baseline corrected. (a) no washing step (b) wetted fiber free paper wash (c) immersion wash (d) pipette wash.*

The spatial distribution of intact proteins has been shown to be affected little by washing procedures prior to MS imaging [130] (Fig. 5). This is attributed to confinement of proteins within the tissue; unlike surface active lipids which are easily removed by washing procedures. In order to assess the diffusion of small molecules subjected to different

washing procedures, three colors of permanent marker were spotted onto a mouse brain and washed by the three methods described above. Figure 7 shows optical images of the tissue sections before and after washing by the wetted paper method (Fig. 7a) and the immersion method (Fig. 7b). The three colors of markers show different solubility in the ethanol wash solvent. This is similar to what is expected on complex tissue sections, where a large number of different moieties of biomolecules are present. While the red marker is nearly washed away by the immersion method, it is only minimally affected during the paper washing procedure.

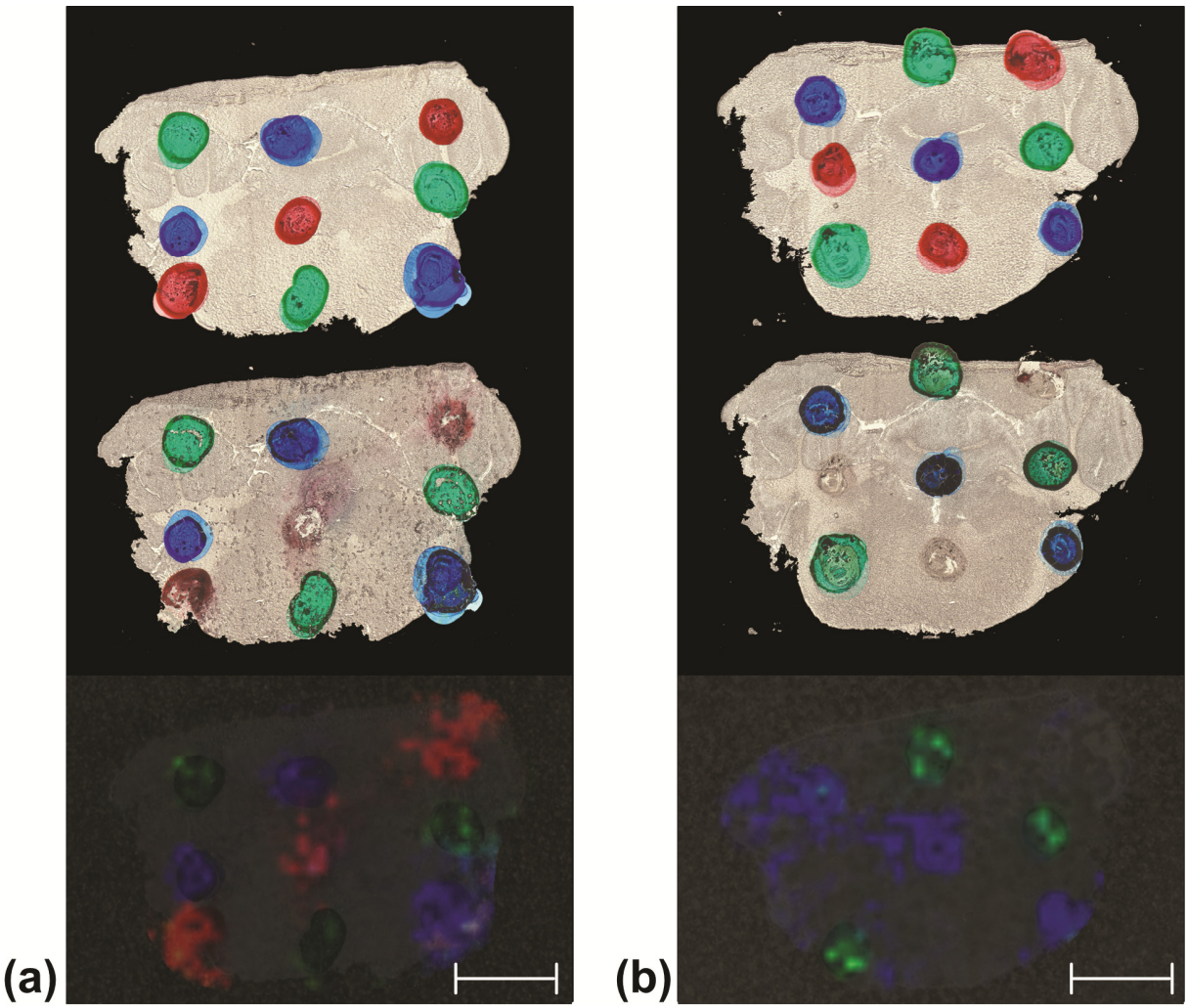

Figure 7: *Optical and mass spectrometric images of three permanent markers (blue, green and red) applied on top of mouse brain sections. The optical images of the sections were*

taken before and after wash by (a) the wetted paper method washing and (b) the immersion wash method. Top: sections before washing. Middle: sections after washing (70% ethanol in H_2O, 60 seconds each). Bottom: The spatial distribution of the masses corresponding to the each marker applied on the tissue sections (Blue: m/z 480 ±0.5, Green: m/z 529.5 and 531.5±0.5 and Red: m/z 444.3 ±0.5) are shown in the bottom row. The red marker is completely washed away by the immersion method, while all three compounds are retained by the wetted paper wash. The blue marker shows more surface diffusion by the immersion method but is localized near the deposition spot after wetted paper wash. The green marker shows little diffusion after cleaning with both methods. Scale bar = 2 mm

Figure 8 shows the photographical documentation of the diffusion process of the markers that occurs during the immersion wash procedure. When analyzed by MALDI imaging MS, it is clear that the red marker has been retained on the sample surface when using the wetted paper method, but was removed completely by the immersion wash method. While not removed completely, the blue marker shows serious diffusion with the immersion method, but little to no diffusion is observed with the wetted paper method. Finally, the spatial localization of the green marker is retained by both methods, an indication that it has lower solubility in the ethanol solvent than the other two colors. While only a test case, the results in Figure 7, combined with those in Figure 5, demonstrate the challenges of choosing a method for tissue washing before MS imaging analysis. The susceptibility of the analytes of interest to surface diffusion during washing will depend not only on their solubility in the wash solvent, but also their surface availability and degree of entrainment within the tissue.

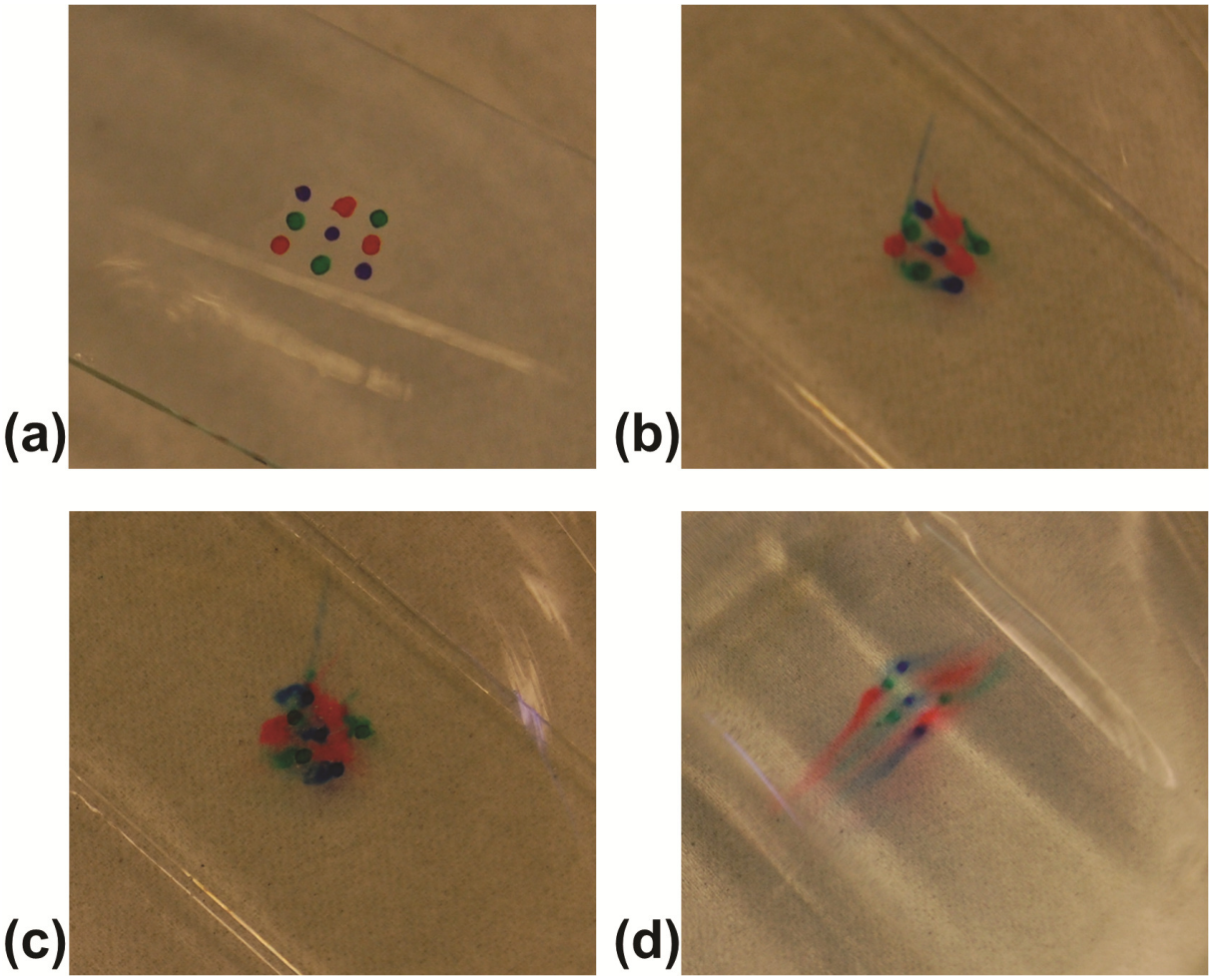

***Figure 8**: Photographical documentation of diffusion of three permanent markers (blue, green and red) applied on top of mouse brain sections during immersion wash procedure. Picture (a) was taken immediately before immersion, (b) after approximately 20s in washing solution (70% ethanol in H_2O), (c) 40s after immersion and (d) during sample removal from washing solution. The total washing time was 60s, with no sample disturbance during immersion.*

3.4 Conclusions

The method described above is a simple, effective method for the washing of biological tissue sections for MALDI and SIMS mass spectrometry imaging. The method uses a common laboratory paper wetted with washing solvent that is blotted onto the tissue sample surface. Fragile tissue sections, not amenable to conventional wet washing methods (thus resulting in poor MALDI MS imaging data quality), can be cleaned with this method and show good MALDI MS imaging spectral and image quality. Localized areas of tissue sections can be selectively washed, and SIMS imaging of a selectively washed tissue section shows increase in signal intensity of small organic molecules and a decrease in signal intensity of salt cations in the washed areas. Contaminant agents such as PDMS can be removed from the analyte surface, improving the data quality. The results of the fiber free paper washing procedure are comparable to accepted standard washing procedures for proteins The method exhibits improved suitability for fragile tissue. Diffusion of small molecules on the tissue surface is substantially lower than the degree of diffusion observed for an immersion wash. The surface cleaning procedure described in this paper is a reproducible, reliable and efficient method that can be applied in any type of sample preparation for SIMS and MALDI-MS imaging.

Chapter 4

4. Feasibility study of drug quantitation in tissue homogenates by MS imaging techniques [*]

Quantitation by mass spectrometry (MS) imaging is in the early stages of development. A number of factors, such as ion suppression, inhomogeneous matrix crystallization and sample preparation can be expected to affect the results of quantitation of drugs in tissue sections by MS imaging. In this chapter we performed a experiment have replaced tissue sections with organ homogenates in order to evaluate tissue-specific effects on the quantitation of risperidone, a psychotropic agent, by MALDI MS and SIMS imaging techniques. This approach allows for the evaluation of drug detection by contact (drug standards on top of homogenates) and full interaction between drugs and cell contents (mixed in-vitro). The different organs evaluated were brain (the primary target organ of the drug), lung, liver, kidney and testis. The results show the mass spectral response for risperidone is strongly organ dependent and is affected by the sample preparation. This suggests that calibration curves created by application of drugs on top of tissue and used for quantitation should be treated with caution in the determination of the actual amount of drug in the tissue section.

[*] Based on: Erika R. Amstalden van Hove, Donald F. Smith, Gert Eijkel, Lieve Dillen, Hilde De Man, Katelijne Anciaux, Filip Cuyckens and Ron M.A. Heeren, *to be submitted.*

4.1 Introduction

The localization and quantitation of pharmaceutical compounds and their metabolites in organs of dosed animals are an essential part of drug discovery research. Currently, whole-body (WB) autoradioluminography is used to visualize the spatial distributions of compounds of interest. This method requires the use of radioactively labeled compounds, which can leave the intact drug and metabolites undistinguishable, as only the label is detectable. Unlabeled drug fragments and metabolites will not be detected. Mass Spectrometry (MS) imaging provides information on molecular composition and spatial localization of compounds without the need of a label [63, 131, 132]. As such, MS imaging is very suitable for qualitative localization of drug compounds and their metabolites. MS imaging however deals with complex biological samples where several molecules compete for the primary ionization source, and drug ionization (and thus detection) may be enhanced or suppressed by the local chemical composition.

Liquid chromatography mass spectrometry (LC-MS) coupled with MS instruments [133] allows for absolute quantitation of analytes, but requires sample homogenization, cleanup and chromatographic separation prior to MS analysis. This allows for confident quantitation without the concern for ionization artifacts from competing molecules. The drawback of this technique is the need for separation and purification steps prior to the MS analyses and loss of spatial information due to homogenization of organs. Therefore a quantitative analysis of drug compounds and their metabolites by MS imaging is highly desirable, where drug/metabolites in different organs can be quantified simultaneously.

Relative quantitation of compounds by Matrix Assisted Laser Desorption Ionization Mass Spectrometry (MALDI-MS) imaging was first reported by Stoeckli et al. [66], who determined the difference in ion suppression for different organs by homogeneous application of a compound of interest on top of a whole-body section prior to the MS imaging experiment for calculation of tissue-specific ionization efficiency factors. Whole-body tissue sections of animals dosed with the same compound were measured, and the

results used for relative drug quantification across the entire whole-body section. This approach is now intensively used in pharmaceutical analysis, complementary to the conventional methods. Alternatively, an analyte with similar chemical structure to the drug of interest, such as a deuterated compound or a radioactively labeled compound, can be deposited on the sample surface to determine the ion suppression for different organs [62, 63, 134]. In addition, quantitation of cocaine in brain [135], tiotropium in lung [136] and olanzapine in liver [137] has been achieved with MS imaging, with the results of tiotropium and olanzapine showing good comparison with LC-MS/MS standard curves from tissue extracts.

It is expected that the complex chemical environment encountered during MS imaging of biological tissue will lead to ion suppression effects [47-51]. When analytes are added on top of a tissue section, factors such as capillary diffusion of the analyte, cell lyses, interaction with tissue contents, and organ chemical environment can affect the ionization yield of the compounds and must be taken into account. Specific sample preparation methods for MS imaging, such as washing procedures [19, 29-31, 34, 52, 78, 135, 138], the use of an ionic matrix [38, 43, 46] and metal coating[37, 139] can be used to enhance detection of certain groups of molecules, but may cause suppression of other substances [52, 53]. Additionally, the interaction of matrix molecules or metals used to enhance desorption and ionization efficiency (e.g in MALDI and metal assisted Secondary Ion Mass Spectrometry (MetA-SIMS)) with the compound of interest is likely to be different when the compound is placed on the surface compared to the same analyte being surrounded by tissue content (intra and extracellular matrix componenents).

In this study we designed a series of experiments using organ homogenates to study ionization effects, with a drug standard applied on top of the homogenates (contact interaction) as well as mixed with homogenates (direct interaction with tissue contents) using both MALDI and SIMS. This allowed us to study the impact of matrix effects on ion suppression, as well as different surface treatments when a drug is applied on top of or mixed with a homogenate. Brain, lung, liver, kidney and testis were used in order to evaluate the possibility of simultaneous quantitation for multiple organs, such as in a

whole-body section. Risperidone, a psychotropic agent with brain as the target organ is reported in this paper. Organ homogenates were used to avoid the influence of sub-regions of organs in analyte ionization and to mimic the complex chemical and physical interaction of standards with cell contents. The results show that most drug-organ combinations show very different ionization behavior depending on the sample preparation method. Standard curves for drug calibration depend strongly on the surface availability of the analyte and the organ type. The absolute quantitation of one compound across different organs is still a challenge. This is directly related to the limitations in analyte detection. Three specific factors determine the boundaries of the quantitation of analytes: limit of detection (LOD), limit of linearity (LOL) and limit of quantitation (LOQ). LOD is related to signal to noise ratio, and it is determinate by the lowest concentration that is different from a blank. LOQ determinate by the lowest analyte concentration that can be quantified with a specific degree of confidence. Both LOD and LOQ are different for each matrix, method and analyte. LOL is determinate by the smallest analyte signal that can be distinguished from background noise, as well as the highest peak before peak saturation occurs. LOL is instrument dependent.

4.2 Materials and Methods

4.2.1 Homogenate preparation

Five different organs from frozen male Sprague-Dawley untreated rats (brain, lung, liver, testis and kidney) were supplied by Janssen Pharmaceuticals, Inc. (Beerse, Belgium).

Lung, testis, half brain, half liver and half kidney were ground in 50% ethanol solution (1g organ/10 ml) using a Potter-Elvehjem Tissue Grinder (Wheaton, USA) with a Teflon® pestle and RW 16 basic rotator (Ika-WERKE GmbH, Germany). Each tissue was

submitted to ten strokes, with a pestle rotation maximum of 960 rpm. The homogenates were kept at -20°C until use, with no further treatment.

4.2.2 Drug standard solutions

Risperidone (M.W. 410.2), a psychotropic agent belonging to the chemical class of benzisoxazole derivatives was provided by Janssen Pharmaceuticals. The drug structure can be found in Figure 1. Risperidone was dissolved in 50% ethanol solution to a final concentration of 20 mM and then diluted to 10 mM, 1 mM, 100 μM, 10 μM and 1 μM in 50% ethanol.

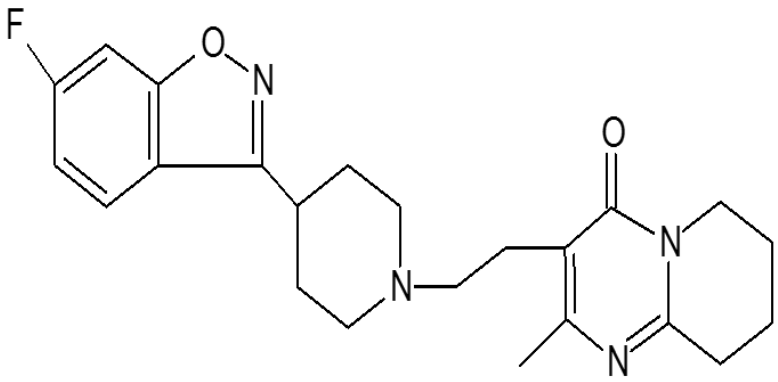

Figure 1: *Structure of risperidone (m/z 410), a psychotropic agent belonging to the chemical class of benzisoxazole derivatives.*

4.2.3 Homogenates and drug standards

4.2.3.1 Drug standards *on top* of organ homogenates

Homogenates of brain, lung, liver, kidney and testis were deposited on stainless steel metal targets. The homogenates were dried in a vacuum desiccator for 30 minutes. The drug standards were applied on top of the dried homogenates (1:1 volume drug/homogenate). For MALDI, the volume per spot (approx. 4 mm diameter well) was 0.5 µL per solution, resulting in a total of 5 nmol, 500 pmol, 50 pmol, 5 pmol and 0.5 pmol of drug standard deposited per spot. For SIMS, the volume per spot (approx. 1.3 mm diameter well) was 0.25 µL per solution, resulting in a final amount of 2.5 nmol, 250 pmol, 25 pmol, 2.5 pmol and 0.25 pmol of drug standard per spot.

4.2.3.2 Drug standards *mixed with* organ homogenates

Organ homogenates and drug standards were mixed 1:1 (v/v) in Eppendorff tubes into a final volume of 6 µL, and then deposited on a metal target. For SIMS, the mixture volume deposited per spot was 0.5 µL, for a final amount of 2.5 nmol, 250 pmol, 25 pmol, 2.5 pmol and 0.25 pmol of drug standard per spot. For MALDI, the volume per spot was 1 µL, for a final amount of 2.5 nmol, 250 pmol, 25 pmol, 2.5 pmol and 0.25 pmol of drug standard per spot.

4.2.4 Metal deposition for MetA-SIMS

Previous studies have shown that a thin metal layer is beneficial for SIMS measurements of whole-body sections [140]. The impact of metal on the detection of standards was investigated by sputter coating half of the samples with gold. The samples were prepared as previously described (4.2.3.1 and 4.2.3.2) and a 1 nm layer of gold was sputter coated on top with a Quorum Technologies (Newhaven, East Sussex, U.K.) SC7640 sputter coater equipped with a FT7607 quartz crystal microbalance stage and a FT7690 film thickness monitor.

4.2.5 MALDI matrix preparation

The matrix solution (1 µL; 10 mg/mL α-Cyano-4-hydroxycinnamic acid in 50% ethanol /water (0.1% trifluoroacetic acid)) was applied on top of previously dried homogenates and drug standards for MALDI analysis. The matrix solution was applied on top of the samples to mimic the conditions for MS imaging, were the matrix solution is typically applied homogenously over the sample surface prior to analysis.

4.2.6 MS data acquisition

MALDI experiments were performed on an Ultraflex III time-of-flight mass spectrometer (Bruker Daltonik GmbH, Bremen, Germany). The acquisition was controlled by FlexControl 2.0 (Bruker Daltonics). The whole sample was imaged with 200 µm raster size. The sample holder was moved to six random positions within a single raster during the spectrum acquisition, acquiring 50 shots per position, in a total of 300 shots per raster. The diameter of the laser spot used was 50 µm.

SIMS experiments were performed on a Physical Electronics (Eden Prairie, MN, USA) TRIFT II time-of-flight secondary ion mass spectrometer with a Au^{1+} primary ion beam current of 450 pA, a primary pulse length of 30 ns, a spot diameter of 500 nm, and a primary ion energy of 22 keV. The data was acquired in mosaic mode, where multiple tiles are collected for large area analysis. Each individual tile has a fixed number of pixels (256x256) that, combined with the selected field-of-view (FOV), defines the ultimate spatial resolution. The FOV is calculated by the maximum tile size and the total measurement area; the FOV used here was 164x164 µm per tile (resulting in a pixel size of 640 nm). The acquisition time was 1 second per tile. The total analyzed area was 1.3 mm^2 for each sample. The data acquisition and analysis was performed by WinCadence 4.4.0.17 software (ULVAC-PHI Inc.), which was also used for data visualization.

4.2.7 Data analysis

Data analysis was performed using our in-house software DEBLIC [86] for integration and baseline correction. Peak picking was performed using our in-house software PEAPI [86]. DEBLIC and PEAPI were developed using Matlab 7.9.0 (R2009b; MathWorks, Natick, MA, USA). For MALDI, raw data were imported and baseline subtracted (DEBLIC). Selected ion counts of interest were calculated by integrating the area under the curve at m/z of the compound of interest (with a width of ± 0.5 m/z) using PEAPI. Peak area distributions per imaged pixel were calculated. Subsequently, data corresponding to the lowest 10% of the intensity distribution was removed as they contained mainly noise. The remaining data were averaged and divided by the number of pixels (>10% of the maximum) to yield the average intensity per pixel. The SIMS raw data were imported and spatially binned (16x16 pixels). Selected ion counts of interest were calculated by extracting the intensity at the m/z of the compound of interest with a selection window of ± 0.5 m/z. The data were then integrated and averaged, with the resulting value presented in counts per pixel and the error bars for both MALDI and SIMS data corresponding to the standard deviation for each averaged spot.

4.3 Results and Discussion

The term "ion suppression", also known as "matrix effect" in SIMS, is normally used to indicate poorly understood effects during ionization that result in low signal intensity, or no signal at all, of a molecule that is known to be present in a sample (such as standards spiked on a surface)[47, 48, 50, 52]. Ion suppression is a common problem in MS, occurring in both MALDI and SIMS experiments [47-51]. The experimental design used here to study both organ-specific effects (ion suppression), as well as the effects of drug standard location, is schematically described in the workflow shown in Figure 2. Drug standards were applied *on top* of homogenates, as is the conventional method for the

construction of standard curves for drugs detected from tissue. In parallel, the same standards were *mixed with* a homogenate solution prior to deposition on target.

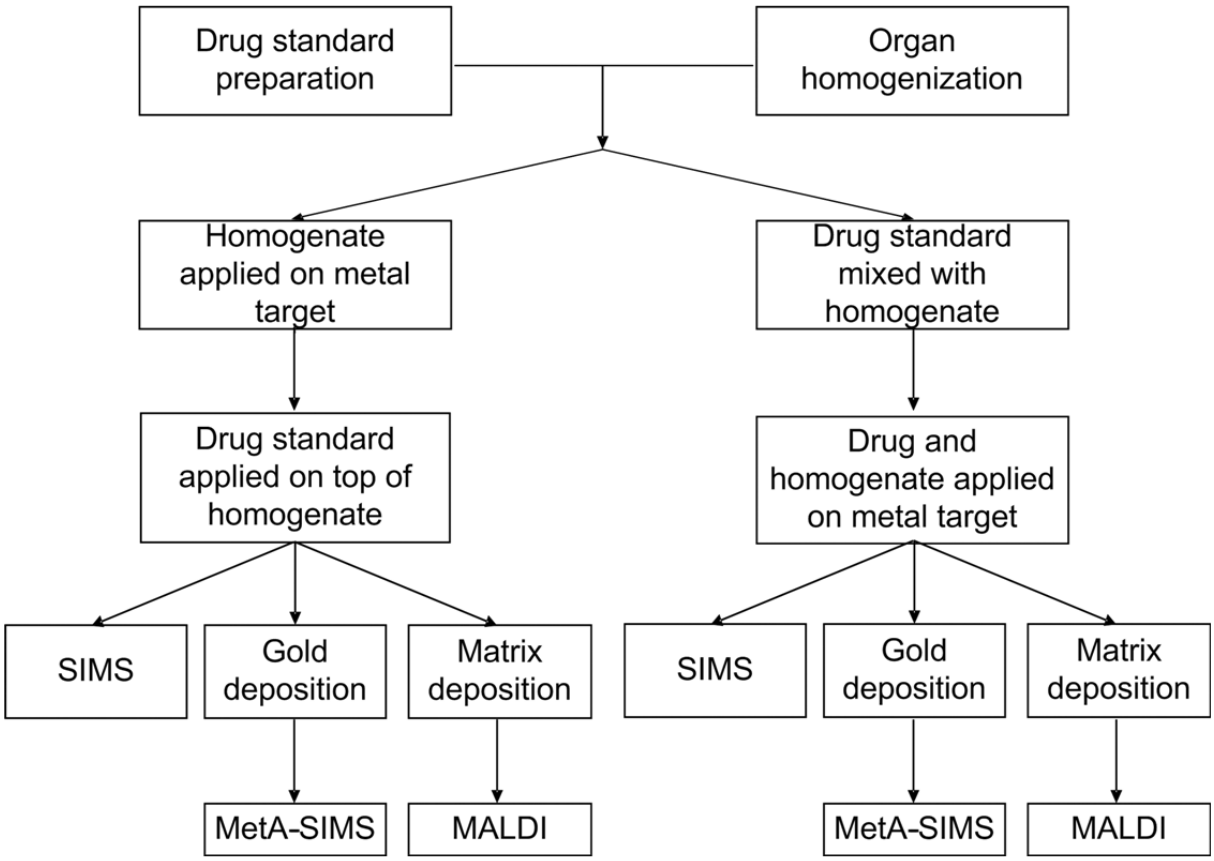

***Figure 2**: Experimental workflow used in this study.*

Conventionally, the construction of standard calibration curves of drugs on top of homogenates is made by the application of the standard with different concentrations on top a tissue section. The tissue section is normally fresh. This means that it has been cut and immediately used or cut, kept at -80C and brought to room temperature before use. As a variation of the standard protocol, the tissue section can also be lyophilized. The reasons to use a lyophilized tissue section are the following: tissue section prepared for other applications such as WB radiography can be used; the sections can be shipped without need of dry ice and can be stored at room temperature. In the initial stages this study, we also

investigated the suitability of lyophilized tissue sections in the detection and quantification of drug standards deposited on top of such tissues.

When a whole body section is used for the construction of a drug standard curve, independent of being fresh or lyophilized, several challenges are encountered. Smaller organs may not present enough surface area for application of standards. Another challenge is the organ inhomogeneity, which can yield different ion suppression effects within one organ. Each organ also shows a different interaction with the drug solution, where diffusion and capillary effects can affect how the drug standard is distributed on the surface. Thus, organ homogenates were used instead of organ sections or whole body sections, in order to avoid such problems and provide comparable ion suppression effects across different organs.

Lyophilized whole body sections present additional challenges for application of drug standards. When the tissue cells have contact with the drug solution, lateral and downwards diffusion of the drug can occur. As a result, most of the drug standards are barely/not detectable at the tissue surface anymore. Figure 3 shows the surface of brain region in a lyopholized whole body section after deposition of a drug standard with an inkjet printer. The dry sample surface is destroyed by the deposition of the standard, although the droplets were very small (100 pL) and only 10 droplets were deposited. In this case, five droplets of 100 μL were deposited on the tissue surface per round, totaling 10nL solution. The deposition of small volumes (with droplet diameters of 100 μm per round) indicates that each time the solutions are deposited a cell layer is depleted, and after a few cycles the standard is deposited on the substrate below the tissue (Figure 3). Since a mammalian cell has approximately 10-20 μm diameter, a small amount of cells (max 100 cells) would be destroyed in each round. Due to the height difference between tissue surface and substrate, as well as the small size hole, it is difficult to the primary ions or laser to ablate the drug molecules deposited in this way. Additionally, the general lack of moisture in the tissue seriously hampered ionization by both MALDI and SIMS. This

problem was alleviated when the tissue was treated with paper wetted with 50% ethanol, using the technique described in Chapter 3.

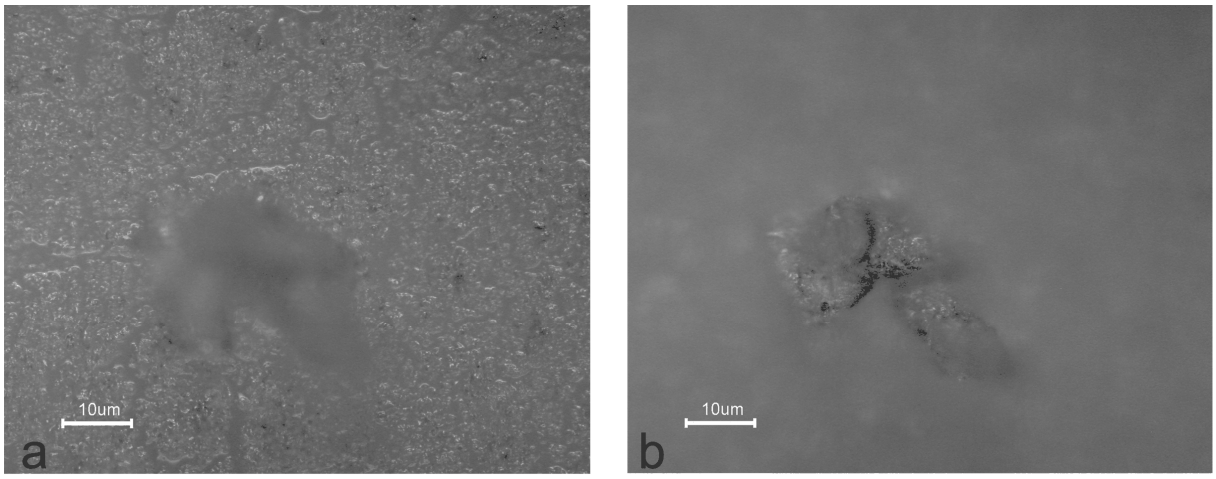

Figure 3*: microscopic image drug standards applied with ChIP on the brain region of a lyophilized whole body section with the focus on (a) the brain tissue surrounding the droplet and (b) the drug droplet itself, with lower focus than used on (a). Scale bar: 10 µm.*

Figure 4 shows the distribution of three principal components before and after surface treatment of a whole body mouse section, and the significant increase in data quality and quantity obtained after the surface treatment. The problems associated with the use of lyophilized whole body sections lead to the decision to use homogenates for the determination of detection and linearity limits if drug standards in different organs.

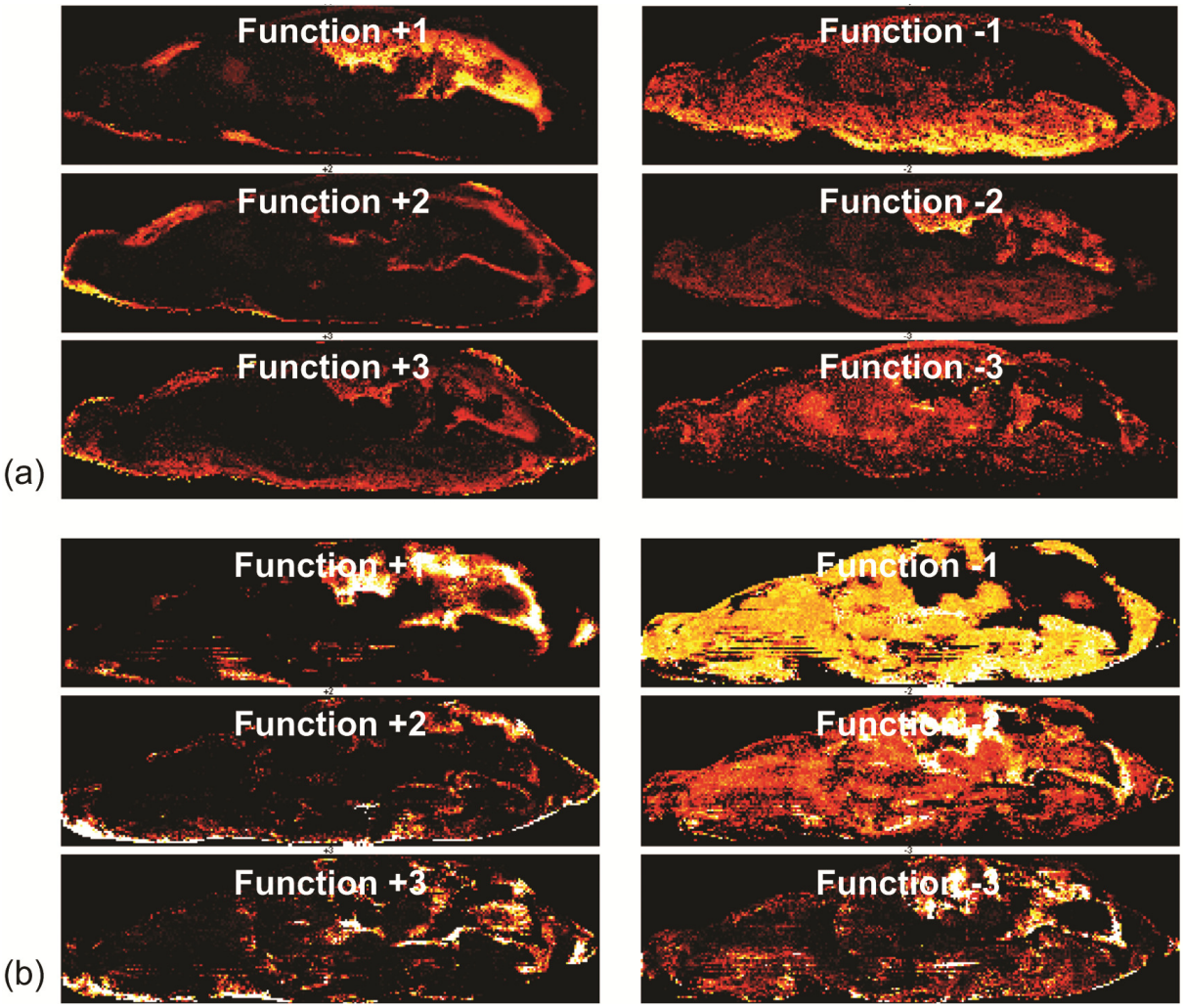

***Figure 4**: Principal component analysis images of the functions +1 and -1, +2 and -2, and +3 and -3 providing inverse images. Panel (a) shows the results obtained for an unwashed mouse whole body section measured by MALDI-MS, whereas panel (b) shows the results obtained for a mouse whole body section measured by MALDI-MS after surface treatment with a wetted paper.*

A very important factor in quantitation by techniques which use surface detection is the sample homogeneity, as discussed above. Areas of high signal, or "hot spots", in MALDI-MS may cause a significant variation of peak intensity/peak area within a dataset. Initially, the data acquisition of drug standards by MALDI was made by sample profiling, where the laser spot would be randomly distributed across the selected sample region. This

technique is fast and the acquisition of multiple datasets from one sample region should provide reliable results. However, insufficient sampling of the entire surface, or conversely over-sampling of hot-spots yielded irreproducible data, even from the same sample. Manual sample profiling showed a completely different result than automated profiling, since in this way it is possible to search for the hot-spots and select the best spectra. After considering the results obtained by sample profiling of spectra obtained by both automated and manual data acquisition, it became clear that both ways could lead to false data interpretation, since it did not represent the analyte distribution across the entire sample surface. The determination of LOL, LOD and LOQ based on a partial surface analysis are also affected by the sample surface coverage. Therefore, the entire sample surface was analyzed in the imaging mode and all results were combined. The effects of sample inhomogeneity and hot spots should be minimized by this approach. Figure 5 shows the spatial distribution of risperidone on top of brain homogenate at six different concentrations. Each homogenate was vortexed immediately before application on the target to minimize sample inhomogeneity. The homogenate was then dried in a desiccator to better reproduce the organ-drug interaction as when the drug is applied on the tissue surface. The difference between this approach and application on top of lyophilized tissue section is that even if downwards diffusion of the drug occurs, part of the drug should still be available at the sample surface, since the homogenate is very thin. Also re-hydration of the tissue can cause the applied standards to be trapped into the cells. The drug standard was also vortexed prior to deposition on top of the homogenate, and the droplet was carefully deposited, to provide homogeneous distribution as good as possible. Results obtained by matrix applied by spray (the most homogeneous coverage possible) and by pipette were similar. The results show that even with a careful approach, the drug distribution on top of a homogenate is still very inhomogeneous, which has a high impact in the data quality.

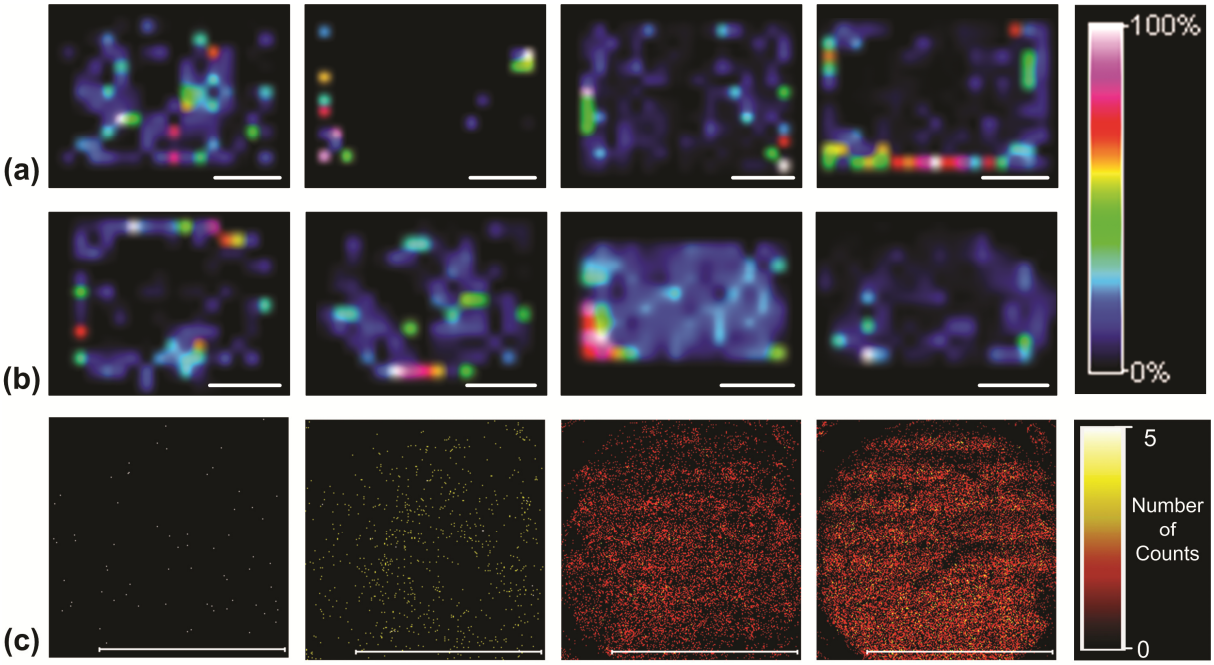

***Figure 5**: Spatial distribution of risperidone m/z 411 ($[M+H]^+$) in contact with brain homogenate measured by MALDI (a and b) and SIMS (c). (a) Risperidone added on top of brain homogenate, (b) risperidone mixed with homogenate and (c) risperidone mixed with homogenate. The same solutions were used for MALDI and SIMS, and the concentrations showed are (from left to right) 10 μM, 100 μM, 1 mM and 10 mM. The total amounts deposited were 5, 50, 500 and 5000 pmol for MALDI and 2.5, 25, 250 and 2500 pmol for SIMS. The ion count scale shown in (c) corresponds to the number of counts measured for 2500 pmol risperidone. Scale bar: 1mm.*

The limits of linearity for a calibration curve measured on a MALDI instrument is very limited, and it has been reported as below a factor of 100 [136]. Such limitation implies that a restricted concentration range that can be used with confidence in the construction of standard curves. Such limitation implies that a restricted concentration range that can be used with confidence in the construction of standard curves. While a drug standard curve can be constructed within the instrument limit of linearity (LOL), a prior knowledge about expected concentration levels of the drug in the organ is necessary. This represents a major problem when comparing drug concentrations in organs at different post-dose times. For

example, the concentration of risperidone in brain can vary with a factor of >100 within 0.25 h and 2 hours after drug administration. Additionally, the concentrations of the drug and metabolites in other organs will also vary considerably with time. While higher drug concentration can be found in the target organ, different organs are likely to have a much lower drug concentration and the amount of drugs found is different organs varies with more than 100 orders of magnitude. Therefore, the limit of linearity (LOL) of MALDI and SIMS mass spectrometers poses another challenge in the absolute quantitation of drugs by MS imaging.

The need of a standard curve with a broader concentration range than the one suitable for MALDI and SIMS instruments was therefore chosen here. The instruments were optimized for 500 pmol for MALDI and 250 pmol for SIMS. A broad concentration range was measured in order to determinate the detection limits of the instruments for risperidone. At the highest amount of material deposited and analyzed, 20 nmol by MALDI and 10 nmol by SIMS, the peaks shape were flattened at the top, indicating that the value was above the instruments dynamic range. The size of the measured area has a direct impact in the determination of LOD, since it is related to the amount of analyte measured per pixel. The spot size used for MALDI measurements was four times bigger than the spot size used for SIMS measurements, while the amount of material deposited was only twice the amount used for SIMS, which causes a change in the amount of analytes per pixel. At low concentrations (0.5 and 5 pmol for MALDI and 0.25 and 2.5 pmol for SIMS), while the risperidone peak was observed, the noise level was very high, and even after a 10% threshold application the intensity obtained corresponds mainly to noise. The standard curves constructed with a broad concentration range by both MALDI and SIMS did show good linearity, but the y-intercepts obtained by extrapolation of the curves were much higher than the values detected in the blank homogenates (data not shown). Intensities of blank homogenates are around 0-1000 counts, whereas the extrapolated values to zero concentration are 5000 – 10,000 counts. This clearly indicates that values below or above the instrument linearity limit do not correspond to real intensity/concentration values, and result in false data interpretation if applied in the

quantitation of drugs in multiple organs. If very low or high concentrations are to be quantified by MALDI and/or SIMS, the instrument settings (such as laser power for MALDI) have to be redefined. The consequence is the inability of MS imaging by MALDI and SIMS to provide absolute quantification in multiple organs in a single experiment. This is directly related to the fact that the amount of drugs found is different organs can vary with more than factor of 100 while the LOQ and LOD can vary per tissue type.

Due to linearity issues discussed above, all comparisons between risperidone on top of and mixed with organ homogenates interactions are based in the values obtained for 1mM and 100µM concentrations (50 and 500 pmol risperidone for MALDI and 25 and 250 pmol for SIMS).

Figure 6 shows the comparison between pure risperidone standard, risperidone applied *on top of* homogenates and *mixed with* homogenates measured by MALDI-MS. Ion suppression is observed when the drug interacts with homogenates, with up to 38 times lower signal in comparison to the pure drug signal (for 500 pmol risperidone *on top of* and *mixed with* testis homogenate). Risperidone standards applied *on top of* kidney and liver homogenates exhibit similar ionization response than when *mixed with* those homogenates within the margin of error. The decrease of ion suppression of risperidone *on top of* kidney and liver homogenates can be explained by the increased surface presence of the drug when applied *on top of* the homogenates and limited interaction between drug and cell contents owing to higher surface availability for MALDI.

A good MALDI signal depends on efficient incorporation of analytes in the matrix and on the amount of matrix surrounding an analyte molecule. When the drug is applied *on top* of homogenates, it is likely to be more efficiently extracted by the matrix solution. This results in an improved incorporation in matrix crystals with less interference from cellular contents. However, the extraction of cell contents by the matrix solution would be expected to influence the drug/matrix interaction when a drug is *mixed with* homogenates. An example is the ionization response increase when risperidone is *mixed with* lung, liver

and brain homogenates. It is expected that the high level of surfactants [141] would aid transport of the hydrophobic drugs into the more polar matrix solution, resulting in the observed enhancement.

When the drug is applied *on top of* the organ, the interaction between drug and the cellular contents of its primary target organ can be significantly different from what was expected, as the drug was designed for optimal effect in this organ. The significant increase in ionization of risperidone (at 500 pmol) when *mixed with* brain cellular content (8x higher than 500 pmol risperidone *on top* of brain) indicates that the risperidone level in brain (the primary target organ) would be highly over-estimated under these conditions. In other words, the intensity of risperidone detected in a dosed brain would be higher than the intensity measured for the same amount applied *on top of* a brain tissue section, resulting in a estimated higher concentration of the drug in the dosed tissue. In addition, there is a large variability of ion intensities for the same amount of drug, dependent on the tissue homogenate type.

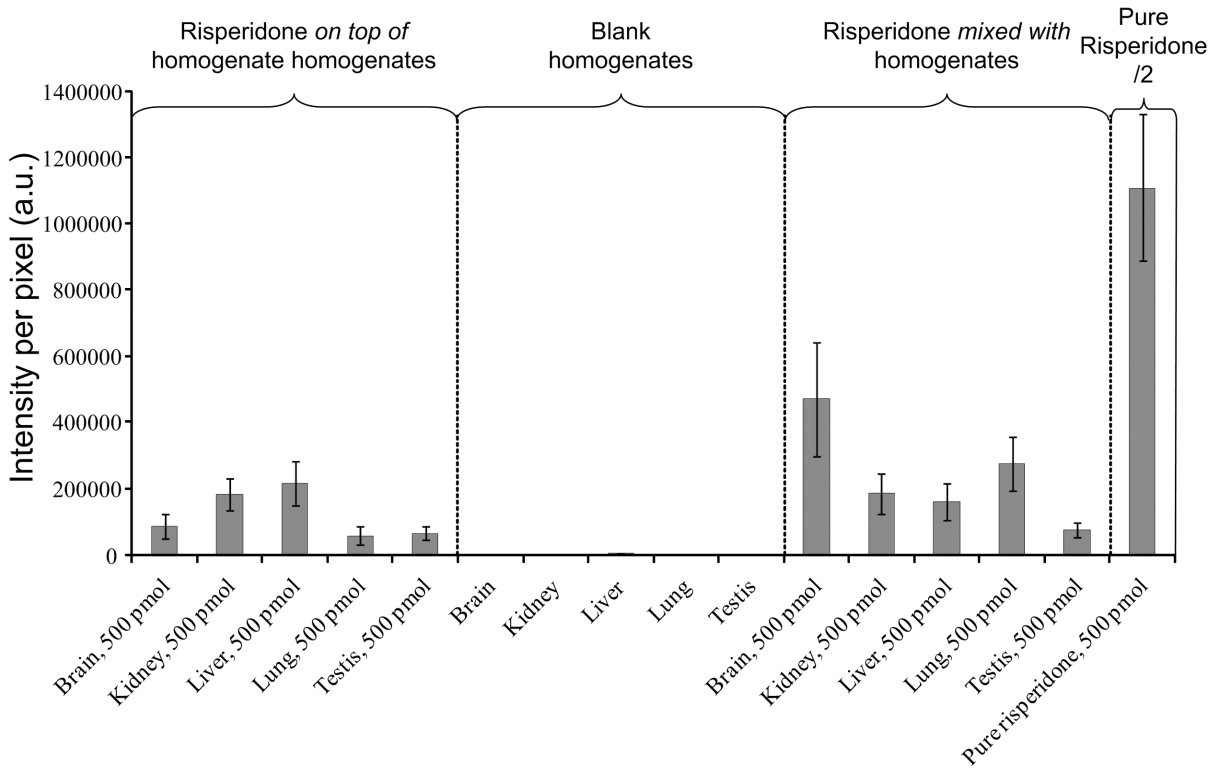

***Figure 6**: Intensity per pixel of risperidone molecular ion $[M+H]^+$ (m/z 411) for 500 pmol, as measured by MALDI-MS. The ion counts of pure risperidone were divided by two.*

Standard calibration curve construction

A drug standard calibration curve must be constructed in order to provide accurate quantification of drugs in specific organs. Here, standard calibration curves that were constructed without the application of an intensity threshold resulted in poor standard curves (data not shown) for both MALDI and SIMS data. This is likely due to erroneous selection of background noise for the selected ion. Figure 7 shows a histogram of the molecular ion peak for risperidone *mixed with* kidney homogenate from a MALDI MS imaging experiment for each pixel over the entire sample spot. The high frequency at low intensity suggests inclusion of noise in the selected ion intensity. An intensity threshold at 10% of the maximum intensity was applied for noise removal. This noise threshold is

indicated with a red dashed line in Figure 7. For each concentration, all intensities above this 10% threshold were averaged and this average value was used in the standard curve. Alternative data treatment, such as 10% threshold of the average intensity and minimum and maximum thresholds provided similar results, but were more time consuming. Therefore the 10% of the maximum intensity threshold was chosen upon the others.

Previous quantitation studies have applied pixel normalization (against the total ion current) and comparison with MS/MS data [136], which should reduce errors at low ion intensity and improve calibration curves. In addition, the MS^n based method reported by Reich *et al.* [135] would reduce errors at low ion intensity by the prerequisite of sufficient parent ion intensity for good MS/MS spectra.

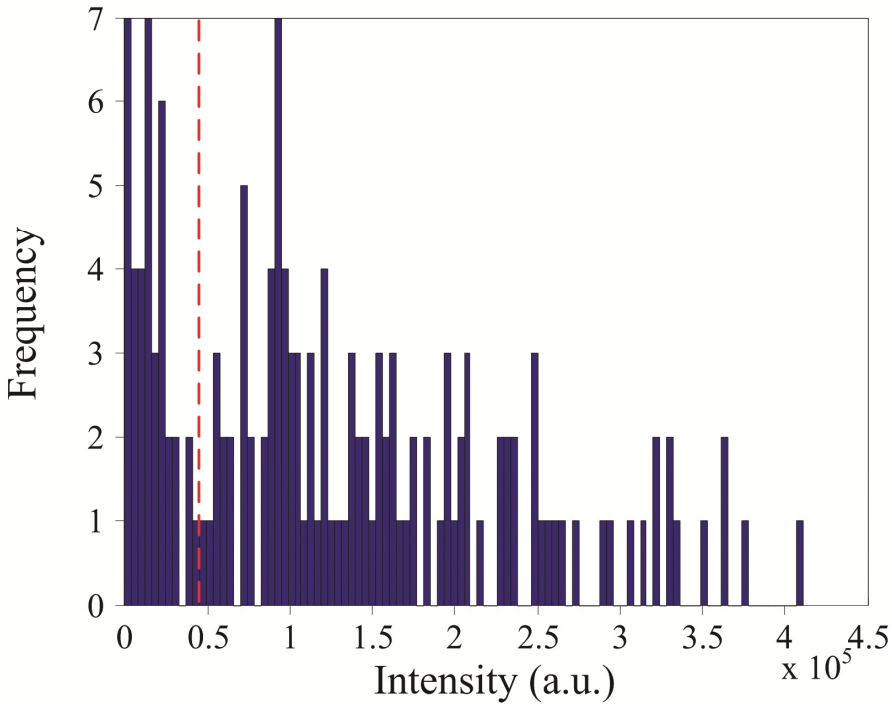

***Figure 7**: Selected ion intensity distribution of the molecular ion of risperidone (m/z 410) in MALDI imaging measurements of the drug mixed with kidney homogenate. The spectra in which the m/z 410 intensity was lower than the red dotted line (10% of the maximum intensity) were removed.*

Figure 8 shows the results of a series of dilutions for risperidone applied *on top of* and *mixed with* organ homogenates. A linear regression model was used for curve fitting with the slope representing the sensitivity of the method. It is important to notice that when a linear regression plot is used, the curve is likely to be strongly influenced by the highest point, as it is the case in the examples shown. The lowest amount investigated are chosen to be well below the instrument LOL to study this limitation. The model obtained for risperidone *on top of* brain homogenate is y= 163.42x + 4529.1 (R^2=0.987) and for risperidone *mixed with* the homogenate is y= 942.16-11754 (R^2=0.994). The steeper slope in the latter case demonstrates an increase of the risperidone signal when in contact with cell contents. The same behavior is observed when risperidone is *mixed with* lung homogenate, due to high level of surfactants, as explained above. However, when risperidone is *mixed with* liver homogenates the $[M+H]^+$ signal decreased in comparison with the $[M+H]^+$ signal when applied *on top of* liver. In terms of MS imaging experiments with a calibration curve being first constructed with standards applied *on top* of the tissue section, the level of risperidone would be over-reported for brain and lung, but under-reported for liver, due to tissue dependent ion suppression. Under these experimental conditions, the amount of risperidone in the kidney and testis would be represented reasonably well.

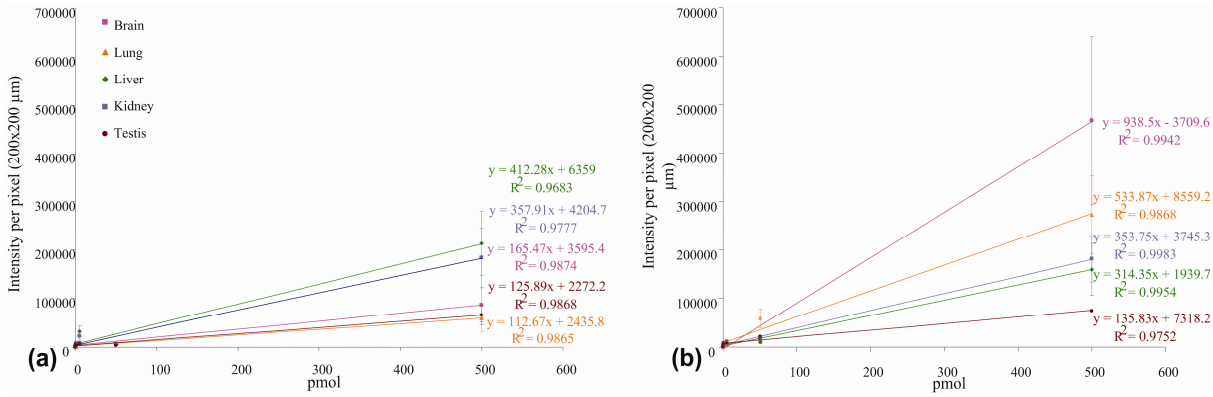

***Figure 8**: Standard curves from (a) risperidone on top of organ homogenates and (b) risperidone mixed with organ homogenates by MALDI-MS. The linear fit for each curve is shown with colored lines.*

SIMS and MetA-SIMS

SIMS imaging offers higher spatial resolution mapping of drugs and metabolites in tissue sections than does MALDI MS imaging. The measurement of whole-body sections by SIMS requires a metal layer in order to prevent surface charging. Surface charging occurs due to the insulating character of the tissue samples when mounted on two layers of non-conducting double-sided tape. In addition to the minimization of surface charging effects [37], qualitative experiments have also demonstrated ionization improvement and molecular ion yield enhancement after gold deposition on tissue section surfaces [142, 143]. Here, we have investigated the effect of a metal layer on SIMS quantification of pharmaceutical compounds *mixed with* and *on top of* tissue homogenates.

Figure 9 shows that drug standards were observed with higher intensity when the drug preparations (both *on top of* and *mixed with* homogenates) were covered with a thin gold layer (e.g. improvement of 250 pmol risperidone *on top of* brain: >40X; kidney: >20X; liver: 10X, lung: 10X; testis: 20X). The gold layer results in a more efficient energy deposition from the primary ion to the surface layer for reduced subsurface damage and an increased emission of larger molecular weight species, similar to the use of a C60 cluster gun as a primary ion source [75, 144-146]. In addition, Figure 9 shows that the use of a gold layer improves detection of the molecular ion. Without a gold layer, fragmentation is very high, and the primary fragment peak (m/z 191) is detected with higher ion counts than the intact molecular ion (m/z 411), as shown in Figure 9a. The peak ratios between the primary fragment ion and the molecular ion of risperidone are listed in Figure 9. In all cases where gold and tissue homogenate were employed together the molecular ion was the base peak in the SIMS spectrum. A comparison with pure risperidone shows that in this case the presence of tissue reduces the amount of fragmentation. MALDI experiments exhibited virtually no fragmentation under any of the conditions studied. All further SIMS experiments in this paper were conducted with a gold layer on top of the sample surface to reduce molecular ion fragmentation.

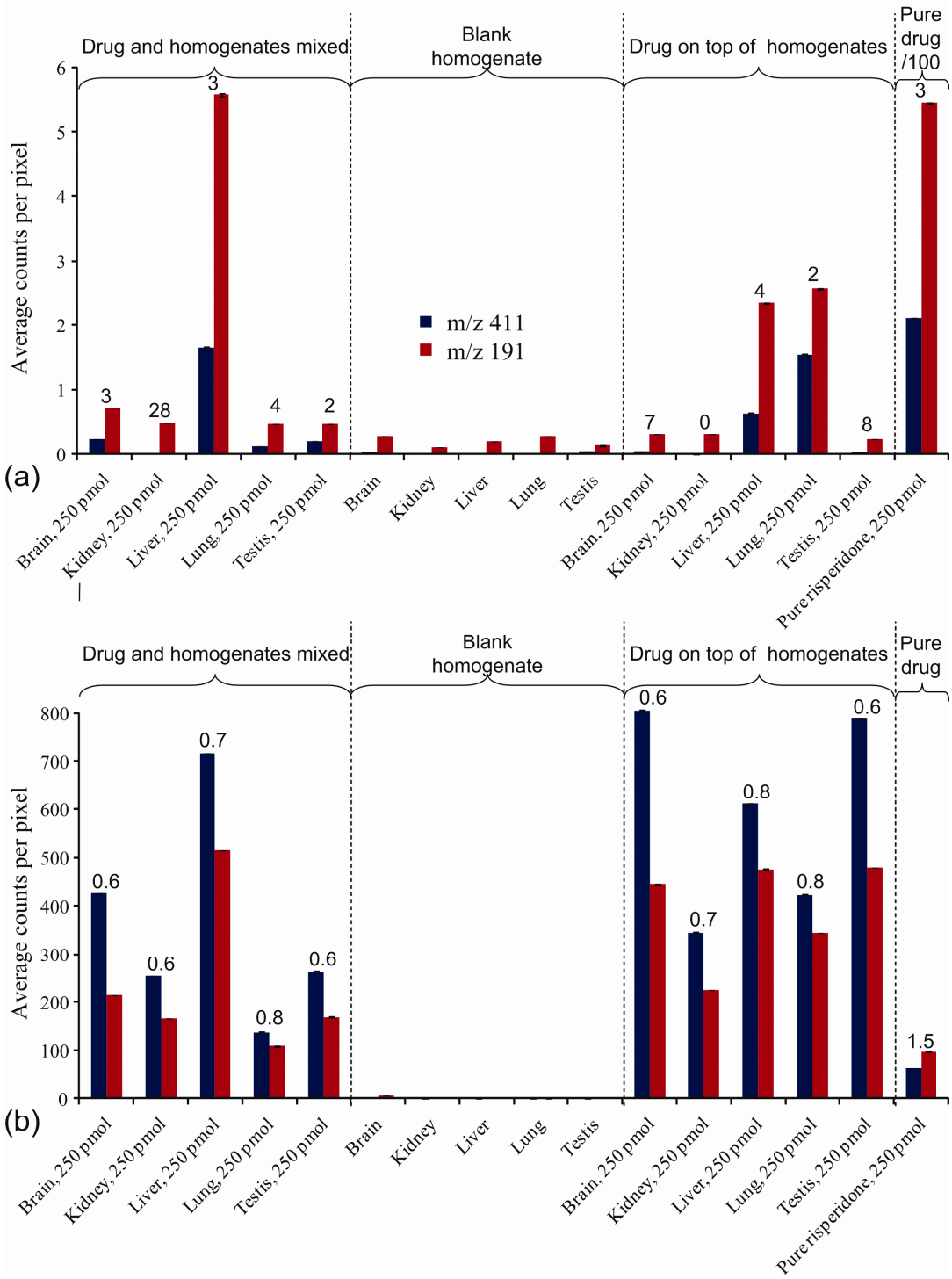

***Figure 9**: Selected ion count of risperidone $[M+H]^+$ (blue, m/z 411) and a fragment ion (red, m/z 191) measured by SIMS, (a) without gold layer and (b) with 1 nm gold layer. Five organ homogenates were used, where the drug standards were applied on top of the*

homogenates or mixed with the homogenates. The ion counts of both risperidone on top of and mixed with homogenates were multiplied by 10 to aid in visualization of the data. Numbers above the histograms reflect the peak area ratio of the risperidone primary fragment ion at m/z 191 over the molecular ion at m/z 411 following SIMS experiments on different tissue types.

The quality of SIMS measurements depends on the amount of material available at the surface, as the first surface layers will predominantly interact with the primary ion beam [147]. Therefore, it is expected that the detection of a drug improves when applied *on top of* an organ homogenate, due to the surface availability of the material. This proves to be true when risperidone is added *on top of* liver homogenate (Fig. 9b). However, a signal enhancement is observed by MetA-SIMS when risperidone is *mixed with* brain, kidney, lung and testis homogenates in comparison with risperidone *on top of* these homogenates (Fig. 9b). Figure 9b suggests that the level of risperidone would be over-reported in all organ homogenates for brain, kidney, lung and testis, but under-reported for liver if no tissue-specific correction factors would be applied when using drug standards deposited on top of tissue. When a drug standard is deposited on top of an organ homogenate, the interaction between drug and homogenate is restricted. Specific characteristics of the homogenates (e.g. hydrophobic or hydrophilic properties) affect the way the drug may be absorbed by or diffuse into the homogenates. The pH of the homogenates can also play a role in the interaction with drugs (lung and liver: pH 5.5; testis: pH 6; kidney and brain: pH 6.5).

The positive matrix effect on risperidone *mixed with* homogenates was confirmed by calibrations curves constructed with the data from the broad concentration range, as shown in Figure 10. The curve fitting was done by the same linear regression model applied for MALDI data. The model for risperidone *mixed with* brain homogenate is y= 0.2538x -0.4337 (R^2=0.99) and shows the best linearity. The linearity of standard

calibration curves by SIMS is much lower and therefore less trustworthy than the curves obtained by MALDI, with exception of risperidone *mixed with* brain and testis homogenate. The difference is likely due to the smaller amount of material ablated from the surface by SIMS and thus a lower signal-to-noise ratio.

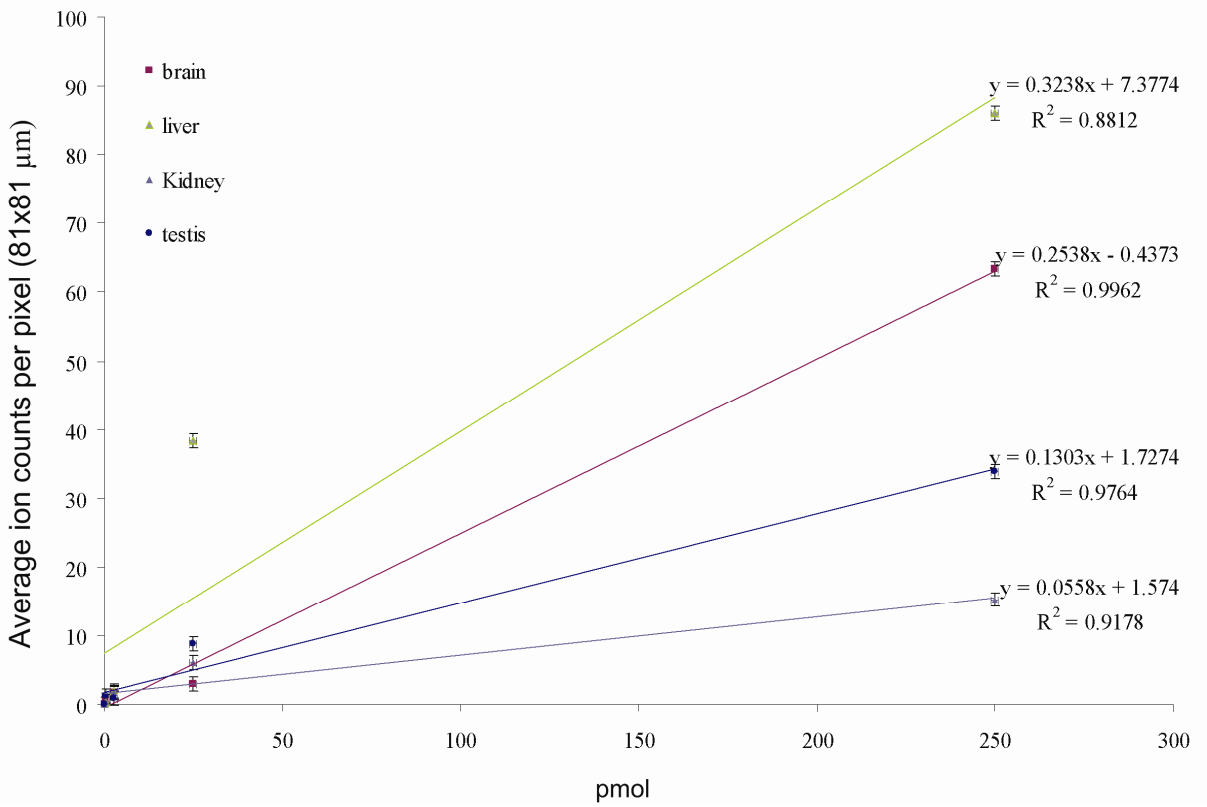

***Figure 10**: Standard curve based on MetA- SIMS data for risperidone $[M+H]^+$ (m/z 411) with drug standards mixed with homogenates.*

A strong increase of ion suppression is observed when risperidone is mixed with liver homogenates for MALDI and MetA-SIMS (Figures 6, 8 and 9). Conversely, lower ion suppression is observed when risperidone is *mixed with* brain and lung homogenates by both MALDI and MetA-SIMS. The signal enhancement of drugs when *mixed with* specific homogenates can be explained by the matrix effect of tissue contents on analyte detection.

4.4 Conclusion

The experiments performed in this study with risperidone demonstrated that the drug standards applied *on top* of an organ homogenate showed different signal response compared to the standards *mixed with* the entire organ tissue contents, and therefore yielded different calibration curves. According to our results, the deposition of standards on top of tissue for calibration purposes could provide inaccurate results for compound quantitation of dosed organ sections. The impact of cell contents to drug availability for ionization is seen in both MALDI and MetA-SIMS.

While successful quantitation by MALDI MS imaging can be performed for individual organs, as recently demonstrated by Ander *et al.* [136], it strongly depends on the organ and the compound chosen. In our study, each organ homogenate has shown a different response to the drug risperidone being *mixed with* or applied *on top of the homogenate*, independent of the ionization method used. Our experiment demonstrates that quantitation by MS imaging with MALDI and SIMS is possible for complex samples such as organs if experimental set-up is carefully designed to deal with such complexity. Additionally, parallel quantification by LC-MS is still needed to support the results obtained by MS imaging. Simultaneous absolute quantitation of a single drug or metabolite in multiple organs continues to represent a challenge due to instrumental limitations such as a narrow linearity limit as well as ion suppression/enhancement effects on the measurability of the analytes. This study confirms the need to carefully determine tissue specific ion suppression factors for quantitative MS imaging experiments.

Spotting compounds on top of tissue has limitations for this purpose. The preparation of a homogeneous layer of the standard drug on top of the homogenates is very difficult, and in some cases impossible to, due to homogenate/drug interactions. In a whole body section, subregions within an organ can also account for different homogenate/drug interactions within one sample region (one concentration spot) and result in inhomogenous standard layers as well. A mixture of tissue homogenate with pharmaceutical compounds is shown to provide better insight in drug-tissue interaction. As a result we propose to use

a combination of the two approaches to determine tissue specific ion suppression factors for analytical quantitative MS imaging studies for each compound of interest.

Chapter 5

5. Multimodal Mass Spectrometric Imaging of Small Molecules Reveals Distinct Spatio-Molecular Signatures in Differentially Metastatic Breast Tumor Models [*]

Phosphocholine (PC) and total choline (tCho) are increased in malignant breast tumors. In this study, magnetic resonance spectroscopic imaging (MRSI), mass spectrometry (MS) imaging, and pathological assessment of corresponding tumor sections have been combined to investigate the localization of choline metabolites and cations in viable *versus* necrotic tumor regions in the nonmetastatic MCF-7, and the highly metastatic MDA-MB-231 breast cancer xenograft models. *In vivo* 3-dimensional MRSI demonstrated that high tCho levels, consisting of free choline (Cho), PC, and glycerophosphocholine (GPC), displayed a heterogeneous spatial distribution in the tumor. MS imaging performed on tumor sections detected the spatial distributions of individual PC, Cho, and GPC, as well as sodium (Na^+) and potassium (K^+), among many others. PC and Cho intensity were increased in viable compared to necrotic regions of MDA-MB-231 tumors, but relatively homogeneously distributed in MCF-7 tumors. Such behavior may be related to the role of PC and PC-related enzymes, such as choline kinase, choline transporters and others in malignant tumor growth. Na^+ and K^+ colocalized in the necrotic tumor areas of MDA-MB-231 tumors, whereas in MCF-7 tumors, Na^+ was detected in necrotic and K^+ in viable tumor regions. This may be attributed to differential Na^+/K^+ pump functions and K^+ channel expressions. Principal component analysis of the MS imaging data clearly identified different tumor microenvironmental regions by their distinct molecular signatures. This molecular information allowed us to differentiate between distinct tumor regions and tumor types, which may, in the future, prove clinically useful in the pathological assessment of breast cancers.

---

[*] Based on: Erika R. Amstalden van Hove, Tiffany R. Blackwell, Ivo Klinkert, Gert Eijkel**,** Ron M. A. Heeren, Kristine Glunde, *Cancer Research*, 2010, **70** (22), 9012-9021

5.1 Introduction

Phosphocholine (PC) and total choline-containing metabolite levels (tCho: glycerophosphocholine (GPC) + PC + free choline (Cho)) are elevated in brain [148], prostate [11, 149], colon [150], and lung tumors [151], in which the most aggressive tumors display the highest PC and tCho levels [152]. Increases in activity and/or expression of several enzymes in choline metabolism, such as choline transporters [153], choline kinase [154], and phospholipases C [155] and D [156, 157] are responsible for the elevated PC and tCho concentrations in cancers, and provide potential therapeutic targets. Choline kinase has already been developed as a target for treatment [14, 151] and a predictive marker for cancer prognosis [151]. Aberrant choline phospholipid metabolism has also been correlated to other diseases, such as neurological disorders including Alzheimer [158, 159], multiple sclerosis [160], inflammation-related pathologies [161], and apoptosis. It is therefore important to develop diagnostic applications to detect choline metabolites that can be translated to the clinic.

Magnetic resonance spectroscopic imaging (MRSI) has been used to detect the extent of invasion of brain, prostatic, and breast tumors [162, 163], and to differentiate between recurrence or necrosis following treatment [148, 164]. Magnetic resonance spectroscopy (MRS) studies have demonstrated an elevation of phosphocholine (PC) and tCho-containing metabolites in breast cancer cells and tumors [10, 13, 14, 157, 165, 166]. However, high spatial resolution *in vivo* MRSI with the chemical specificity to resolve PC, GPC, Cho is currently unavailable. MS imaging of histological tumor sections is able to detect the spatial localization of these choline metabolites and hundreds of other molecules from the tissue surface. In this study, MS imaging techniques have been applied to investigate the spatial distributions of Cho, PC, and other choline-related phospholipids in microenvironmental regions of breast cancer xenograft tumors to further elucidate the involvement of choline metabolism in cancer growth and spread [165].

MS imaging provides molecular identification of lipids, peptides, and proteins by their molecular weight and determines their spatial distribution on the tissue surface at the same time [66, 111, 124, 167]. Sectioned samples from biopsies or other biological materials can be directly analyzed without the need for chemical labeling or extended sample preparation, and hundreds of biomolecules can be detected on a single tissue slide. Secondary ion mass spectrometry (SIMS) and matrix assisted laser desorption ionization (MALDI) are able to detect molecular distributions on histological tissue sections [139] at high spatial resolution, reaching spatial resolutions bellow 50 μm with MALDI-MS imaging and in the sub-micrometer range with SIMS [19, 132], while in-vivo MRSI provides 500 μm spatial resolution [57]. Here, an approach has been developed using complementary desorption and ionization techniques directly applied on tissue obtained from breast cancer xenograft models.

The purpose of this study was to further elucidate the spatial and molecular characteristics of the altered choline phospholipid metabolism typically observed in breast cancers. To this end, MRS studies have been combined with newly developed MS imaging approaches, and corresponding hematoxylin and eosin stains have been analyzed to differentiate invasive and noninvasive breast cancer models based on their molecular signatures, with a special focus on choline metabolites. Increased PC levels have been observed in viable tumor regions of a highly metastatic breast tumor model, and a close to homogeneous PC distribution in a nonmetastatic, estrogen-sensitive breast tumor model. MS imaging also detected Cho, sodium and potassium among other molecules, in distinct tumor regions.

5.2 Material and Methods

5.2.1 Cell lines, tumor model and inoculations

MDA-MB-231, a highly metastatic human mammary epithelial cancer cell line, and MCF-7, a nonmetastatic, estrogen-sensitive (estrogen-dependent) line, were used for inoculation to generate breast tumor xenograft models. MCF-7 and MDA-MB-231 breast cancer cell lines were purchased from the American Type Culture Collection (ATCC, Manassas, VA). Cell culture of these cell lines was performed as previously described [168]. MCF-7 or MDA-MB-231 cells were inoculated in the upper left thoracic mammary fat pad of female severe combined immunodeficient (SCID) mice. For MCF-7 cell inoculations, 0.18 mg 60-day release 17□-Estradiol Pellets (Innovative Research of America, Sarasota, Florida) were subcutaneously implanted near the left shoulder of SCID mice one week prior to inoculation. 2×10^6 tumor cells were inoculated in a volume of 0.05 ml Hanks balanced solution (HBSS, Sigma, and St. Louis, MO; no matrigel was used). Mice weighed between 19 g – 24 g and tumor sizes ranged between 75 mm^3 – 375 mm^3 when experiments were performed. All experimental animal protocols were approved by the Institutional Animal Care and Use Committee of the Johns Hopkins University School of Medicine.

5.2.2 Sample preparation

Tumors frozen in gelatin were sectioned at 10-μm thickness using a cryo-microtome (Microm Int., Walldorf, Germany) and attached to a cold indium tin oxide (ITO)-coated glass slide (Delta technologies, Stillwater, MN, USA) and stored at -80°C. Prior to analysis, each tumor section was put into a dessicated chamber until it reached room temperature to avoid water film formation on the tissue surface. After the sections

reached room temperature, different sample preparation procedures were applied depending on the MS imaging techniques used in this study.

No tissue washing step of tumor sections was required prior to SIMS experiments.

For Metal Assisted (MetA)-SIMS, a thin layer of gold was applied to the tissues surface. The tumor sections were sputter coated with 1 nm gold using a Quorum Technologies (Newhaven, East Sussex, U.K.) SC7640 sputter coater equipped with a FT7607 quartz crystal microbalance stage and a FT7690 film thickness monitor.

For Matrix Enhanced (ME)-SIMS and MALDI-MS, the tissues were covered with 2,5-Dihydroxybenzoic acid (DHB) 30mg/mL in 50% acetonitrile/0.1% aqueous trifluoroacetic acid using air driven thin liquid chromatography sprayer (Sigma). The nitrogen pressure required for efficient nebulization was 0.3-0.4 bar, resulting in matrix crystals of µm size. Alternatively, matrix was deposited on the tissue sections with a vibrational spray coater ImagePrep instrument (Bruker Daltonics, Bremen, Germany). The parameters for each cycle were 1.5 s spray time, 0.3 s incubation time and 0.7 s drying time. The chosen amplitude was of 20% spray power and the membrane offset was optimized with pure ethanol at 10% spray power as recommended by the manufacturer. The membrane was cleaned after every 30 cycles to eliminate clogging effect caused by matrix.

For some MALDI studies and ME-SIMS, a thin layer of gold was applied to the surface after matrix application. The tissues were sputter coated with 1 nm gold as described above for MetA-SIMS.

5.2.3 *In vivo/ex vivo MRS measurements*

Noninvasive ^{1}H MRSI was performed on a 9.4-T Bruker Biospec Small Animal MR Scanner using a surface coil as previously described [149]. Briefly, mice were anesthetized with an i.p. injection of ketamine (25 mg/kg; Phoenix Scientific, Inc.) and acepromazine (2.5 mg/kg; Aveco, Phoenix Scientific) diluted in saline. Body temperature was maintained using a blanket circulated with warm water. Water-suppressed MRSI spectra were acquired of tumors using 3-dimensional (3D) chemical shift imaging (CSI) with VAPOR water suppression. The acquisition parameters were as follows: sweep width 7000 Hz, data size of 512 points, echo time 82 ms, repetition time 1 s, field of view 8 mm × 8 mm × 8 mm, and voxel size of 1 mm × 1 mm × 1 mm, zero filling to 32 × 32 × 32. For spatial referencing of the tumor shape, water-unsuppressed MRSI spectra were acquired with an echo time of 15 ms, and all other parameters were the same as for water-suppressed spectra. Spectra were processed with in-house IDL software, and displayed in AMIRA 5.2.1 (Visage Imaging, Inc., San Diego, CA). High-resolution MRS was acquired of the water-soluble dual-phase extract fractions from the respective breast cancer cell lines as previously described [169]. Briefly, approximately 3×10^{7} cells were harvested by trypsinization and dual-phased extraction was performed with methanol/chloroform/water (1:1:1, v/v/v) as previously described [169]. Samples were vortexed, incubated overnight at 4 °C, and the phases were separated by centrifugation. Divalent cations were removed from the water-methanol phase using chelex (Sigma-Aldrich, City, Country), methanol was removed by rotary evaporation, and the remaining water phase lyophilized and stored at -80 °C. The samples were dissolved in D_2O, containing 3-(trimethylsilyl)propionic-2,2,3,3-d_4 acid (TSP; Sigma-Aldrich) as chemical shift reference. Fully relaxed high-resolution ^{1}H MR spectra were acquired on a Bruker Avance 500 spectrometer operating at 11.7 T using a 5-mm HX inverse probe as previously described [169, 170]. MR spectra were processed as previously described using Bruker XWIN-NMR 3.5 software (Bruker BioSpin) [169, 170].

5.2.4 Ex vivo MS imaging measurements

SIMS

SIMS imaging experiments (SIMS, MetA-SIMS and ME-SIMS) were performed on a Physical Electronics (Eden Prairie, MN) TRIFT II time-of-flight SIMS (ToF-SIMS) equipped with either $^{115}In^+$ or Au^+ liquid metal ion gun. Experiments with the Indium gun were performed with a primary ion beam current of 450 pA, a primary pulse length of 30 ns, a spot diameter of 500 nm, and a primary ion energy of 15 keV. The raster size (or field of view-FOV) chosen for these SIMS experiments varied from a minimum of 62.5 µm up to 200 µm per tile, and were constant throughout the experiment, covering the entire tumor surface. The FOV is calculated by WinCadence 4.4.0.17 software (ULVAC-PHI Inc.) based on the maximum tile size and the total measurement area defined by the user. The data acquisition and analysis was performed by WinCadence 4.4.0.17 software.

MS microscope mode MALDI

MALDI stigmatic MS imaging was performed on a modified TRIFT-II instrument equipped with a Nd:YAG 355 nm laser and a DMCP-PS CCD camera combination as previously described [20]. The sample was completely scanned with a homogeneous laser pulse of 150 x 200 µm and a laser repetition rate of 10 Hz, while the sample stage moved at a constant velocity of 100 µm/s. For MALDI data, single-shot 200 µm Total Ion Count (TIC) MALDI stigmatic images were acquired with DaVis software (LaVision, Göttingen, Germany) and stored as tagged image file format (tiff) files with the corresponding synchronized ADC signals (Acqiris, Geneva, Switzerland). To image an entire section, the sample stage was moved at 100 µm/s at a laser repetition rate of 10 Hz in a line-scan, which was repeated until the entire tumor surface was imaged [128].

MS Microprobe MALDI

MALDI microprobe MS imaging was performed on an Ultraflex-ToF (Bruker, Germany), with an accumulation of 500 shots per position and each position covered by a 150x150 µm area. The acquisition was controlled by FlexControl 2.0 (Bruker Daltonics) and the measurement area selection as well as data visualization was executed with FlexImaging 2.0 software (Bruker Daltonics).

5.2.5 Data processing and principal component analysis (PCA)

The data acquired in microscope mode were processed with our in-house developed imaging software (SIC) which aligned all the acquired data into a Total Ion Image [171].

All MS imaging raw data acquired on different MS instrumentation were converted to the generic MS imaging data format datacube (x, y, m/z) using in-house developed software. Images were generated with publically available software "Datacube Explorer" (www.imzml.org).

Principal component analysis (PCA) was performed using in-house developed ChemomeTricks toolbox for MATLAB version 7.0 (The MathWorks, Natick, MA) [86]. PCA is a widely used multivariate data analysis method, described in numerous articles [119, 120]. In short, PCA reduces the dimensionality of the dataset by the creation of a new set of variables, the principal components. These principal components are linear combinations of the original variables. Closely correlated variables (i.e. mass channels originating from the same chemical compound) are grouped into the same principal component. The principal components are hierarchically sorted by the amount of the total variance they describe. The first principal component (PC1) represents the largest amount of the total variance; noise-related signals are found in the higher-ranked principal components. Discarding these higher-ranked principal components from further data processing greatly reduces the noise in the data [86].

5.3 Results

MS imaging analyses showed a distinct difference in the lipid, and more specifically PC distribution of the highly invasive and metastatic, triple negative (estrogen-, progesterone-, and ErbB2-negative) MDA-MB-231 breast tumor model compared to the nonmetastatic, estrogen- and progesterone-positive and ErbB2-negative MCF-7 breast tumor model. Increased PC and overall choline-containing compound levels in breast tumors have been related to tumor aggressiveness in previous studies [14, 157, 165, 166, 172] and are shown as representative *in vivo* ^{1}H MR spectrum in Figure 1A and 3D ^{1}H MRSI data in red Figure 1B. These spatially resolved data provided *in vivo* information on the tCho distribution, and showed that high tCho levels were typically found only in specific regions within the tumor. The tCho signal consisted of at least three individual compounds: free choline, PC, and GPC, which were resolved by *ex vivo* MRS at 11.7 T in water-soluble extracts from MDA-MB-231 breast cancer cells as shown in Figure 1C.

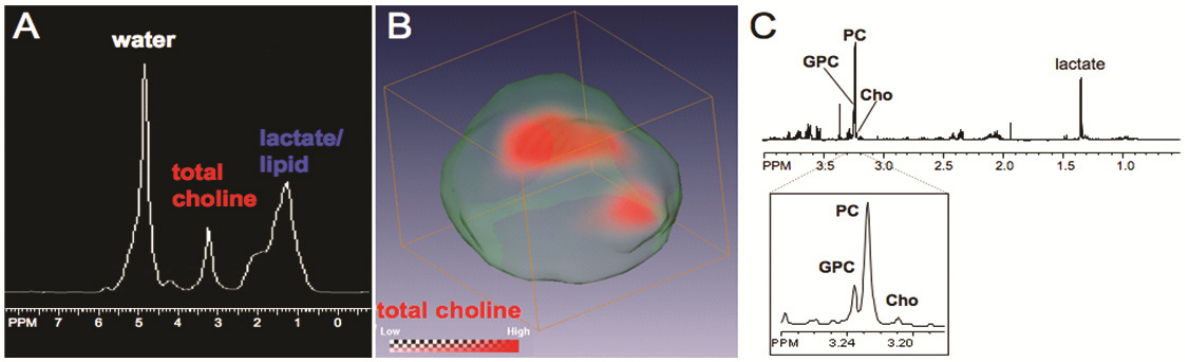

Figure 1: *(A) Representative in vivo ^{1}H MR spectrum demonstrating that the total choline signal cannot be spectrally resolved in vivo. (B) Representative ^{1}H MRSI data set showing the spatial distribution of tCho displayed in red within an MDA-MB-231 tumor as described in the experimental section. (C) High-resolution MR spectrum obtained from a representative water-soluble MDA-MB-231 cell extract resolving GPC, PC, and Cho spectrally.*

Table 1: *List of detected compounds.*

Compound	Formula and common name	Designation	Calculated m/z	MALDI	SIMS	MCF-7 predominant region	MDA-MB-231 predominant region
Sodium	Na	$[M]^+$	22.98		•	Necrotic region	Necrotic region
Potassium	K	$[M]^+$	39.09		•	Viable tumor	Necrotic region
Choline (Cho)	$C_5H_{14}NO$	$[M]^+$	104.17	•	•	Homogeneous	Slightly stronger in necrotic region
Cho.H_2O	$C_5H_{14}NO.H_2O$	$[M+H_2O]^+$	122.18	•	•		Viable tumor
Phosphocholine (PC)	$C_5H_{15}PNO_4$	$[M]^+$	184.07	•	•	Homogeneous	Viable tumor
1,2-Diacylglycerol	$C_{36}H_{66}O_5$ DG(16:1(9Z)/17:1(9Z)/0:0) or DG(16:0/17:2(9Z,12Z)/0:0)	$[M]^+$	578.49	•		Homogeneous	Homogeneous
Phosphatidylcholine (PtdCho) dipalmitoyl	$C_{38}H_{74}NO_{10}P$ PS(16:0/16:0)	$[M]^+$	735.50			Barely detected	Outer part

MS imaging was able to detect Cho, PC, and several other ions and biomolecules in the tumor models, and to localize them to specific tumor regions, as summarized in Table 1. The ratio of elements sodium (Na^+) and potassium (K^+) changed in two tumor regions (e.g. viable tumor and necrotic region) as shown in Table 2 and Figure 2. Several other molecules were also found in both tumor types and are shown in the overall spectra (m/z 0 to 1000) in Figure 2. The spatial distribution of an array of biomolecules was able to discern several tumor microenvironments in the two tumor models, as shown in Figures 3 and 4. The assignments of molecules were made based on the unique masses of single elements (e.g. Na^+ (M.W. 22.989), K^+ (M.W. 39.098), the calculated molecular weight of

more complex substances, and by measurement of standards. The lipid database Lipid Maps (http://www.lipidmaps.org) was also used in the identification process. In each tumor section, the distinction between these different tumor microenvironments was possible solely based on the mass distribution of these molecules (Fig. 3, 4). To correlate substances found by MS imaging within these tumor microenvironments, adjacent tumor sections were hematoxylin and eosin (H&E) stained, and compared to the MS imaging data sets, which enabled the distinction of viable and necrotic tumor regions. Viable tumor regions were characterized by purple hematoxylin-stained nuclei of cancer cells, and necrotic tumor regions by the absence of nuclei. Individual molecules could be visualized at cellular level by high spatial resolution MetA-SIMS (Figure 5). The analyzed sections by MetA-SIMS were H&E stained afterwards.

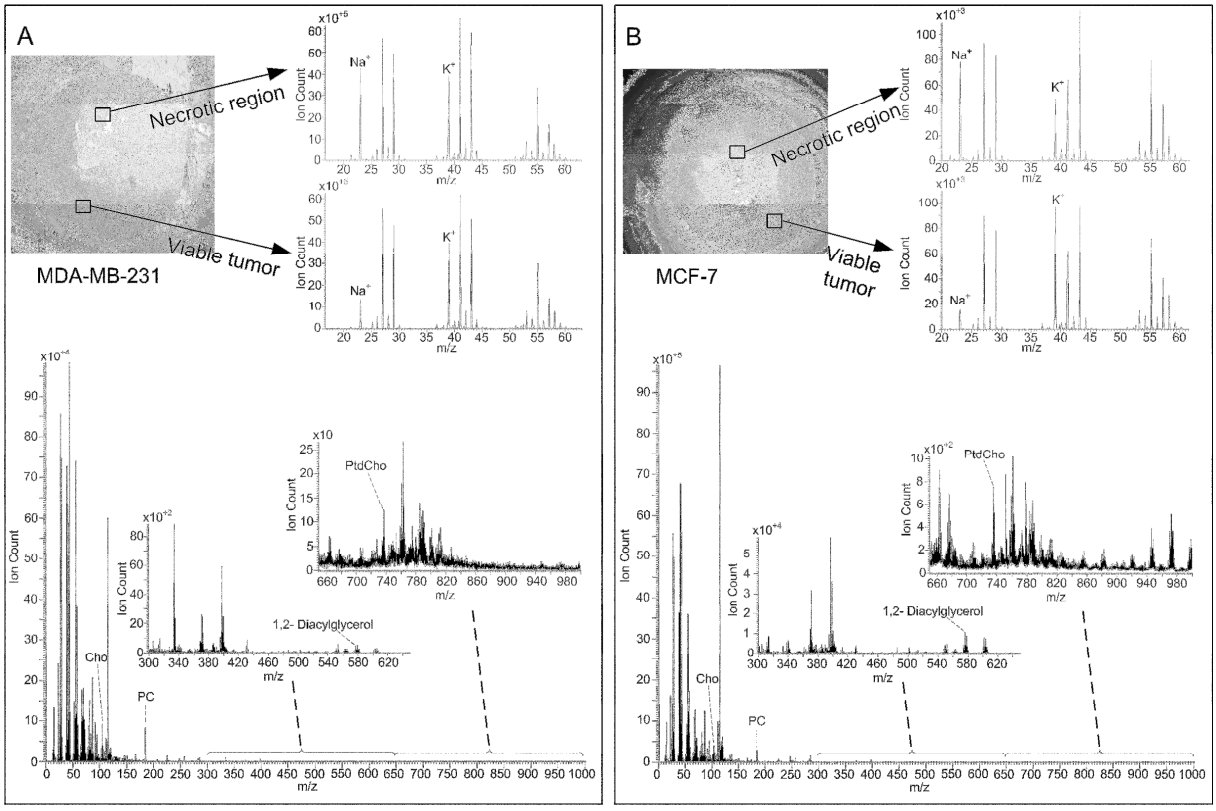

Figure 2: *Optical images of H&E stained of (A) a representative MDA-MB-231 tumor and (B) a representative MCF-7 tumor. The MS spectra are provided for two selected areas, containing two expanded mass regions (m/z 15 to 65) with peak assignment of Na^+ and K^+, and the total area spectrum (m/z 1 to 1000) including two expanded spectral regions (m/z 300 to 640, m/z 640 to 1000) with peak assignments for Cho, PC, cholesterol, 1,2-Diacylglycerol and PtdCho.*

Table 2: *relative intensity scale (3x3 tiles) of Na^+ and K^+ distribution on MDA-MB-231 and MCF-7 tumors.*

Compound	Region selection	MDA-MB-231 Relative intensity	MDA-MB-231 Normalized value	MCF-7 Relative intensity	MCF-7 Normalized value
Na+	necrotic region	$26.6x10^{+5}$	1.3	$100x10^{+4}$	5.88
	viable region	$15.4x10^{+5}$	1	$17x10^{+4}$	1
K+	necrotic region	$57x10^{+5}$	3.7	$59x10^{+4}$	3.47
	viable region	$42x10^{+5}$	2.2	$98x10^{+4}$	5.76

The distribution of PC in highly metastatic MDA-MB-231 tumors was heterogeneous, as shown by the MALDI-MS data shown in Figure 3A, with high PC concentrations, displayed in blue, localized to distinct tumor regions within viable tumor regions (Fig. 3). By applying PCA, PC was identified to be the most important compound in differentiating these tumor microenvironmental regions in MDA-MB-231 tumors, as evident in PCA function +2 (Figure 3A). In contrast, the PC intensity was relatively homogeneously distributed in nonmetastatic MCF-7 tumor models as shown by the SIMS data in Figure 3B, and was not a determining factor in the tumor region assignment using PCA in the MCF-7 tumor model. This was evident from both PCA functions +2 and -2, describing 1.6% of the total variation in Figure 3B, which did not match the PC distribution in MCF-7 tumors and used different molecules for the region assignment. PCA function +2 in MCF-7 tumors outlined distinct tumor microenvironmental regions within the hematoxylin-stained viable tumor regions.

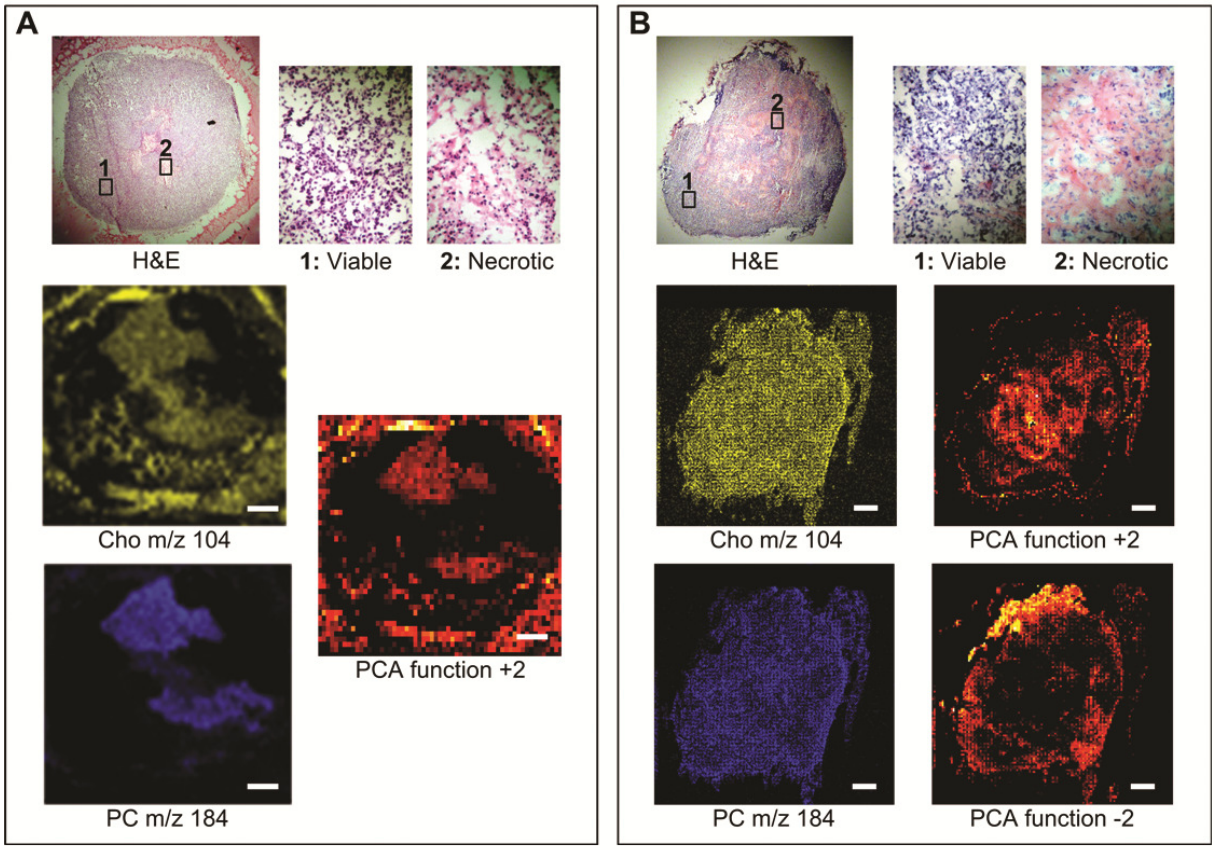

Figure 3: *(A) MALDI-MS microscope mode data set of a representative MDA-MB-231 tumor showing the H&E image, the corresponding MS imaging of Cho and PC, and the PCA image of the function +2. (B) SIMS microprobe data set of a representative MCF-7 tumor showing the H&E image, the corresponding MS imaging of Cho and PC, and the PCA images of the functions +2 and -2 providing inverse images, in which tumor regions are defined by masses other than Cho and PC. Scale bar: 1 mm*

Other lipids also demonstrated a heterogeneous spatial distribution in the MDA-MB-231 tumor model in MALDI-MS, SIMS, ME-SIMS (data not shown) and MetA-SIMS modes, such as the distribution of Cho by MALDI-MS, shown in yellow in Figure 3. Cho was present in several regions, and overlapped with PC. In contrast, such heterogeneous spatial distributions were not observed in the MCF-7 tumor model in the case of molecules

ranging between m/z 100 to 1000 with MALDI-MS (data not shown), SIMS, ME-SIMS (data not shown) and MetA-SIMS (data not shown), with emphasis on PC, which showed a relatively homogeneous distribution throughout the entire tumor section (Fig. 3B, acquired with SIMS).

The spatial distributions of Na^+ and K^+, detected with SIMS and MetA-SIMS, were also distinctively different between MCF-7 and MDA-MD-231 tumors, as shown in Table 1 and Figure 4. In MDA-MD-231 tumors shown in Figure 4A, Na^+ and K^+ displayed the same spatial distributions and were positively correlated in PCA. In MCF-7 tumors, Na^+ and K^+ were present in different regions, negatively correlated, and a determining factor in the PCA (Figure 4B), showing the inverse images of PCA function +2, with Na^+ as the determinant region assignment factor and function -2, where K^+ provides the determinant region assignment factor. This characteristic finding could be used as a criterion for region assignment in MCF-7 tumors and as a criterion to differentiate between the two tumor types. It is also evident that levels of high Na^+ mostly overlap with necrotic regions in the H&E-stained adjacent sections in both tumor models. Levels of high K^+ mostly overlap with necrotic regions in MDA-MB-231, and with viable regions in MCF-7 tumors. Experiments performed at high spatial resolution in MDA-MB-231 tumors show that high K^+ concentrations localized to hematoxylin-positive bodies in necrotic regions, and that a homogeneous K^+-distribution was detected in the viable tumor (Fig. 5). Simultaneously, it is possible to visualize the hematoxylin-positive-, K^+-colocalized Na^+ distribution in the necrotic region, and a homogeneous distribution of Na^+ in the viable region (Figure 5). All experiments were repeated in 7 MDA-MB-231 tumors and 6 MCF-7 tumors with consistent reproducibility in both tumor models, and by using different mass spectrometers and tissue preparation methods.

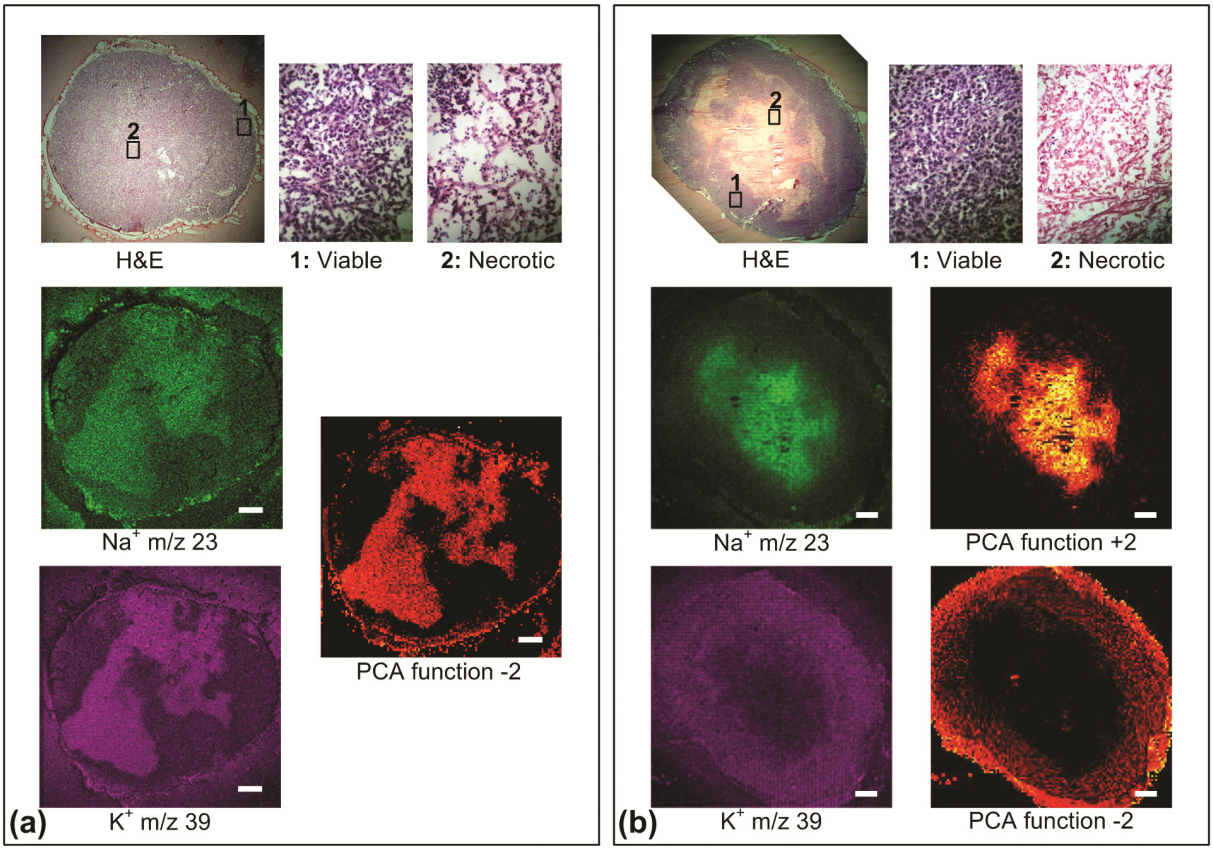

Figure 4: *(A) SIMS microprobe data set of a representative MDA-MB-231 tumor showing the H&E image, the corresponding MS imaging of Na^+ and K^+, and the PCA image of the function -2. (B) SIMS microprobe data set of a representative MCF-7 tumor showing the H&E image, the corresponding MS imaging of Na^+ and K^+, and the inverse PCA images of the functions +2 and -2. Scale bar: 1 mm.*

The use of different ionization techniques in both tumor xenograft models provided complementary data regarding the spatial localization of Cho (m/z 104, $[M]^+$, shown in Figure 3 and Cho with a water molecule attached to it (m/z 122, $[M+H_2O]^+$), both of which were well visualized with SIMS and MALDI and displayed identical spatial distributions. Cho colocalized with regions were PC was present, but also to regions where PC was absent or below the detection limit (Fig. 3). The same behavior was found for

GPC (m/z 524, $[M]^+$) (data not shown). The mass values for Na^+, K^+, Cho, PC and GPC were typically observed in both tumor types, with experiments under the exact same conditions running in parallel.

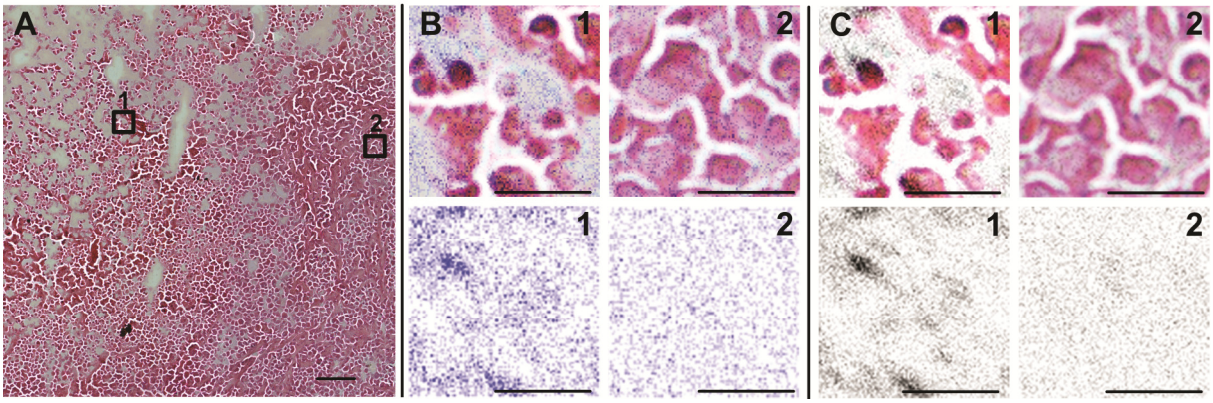

Figure 5: *(A) Optical image of a small part of MDA-MB-231 tumor, stained with H&E after concluding a MetA-SIMS experiment with (1) necrotic region and (2) viable tumor areas selected. (B) Na^+ and (C) K^+ distribution from MetA-SIMS data and overlay with microscopic image in regions (1) and (2) are shown the upper part; the individual ion distributions on areas (1) and (2) are shown at the bottom. Due to previous gold coating of the tissue, the hematoxilin staining was less efficient, therefore the visibility of cell nuclei is less pronounced. Scale bar: (A) 100 µm; (B) and (C) 25 µm.*

5.4 Discussion

Previous studies have demonstrated the importance of abnormal PC levels and other choline related lipid metabolites in cancer cells [13, 157, 166], but the techniques used in these studies were unable to identify distinct tumor regions containing high PC levels. Spatially resolved MRSI merely provided the tumoral tCho distribution, but was not able to

resolve the individual compounds contributing to the tCho signal, such as PC, Cho, and GPC.

In order to validate the experiments described above, several SIMS, ME-SIMS, MetA-SIMS and MALDI measurements were performed on adjacent slides. The analysis of all samples (with and without any surface treatment) showed similar PC localizations, validating the conclusion that PC localization was not due to artifacts of the sample preparation protocols used.

The measurement time for MS imaging depends on the desired spatial resolution, sample size, and the number of spectra collected. A quick survey scan with low spatial resolution can be combined with a longer analytical scan if more detailed spatial and spectral information are required. The FOV may vary from a few micrometers up to 200 µm per tile, depending on the desired spatial resolution. Both techniques provide extensive molecular information per μm^2 of the sample surface.

The MS Imaging applications used detected high PC levels in viable, non-necrotic tumor regions in the invasive/metastatic MDA-MB-231 tumor model, which is in good agreement with previous studies that revealed the importance of PC and related compounds in metastatic tumor growth [13, 157, 166]. Free choline (m/z 104) was present in viable tumor with a lower intensity than PC, and it was also detected in necrotic regions, which was confirmed by PCA of this data. PCA demonstrated that PC and Cho positively correlated in active MDA-MB-231 tumor regions and negatively correlated in necrotic areas. With this information, we were able to differentiate tumor microenvironments based on their molecular signatures with precision. The distribution of Na^+, K^+, Cho and PC in the MDA-MD-231 tumor model revealed tumor microenvironments with distinct molecular compositions, identified by PCA. The molecular distributions of PC and other compounds detected by MS Imaging reveal several sub-regions and features within the viable tumor regions than those determined by H&E staining alone. With the use of PCA, it was also possible to assign complementary regions based on the intensity of certain mass spectral

peaks such as PC and Cho. Future MS Imaging fingerprinting applications can potentially identify distinct tumor regions with diagnostic and therapeutic relevance.

The MS Imaging-detected spatial PC distribution was also able to differentiate between the two tumor xenograft models. The borders between necrotic and viable region were sharply defined by PC in highly invasive/metastatic MDA-MB-231 tumors, whereas in MCF-7 tumors, these regions were less defined. In addition, PC was a major principal component in the MDA-MB-231 tumor. However, PC was not relevant for tumor region assignment in MCF-7 tumors, likely due to the lower concentration of PC in MCF-7 compared to MDA-MB-231 tumors [10]. Our MS imaging findings confirm the importance of PC in malignant tumor growth [10]. Altered expression and activity levels of phosphatidylcholine metabolism-related enzymes, such as choline kinase [151, 154, 170], phospholipases C and D [173] and specific choline transporters [174] may account for the higher MS imaging-detected PC intensity in viable regions of the more aggressive tumor model. A recent studies in prostate tumor models detected increased tCho and PC concentrations in hypoxic tumor regions, and showed that hypoxia inducible factor-1 (HIF-1) signaling increased choline kinase expression, and hence PC production, under hypoxic conditions [149]. It is possible that HIF-1 signaling in hypoxic tumor regions increased the PC concentrations in the MDA-MB-231 breast tumor models, thereby potentially leading to a heterogeneous PC distribution in viable tumor regions as observed in our MS imaging data.

Both Na^+ and K^+ displayed heterogeneous spatial distributions in the breast tumor models investigated in our study. The correlation between Na^+ and K^+ ions revealed distinct differences between the invasive/metastatic and the nonmetastatic tumor model, as Na^+ and K^+ were negatively correlated in MCF-7 tumors, and positively correlated in MDA-MB-231 tumors. These different Na^+ and K^+ correlations may in the future be useful for differentiating breast tumor types. Na^+ has previously been related to tumor growth and attributed to alterations in Na^+/K^+ pump functions [54]. Our MS imaging data displayed a heterogeneous spatial distribution of the Na^+ intensity in both breast tumor models, which is in good agreement with these Na^+ MRSI studies [54]. The high Na^+ levels in the necrotic

regions of both tumor types support previous findings that correlated such high Na^+ levels with a decrease in Na^+/K^+ pump activity and an increase in cell membrane permeability in the necrotic region [175]. The same study reported higher K^+ levels in viable tumor regions compared to necrotic areas, due to high Na^+/K^+ pump activity in viable regions. In MCF-7 tumors, the low K^+ levels in necrotic regions and high K^+ levels in viable regions are in agreement with this study [175]. At high spatial resolution, increased Na^+ and K^+ were observed in hematoxylin-positive bodies in necrotic regions of MDA-MB-231 tumors, which likely originated from dead or dying cells. Both ions were decreased and homogenously distributed in viable regions, opposing the above explanation based on Na^+/K^+ pump activation, in which high levels of Na^+ would be expected in the extracellular space of viable tumor regions and decreased K^+ in necrotic regions. Breakdown of voltage-gated K^+ channels in necrotic MDA-MB-231 tumor regions may explain the increased K^+ in these regions. Voltage-gated K^+ channels were reported to be involved in breast cancer cell proliferation [55, 176], and to play an important role in the regulation of cell apoptosis [177]. In our study, high K^+ levels in necrotic regions of highly metastatic MDA-MB-231 tumors contrasting low K^+ levels in necrotic regions of nonmetastatic MCF-7 tumors, suggest that a dysfunction in voltage-gated K^+ channels in highly metastatic tumors may contribute to tumor malignancy. Further studies are necessary to elucidate the exact roles of voltage-gated K^+ channels and Na^+/K^+ pump in necrosis, apoptosis, and tumor aggressiveness.

5.5 Conclusions

The MS imaging data demonstrate that several important cancer-related molecules and spatial features can be readily identified in a single MS imaging experiment. In comparison, immunohistochemical stainings of breast biopsies, which are the current clinical standard in diagnostic pathology laboratories, require the use of one tissue section per type of immunostaining, and complex spatial and molecular correlations may be lost. The combination of MS imaging with MRSI data from the same tumors corroborate the validity of results by combining in-vivo and ex-vivo imaging techniques on the same

target, with agreeable results. The information that can be obtained by MS imaging of breast tumor sections may in the future provide spatially resolved molecular fingerprinting applications to help guide molecular diagnosis and treatment planning of breast cancer patients.

Summary

The insights derived from spatial localization of molecules in tissue sections are of great value for understanding and treating cancer and other diseases. These insights can relate to molecules linked to a disease as well as to drug molecules distributed across organs of interest. In the case of disease related molecules, such as phosphocholine and choline, linked to both tumor growth and malignancy, mass spectrometry (MS) imaging can not only provide the molecular and spatial information of single molecules, but can do so for a broad range of substances, from elements to proteins. In one single measurement, the impact of these molecules in multiple physiological and pathological pathways can be analyzed. In pharmaceutical research MS imaging can provide information about the drug as well as drug metabolites. Sample preparation remains a crucial step for any MS imaging experiment to be successful. Such challenges, in this thesis, were fragile tissue samples that had to be washed but could not be submitted to conventional tissue washing methods, the possibility of quantification of pharmaceutical compounds in organ tissues by MS imaging only, and the optimal sample preparation and analysis conditions for comparison between different tumor types. In this thesis, new methods, experimental settings, and applications of appropriate treatments for diverse tissue types are discussed.

Instrumentation, ionization and applications of MS imaging are discussed in Chapter 2. This chapter is centered on the two MS imaging techniques utilized and applied in this thesis, secondary ion mass spectrometric (SIMS) imaging and matrix assisted laser desorption ionization (MALDI) MS imaging. In a continuous effort to improve the quality of results provided by MS imaging, a series of instrumental developments have taken place recently. These developments include new gas phase separation capabilities and the increase of mass resolving power, mass accuracy, spatial resolution and tandem MS capabilities. While instrumentation has been developed to provide maximum information from tissue sections, sample preparation is intrinsically linked to reliable results. Sample preparation includes tissue section preparation, e.g. cutting temperature and substrate onto

which to apply the tissue section, sample storage and further handling such as washing steps, matrix and/or metal deposition on the sample surface. In order to improve detection of certain classes of molecules such as peptides and proteins, specific sample washing methods are necessary. Finally, one can only fully benefit from optimized sample preparation when combining it with the appropriate data interpretation method. This is addressed in chapter 2 with the use of the best data analysis strategy to ensure reliable data interpretation.

Because sample handling is of such importance to the success of MS imaging experiments, Chapter 3 is dedicated to a new surface cleaning method. This new method consists of the use of a wetted laboratory paper that can be used for local sample washing as well as for cleaning extremely fragile tissue sections. It consists of a wetted paper with the solvent of choice applied directly onto the biological tissue surface. The washing solution is spatially contained by the paper structure, thus the formation of a liquid film on the tissue surface is avoided. An additional advantage is that the paper used in the washing step can also be analyzed by MS imaging, providing additional information of components removed from the tissue surface while retaining their spatial organization.

While the appropriate sample preparation requires attention, the demand for quantitation by MS imaging methods is also increasing. In drug discovery research, it is important to know not only in which organs drug and drug metabolites can be found after drug administration, but also how much of drug and metabolites are present in each organ. This information is related to both drug efficacy and toxicity, depending on the organ where it can be found. However, quantification by MS imaging is challenging, with several factors contributing to its accuracy such as ion suppression, sample preparation and inhomogeneous matrix crystallization, expected to affect the results of quantitation of drugs in tissue sections. Chapter 4 provides an experimental setting designed to address ion suppression and sample preparation impact on drug quantitation. It also provides data that show the effect of different sample preparation techniques and organ dependence on mass spectrometric response of the drug. While quantitation by MS imaging is not possible at

this moment, this study sheds light on where the problems lie and demonstrates that by using a carefully designed experimental set-up it is possible to address these problems.

Finally, the application of MS imaging in cancer research is the focus of Chapter 5. This chapter comprises a comprehensive study of two breast cancer xenograft models, the nonmetastatic MCF-7 and highly metastatic MDA-MB-231 tumors, by SIMS and MALDI MS imaging in combination with magnetic resonance spectroscopic imaging (MRSI). The study is focused on the distribution of phosphocholine (PC), total choline (tCho), free choline (Cho), sodium and potassium in the two different tumors. *In vivo* 3-dimensional MRSI demonstrated that high tCho levels, consisting of free choline (Cho), PC, and glycerophosphocholine (GPC), displayed a heterogeneous spatial distribution in the tumor. MS imaging data provided information about the spatial distribution of each individual molecule, with increased PC and Cho in viable tumor regions compared to necrotic regions in the highly metastatic MDA-MB-231 tumor type. The same molecules were homogeneously distributed in the nonmetastatic MCF-7 tumor type, which may be related to the role of PC and Cho. Also, significant differences in the spatial distribution of Na^+ and K^+ in the these two tumor types suggested differential Na^+/K^+ pump functions and K^+ channel expressions. It is important to note that the combined results provide a link to the impact of multiple pathways in tumor malignancy in one single study.

All the above aspects make MS imaging a very useful and rewarding technique, which can be applied effectively in several fields when using suitable methodology. Therefore, together with instrumentation improvement, methodology development is essential for high quality imaging experiments.

Samenvatting

De inzichten uit plaatsbepaling van moleculen in weefsels zijn van grote waarde voor het begrijpen en behandelen van kanker en andere ziekten. Deze inzichten kunnen betrekking hebben op moleculen die gerelateerd zijn aan een bepaalde ziekte maar ook op medicijnen en hun verspreiding in bepaalde organen. In het geval van ziekte gerelateerde moleculen, zoals phosphocholine en choline, die in verband worden gebracht met zowel de groei als met de kwaadaardigheid van tumoren, kan massaspectrometrie (MS) niet alleen de aard en locatie van individuele moleculen ophelderen, maar kan dat ook voor een heel scala van stoffen, van elementen tot eiwitten. In één enkele meting kan de impact van deze moleculen worden geanalyseerd in diverse fysiologische en pathologische processen. In farmaceutisch onderzoek kan MS imaging informatie verschaffen over zowel het medicijn alsook metabolieten daarvan. Het prepareren van monsters blijft een cruciale stap voor elk succesvol MS imaging experiment. Uitdagingen daarbij in dit proefschrift waren delicate weefselmonsters die gewassen moesten worden maar niet onderworpen konden worden aan traditionele methodes daarvoor, kwantificatie van medicijnen in orgaanweefsels die alleen middels MS imaging mogelijk was, en het bepalen van de optimale condities voor het prepareren en analyseren van monsters om verschillende tumor types te vergelijken. In dit proefschrift worden nieuwe methodes, experimentele opstellingen, en geschikte behandelingen van diverse weefseltypes aangedragen en bediscussieerd.

Instrumentatie, ionisatie en de toepassing van MS imaging worden bediscussieerd in hoofdstuk 2. Dat hoofdstuk is gericht op de twee MS imaging technieken die voor dit proefschrift zijn toegepast, te weten ‘secondary ion mass spectrometric (SIMS) imaging’ en ‘matrix assisted laser desorption ionization (MALDI) MS imaging’. Uit de voortdurende inspanningen om de kwaliteit van de resultaten uit MS imaging te verbeteren, zijn recent een aantal instrumentele ontwikkelingen voortgekomen. Deze ontwikkelingen omvatten nieuwe mogelijkheden voor gas fase scheiding, en verbeteringen in massa resolutie, massa nauwkeurigheid, resolutie en mogelijkheden met tandem MS. Terwijl instrumentatie

ontwikkeld is om zo veel mogelijk informatie van weefsels te verkrijgen, is monsters bereiding intrinsiek verweven met de betrouwbaarheid van resultaten. Zo is bij het bereiden van weefselpreparaten onder andere de snijdtemperatuur van belang, net als het substraat waarop het weefsel wordt aangebracht, de bewaarcondities van het monster en verdere behandelingen zoals wassen en het aanbrengen van een matrix en/of metaal op het monster oppervlak. Om de opsporing van bepaalde klassen van moleculen zoals peptiden en proteïnen te verbeteren, zijn specifieke wasmethodes noodzakelijk. En uiteindelijk kan men pas ten volle profiteren van optimale monster bereiding wanneer dat gecombineerd wordt met de passende methode voor data interpretatie. In hoofdstuk 2 komt dit tot uiting door gebruik van de best mogelijke analysestrategie om betrouwbare gegevensinterpretatie te verzekeren.

Omdat monster bereiding zo belangrijk is voor het slagen van MS imaging experimenten, is hoofdstuk 3 gewijd aan een nieuwe methode voor het schoonmaken van oppervlaktes. Deze nieuwe methode bestaat uit het gebruik van natgemaakt lab papier voor zowel het lokaal wassen van monsters als voor het schoonmaken van zeer delicate weefsel preparaten. Het natte papier met het gekozen oplosmiddel wordt direct op het oppervlak van het biologische weefsel aangebracht. Het wasmiddel wordt daarbij vastgehouden door de papierstructuur, zodat de vorming van een vloeistoffilm op het weefseloppervlak wordt voorkomen. Aanvullend voordeel is dat het papier dat gebruikt wordt bij het wassen ook met MS imaging geanalyseerd kan worden, hetgeen aanvullende informatie oplevert over de componenten die van het weefseloppervlak zijn verwijderd met behoud van hun ruimtelijke structuur.

Zoals de juiste bereidingswijze van monsters aandacht behoeft, neemt ook de vraag naar kwantificatie middels MS imaging toe. In medicijnenonderzoek is het niet alleen belangrijk te weten in welke organen een medicijn en haar metabolieten aangetroffen kunnen worden na toediening, maar ook hoe veel er van dat medicijn en die metabolieten aanwezig is in elk orgaan. Deze informatie is gerelateerd aan zowel doeltreffendheid als toxiciteit van het medicijn, afhankelijk van het orgaan waar het aangetroffen wordt.

Kwantificatie middels MS imaging is echter een uitdaging, daar diverse factoren als ion suppressie, monster bereiding and niet-homogene matrix kristallisatie, de nauwkeurigheid bepalen en naar verwachting van invloed zijn op de resultaten van kwantificatie van medicijnen in weefsels. In hoofdstuk 4 wordt een experimentele opstelling gepresenteerd, die ontworpen is de invloed van ion suppressie en monster bereiding op kwantificatie van medicijnen te kunnen bepalen. In dit hoofdstuk wordt data gepresenteerd die de invloed aantonen van verschillende monster bereidingswijzen en van de afhankelijk van het orgaan op de wijze waarop het medicijn waargenomen kan worden in een MS meting. Waar kwantificatie middels MS imaging momenteel nog niet mogelijk is, geeft dit onderzoek inzicht in de problemen daarbij en toont het aan dat die met een zorgvuldig ontwikkelde experimentele opstelling aangepakt kunnen worden.

Tenslotte komt de toepassing van MS imaging in kankeronderzoek onder de aandacht in hoofdstuk 5. Dat hoofdstuk bestaat uit een veelomvattende studie naar twee kanker xenograft modellen, de niet-metastatische MCF-7 en de hoog-metastatische MDA-MB-231 tumoren, die met SIMS en MALDI MS imaging onderzocht zijn in combinatie met magnetic resonance spectroscopic imaging (MRSI). Dit onderzoek heeft zich gericht op de distributie van phosphocholine (PC), totaal choline (tCho), vrij choline (Cho), sodium en potassium in twee verschillende tumoren. Met *in vivo* 3-dimensionele MRSI werd aangetoond, dat hoge tCho niveaus, bestaande uit vrij choline (Cho), PC, en glycerophosphocholine (GPC), een heterogene ruimtelijke verspreiding in de tumor lieten zien. MS imaging data gaf inzicht in de ruimtelijke distributie van elk individuele molecuul, met verhoogde aanwezigheid van PC en Cho in levensvatbare tumor regio's ten opzichte van necrotische regio's in het hoog-metastatische MDA-MB-231 tumor type. Dezelfde moleculen waren homogeen verspreid in het niet-metastatische MCF-7 tumor type, hetgeen gerelateerd kan worden aan de rol van PC en Cho. Tevens suggereren significante verschillen in de ruimtelijke distributie van Na^+ en K^+ in deze twee tumor types verschillende Na^+/K^+ pomp functies en K^+ kanaal uitingen. Het is belangrijk daarbij op te merken dat deze gecombineerde resultaten uit één enkel onderzoek

aanknopingspunten bieden voor inzicht in de effecten van een veelvoud aan processen met betrekking tot de kwaadaardigheid van tumoren.

Alle bovenstaande aspecten maken MS imaging een zeer bruikbare en waardevolle techniek, die met de juiste aanpak effectief kan worden ingezet in verschillende toepassingsgebieden. Daarom blijft verdere methodologische ontwikkeling , net als verbetering van instrumenten, essentieel voor imaging experimenten van hoge kwaliteit.

Bibliography

1. Bedair, M.; Sumner, L. W., Current and emerging mass-spectrometry technologies for metabolomics. *Trac-Trends in Analytical Chemistry* **2008,** 27, (3), 238-250.
2. Hu, C. X.; van der Heijden, R.; Wang, M.; van der Greef, J.; Hankemeier, T.; Xua, G. W., Analytical strategies in lipidomics and applications in disease biomarker discovery. *Journal of Chromatography B-Analytical Technologies in the Biomedical and Life Sciences* **2009,** 877, (26), 2836-2846.
3. Kumar, C.; Mann, M., Bioinformatics analysis of mass spectrometry-based proteomics data sets. *FEBS letters* **2009,** 583, (11), 1703-1712.
4. Mann, M.; Kelleher, N. L., Precision proteomics: The case for high resolution and high mass accuracy. *Proceedings of the National Academy of Sciences of the United States of America* **2008,** 105, (47), 18132-18138.
5. Borrebaeck, C. A. K.; Wingren, C., Design of high-density antibody microarrays for disease proteomics: Key technological issues. *Journal of Proteomics* **2009,** 72, (6), 928-935.
6. Mischak, H.; Coon, J. J.; Novak, J.; Weissinger, E. M.; Schanstra, J. P.; Dominiczak, A. F., Capillary electrophoresis-mass spectrometry as a powerful tool in biomarker discovery and clinical diagnosis: an update of recent developments. *Mass Spectrometry Reviews* **2009,** 28, (5), 703-724.
7. Wu, T. F.; Mohan, C., Proteomic toolbox for autoimmunity research. *Autoimmunity Reviews* **2009,** 8, (7), 595-598.
8. Ladanyi, A.; Sipos, F.; Szoke, D.; Galamb, O.; Molnar, B.; Tulassay, Z., Laser microdissection in translational and clinical research. *Cytometry Part A* **2006,** 69A, (9), 947-960.
9. Pinzani, P.; Orlando, C.; Pazzagli, M., Laser-assisted microdissection for real-time PCR sample preparation. *Molecular Aspects of Medicine* **2006,** 27, (2-3), 140-159.
10. Aboagye, E. O.; Bhujwalla, Z. M., Malignant Transformation Alters Membrane Choline Phospholipid Metabolism of Human Mammary Epithelial Cells. *Cancer Research* **1999,** 59, (1), 80-84.
11. Ackerstaff, E.; Artemov, D.; Gillies, R. J.; Bhujwalla, Z. M., Hypoxia and the presence of human vascular endothelial cells affect prostate cancer cell invasion and metabolism. *Neoplasia* **2007,** 9, (12), 1138-1151.
12. Glunde, K., Ackerstaff, E., Natarajan, K., Artemov, D., and Bhujwalla, Z. M. , Real-time changes in 1H and 31P NMR spectra of malignant human mammary epithelial cells during treatment with the anti-inflammatory agent indomethacin. *Magnetic Resonance in Medicine* **2002,** 48, 819-825.
13. Glunde, K.; Jacobs, M. A.; Pathaka, A. P.; Artemov, D.; Bhujwalla, Z. M., Molecular and functional imaging of breast cancer. *NMR in biomedicine* **2009,** 22, (1), 92-103.

14. Glunde, K.; Bhujwalla, Z. M., Choline kinase alpha in cancer prognosis and treatment. *Lancet Oncology* **2007,** 8, (10), 855-857.
15. Giepmans, B. N. G.; Adams, S. R.; Ellisman, M. H.; Tsien, R. Y., The Fluorescent Toolbox for Assessing Protein Location and Function. *Science* **2006,** 312, (5771), 217-224.
16. Mamidi, R.; Mannens, G.; Annaert, P.; Hendrickx, J.; Goris, I.; Bockx, M.; Janssen, C. G. M.; Kao, M.; Kelley, M. F.; Meuldermans, W., Metabolism and excretion of RWJ-333369 [1,2-ethanediol, 1-(2-chlorophenyl)-, 2-carbamate, (S)-] in mice, rats, rabbits, and dogs. *Drug Metabolism and Disposition* **2007,** 35, (4), 566-575.
17. MacAleese, L.; Stauber, J.; Heeren, R. M. A., Perspectives for imaging mass spectrometry in the proteomics landscape. *Proteomics* **2009,** 9, (4), 819-834.
18. Todd, P. J.; McMahon, J. M.; Short, R. T.; McCandlish, C. A., Organic SIMS of biological tissue. *Analytical Chemistry* **1997,** 69, 529A-535A.
19. Altelaar, A. F. M.; Luxembourg, S. L.; McDonnell, L. A.; Piersma, S. R.; Heeren, R. M. A., Imaging mass spectrometry at cellular length scales. *Nature Protocols* **2007,** 2, (5), 1185-1196.
20. Luxembourg, S. L.; Mize, T. H.; McDonnell, L. A.; Heeren, R. M. A., High-spatial resolution mass spectrometric imaging of peptide and protein distributions on a surface. *Analytical Chemistry* **2004,** 76, (18), 5339-5344.
21. Rohner, T. C.; Staab, D.; Stoeckli, M., MALDI mass spectrometric imaging of biological tissue sections. *Mechanisms of Ageing and Development* **2005,** 126, (1), 177-185.
22. Langstrom, B.; Andren, P. E.; Lindhe, O.; Svedberg, M.; Hall, H., In vitro imaging techniques in Neurodegenerative diseases. *Molecular Imaging and Biology* **2007,** 9, (4), 161-175.
23. Baker, M. J.; Brown, M. D.; Gazi, E.; Clarke, N. W.; Vickerman, J. C.; Lockyer, N. P., Discrimination of prostate cancer cells and non-malignant cells using secondary ion mass spectrometry. *Analyst* **2008,** 133, (2), 175-9.
24. Trim, P. J.; Henson, C. M.; Avery, J. L.; McEwen, A.; Snel, M. F.; Claude, E.; Marshall, P. S.; West, A.; Princivalle, A. P.; Clench, M. R., Matrix-Assisted Laser Desorption/Ionization-Ion Mobility Separation-Mass Spectrometry Imaging of Vinblastine in Whole Body Tissue Sections. *Analytical Chemistry* **2008,** 80, (22), 8628-8634.
25. Ifa, D. R.; Jackson, A. U.; Paglia, G.; Cooks, R. G., Forensic applications of ambient ionization mass spectrometry. *Analytical and Bioanalytical Chemistry* **2009,** 394, (8), 1995-2008.
26. Ifa, D. R.; Manicke, N. E.; Dill, A. L.; Cooks, R. G., Latent Fingerprint Chemical Imaging by Mass Spectrometry. *Science* **2008,** 321, (5890), 805.
27. Lemaire, R.; Wisztorski, M.; Desmons, A.; Tabet, J. C.; Day, R.; Salzet, M.; Fournier, I., MALDI-MS Direct Tissue Analysis of Proteins: Improving Signal Sensitivity Using Organic Treatments. *Analytical Chemistry* **2006,** 78, (20), 7145-7153.
28. Schuerenberg, M.; Luebbert, C.; Deininger, S. O.; Ketterlinus, R.; Suckau, D., MALDI tissue imaging: mass spectrometric localization of biomarkers in tissue slices. *Nature Methods* **2007,** 4, (5), iii-iv.
29. Schwartz, S. A.; Reyzer, M. L.; Caprioli, R. M., Direct tissue analysis using matrix-assisted laser desorption/ionization mass spectrometry: practical aspects of sample preparation. *Journal of Mass Spectrometry* **2003,** 38, (7), 699-708.

30. Seeley, E. H.; Oppenheimer, S. R.; Mi, D.; Chaurand, P.; Caprioli, R. M., Enhancement of Protein Sensitivity for MALDI Imaging Mass Spectrometry After Chemical Treatment of Tissue Sections. *Journal of the American Society for Mass Spectrometry* **2008,** 19, (8), 1069-1077.
31. Kaletaş, B. K.; van der Wiel, I. M.; Stauber, J.; Lennard, J. D.; Güzel, C.; Kros, J. M.; Luider, T. M.; Heeren, R. M. A., Sample preparation issues for tissue imaging by imaging MS. *Proteomics* **2009,** 9, (10), 2622-2633.
32. Djidja, M. C.; Francese, S.; Loadman, P. M.; Sutton, C. W.; Scriven, P.; Claude, E.; Snel, M. F.; Franck, J.; Salzet, M.; Clench, M. R., Detergent addition to tryptic digests and ion mobility separation prior to MS/MS improves peptide yield and protein identification for in situ proteomic investigation of frozen and formalin-fixed paraffin-embedded adenocarcinoma tissue sections. *Proteomics* **2009,** 9, (10), 2750-2763.
33. Groseclose, M. R.; Andersson, M.; Hardesty, W. M.; Caprioli, R. M., Identification of proteins directly from tissue: in situ tryptic digestions coupled with imaging mass spectrometry. *Journal of Mass Spectrometry* **2007,** 42, (2), 254-262.
34. Lemaire, R.; Desmons, A.; Tabet, J. C.; Day, R.; Salzet, M.; Fournier, I., Direct analysis and MALDI imaging of formalin-fixed, paraffin-embedded tissue sections. *Journal of Proteome Research* **2007,** 6, (4), 1295-1305.
35. Petyuk, V. A.; Qian, W. J.; Chin, M. H.; Wang, H. X.; Livesay, E. A.; Monroe, M. E.; Adkins, J. N.; Jaitly, N.; Anderson, D. J.; Camp, D. G.; Smith, D. J.; Smith, R. D., Spatial mapping of protein abundances in the mouse brain by voxelation integrated with high-throughput liquid chromatography-mass spectrometry. *Genome Research* **2007,** 17, (3), 328-336.
36. Stauber, J.; Lemaire, R.; Franck, J.; Bonnel, D.; Croix, D.; Day, R.; Wisztorski, M.; Fournier, I.; Salzet, M., MALDI Imaging of formalin-fixed paraffin-embedded tissues: Application to model animals of Parkinson disease for biomarker hunting. *Journal of Proteome Research* **2008,** 7, (3), 969-978.
37. Altelaar, A. F. M.; Klinkert, I.; Jalink, K.; de Lange, R. P. J.; Adan, R. A. H.; Heeren, R. M. A.; Piersma, S. R., Gold-Enhanced Biomolecular Surface Imaging of Cells and Tissue by SIMS and MALDI Mass Spectrometry. *Analytical Chemistry* **2005,** 78, (3), 734-742.
38. Fournier, I.; Marinach, C.; Tabet, J. C.; Bolbach, G., Irradiation effects in MALDI, ablation, ion production, and surface modifications. Part II: 2,5-dihydroxybenzoic acid monocrystals. *Journal of the American Society for Mass Spectrometry* **2003,** 14, (8), 893-899.
39. Strupat, K.; Karas, M.; Hillenkamp, F., 2,5-Dihydroxybenzoic acid: a new matrix for laser desorption--ionization mass spectrometry. *International Journal of Mass Spectrometry and Ion Processes* **1991,** 111, 89-102.
40. Tholey, A.; Heinzle, E., Ionic (liquid) matrices for matrix-assisted laser desorption/ionization mass spectrometry—applications and perspectives. *Analytical and Bioanalytical Chemistry* **2006,** 386, (1), 24-37.
41. Beavis, R. C.; Chaudhary, T.; Chait, B. T., alpha-Cyano-4-hydroxycinnamic acid as a matrix for matrix assisted laser desorption mass spectrometry. *Organic Mass Spectrometry* **1992,** 27, (2), 156-158.

42. Beavis, R. C.; Chait, B. T.; Standing, K. G., Matrix-assisted laser-desorption mass spectrometry using 355 nm radiation. *Rapid Communications in Mass Spectrometry* **1989,** 3, (12), 436-439.
43. Fournier, I.; Tabet, J. C.; Bolbach, G., Irradiation effects in MALDI and surface modifications: Part I: Sinapinic acid monocrystals. *International Journal of Mass Spectrometry* **2002,** 219, (3), 515-523.
44. Pan, C.; Xu, S.; Zhou, H.; Fu, Y.; Ye, M.; Zou, H., Recent developments in methods and technology for analysis of biological samples by MALDI-TOF-MS. *Analytical and Bioanalytical Chemistry* **2007,** 387, (1), 193-204.
45. Jackson, S. N.; Wang, H.-Y. J.; Woods, A. S., In Situ Structural Characterization of Phosphatidylcholines in Brain Tissue Using MALDI-MS/MS. *Journal of the American Society for Mass Spectrometry* **2005,** 16, (12), 2052-2056.
46. Lemaire, R.; Tabet, J. C.; Ducoroy, P.; Hendra, J. B.; Salzet, M.; Fournier, I., Solid Ionic Matrixes for Direct Tissue Analysis and MALDI Imaging. *Analytical Chemistry* **2006,** 78, (3), 809-819.
47. Knochenmuss, R.; Dubois, F.; Dale, M. J.; Zenobi, R., The Matrix Suppression Effect and Ionization Mechanisms in Matrix-assisted Laser Desorption/Ionization. *Rapid Communications in Mass Spectrometry* **1996,** 10, (8), 871-877.
48. Knochenmuss, R.; Karbach, V.; Wiesli, U.; Breuker, K.; Zenobi, R., The matrix suppression effect in matrix-assisted laser desorption/ionization: application to negative ions and further characteristics. *Rapid Communications in Mass Spectrometry* **1998,** 12, (9), 529-534.
49. Knochenmuss, R.; Stortelder, A.; Breuker, K.; Zenobi, R., Secondary ion–molecule reactions in matrix-assisted laser desorption/ionization. *Journal of Mass Spectrometry* **2000,** 35, (11), 1237-1245.
50. McCombie, G.; Knochenmuss, R., Small-Molecule MALDI Using the Matrix Suppression Effect To Reduce or Eliminate Matrix Background Interferences. *Analytical Chemistry* **2004,** 76, (17), 4990-4997.
51. McCombie, G.; Knochenmuss, R., Enhanced MALDI Ionization Efficiency at the Metal-Matrix Interface: Practical and Mechanistic Consequences of Sample Thickness and Preparation Method. *Journal of the American Society for Mass Spectrometry* **2006,** 17, (5), 737-745.
52. Heeren, R. M. A.; Kukrer-Kaletas, B.; Taban, I. M.; MacAleese, L.; McDonnell, L. A., Quality of surface: The influence of sample preparation on MS-based biomolecular tissue imaging with MALDI-MS and (ME-)SIMS. *Applied Surface Science* **2008,** 255, (4), 1289-1297.
53. Stauber, J.; MacAleese, L.; Franck, J.; Claude, E.; Snel, M.; Kaletas, B. K.; Wiel, I.; Wisztorski, M.; Fournier, I.; Heeren, R. M. A., On-Tissue Protein Identification and Imaging by MALDI-Ion Mobility Mass Spectrometry. *Journal of the American Society for Mass Spectrometry* **2009,** 21, (3), 338-347.
54. Ouwerkerk, R.; Bleich, K. B.; Gillen, J. S.; Pomper, M. G.; Bottomley, P. A., Tissue sodium concentration in human brain tumors as measured with 23Na MR imaging. *Radiology* **2003,** 227, (2), 529-537.

55. Brevet, M.; Ahidouch, A.; Sevestre, H.; Merviel, P.; El Hiani, Y.; Robbe, M.; Ouadid-Ahidouch, H., Expression of K+ channels in normal and cancerous human breast. *Histology and Histopathology* **2008,** 23, (8), 965-972.
56. Caprioli, R. M.; Farmer, T. B.; Gile, J., Molecular imaging of biological samples: Localization of peptides and proteins using MALDI-TOF MS. *Analytical Chemistry* **1997,** 69, (23), 4751-4760.
57. Zierhut, M. L.; Ozturk-Isik, E.; Chen, A. P.; Park, I.; Vigneron, D. B.; Nelson, S. J., ^{1}H spectroscopic imaging of human brain at 3 Tesla: Comparison of fast three-dimensional magnetic resonance spectroscopic imaging techniques. *Journal of Magnetic Resonance Imaging* **2009,** 30, (3), 473-480.
58. Lewellen, T. K., Recent developments in PET detector technology. *Physics in Medicine and Biology* **2008,** 53, (17), R287-R317.
59. Andersson, M.; Groseclose, M. R.; Deutch, A. Y.; Caprioli, R. M., Imaging mass spectrometry of proteins and peptides: 3D volume reconstruction. *Nature Methods* **2008,** 5, (1), 101-108.
60. Sinha, T. K.; Khatib-Shahidi, S.; Yankeelov, T. E.; Mapara, K.; Ehtesham, M.; Cornett, D. S.; Dawant, B. M.; Caprioli, R. M.; Gore, J. C., Integrating spatially resolved three-dimensional MALDI IMS with in vivo magnetic resonance imaging. *Nature Methods* **2008,** 5, (1), 57-59.
61. Amstalden van Hove, E. R.; Blackwell, T. R.; Klinkert, I.; Eijkel, G. B.; Heeren, R. M. A.; Glunde, K., Multimodal mass spectrometric imaging of small molecules reveals distinct spatio-molecular signatures in differentially metastatic breast tumor models. *Cancer Research* **2010,** 70, (22), 9012-21.
62. Prideaux, B.; Staab, D.; Stoeckli, M., Applications of MALDI-MSI to pharmaceutical research. *Methodsin Molecular Biology* **2010,** 656, 405-13.
63. Solon, E. G.; Schweitzer, A.; Stoeckli, M.; Prideaux, B., Autoradiography, MALDI-MS, and SIMS-MS Imaging in Pharmaceutical Discovery and Development. *Aaps Journal* **2010,** 12, (1), 11-26.
64. Wiseman, J. M.; Puolitaival, S. M.; Takáts, Z.; Cooks, R. G.; Caprioli, R. M., Mass Spectrometric Profiling of Intact Biological Tissue by Using Desorption Electrospray Ionization13. *Angewandte Chemie International Edition* **2005,** 44, (43), 7094-7097.
65. Grossi, C.; Francese, S.; Casini, A.; Rosi, M. C.; Luccarini, I.; Fiorentini, A.; Gabbiani, C.; Messori, L.; Moneti, G.; Casamenti, F., Clioquinol Decreases Amyloid-beta Burden and Reduces Working Memory Impairment in a Transgenic Mouse Model of Alzheimer's Disease. *Journal of Alzheimers Disease* **2009,** 17, (2), 423-440.
66. Stoeckli, M.; Staab, D.; Schweitzer, A., Compound and metabolite distribution measured by MALDI mass spectrometric imaging in whole-body tissue sections. *International Journal of Mass Spectrometry* **2007,** 260, (2-3), 195-202.
67. Debois, D.; Bralet, M. P.; Le Naour, F.; Brunelle, A.; Laprevote, O., In Situ Lipidomic Analysis of Nonalcoholic Fatty Liver by Cluster TOF-SIMS Imaging. *Analytical Chemistry* **2009,** 81, (8), 2823-2831.
68. Wiseman, J. M.; Ifa, D. R.; Zhu, Y.; Kissinger, C. B.; Manicke, N. E.; Kissinger, P. T.; Cooks, R. G., Desorption electrospray ionization mass spectrometry: Imaging drugs and metabolites in tissues. *Proceedings of the National Academy of Sciences of the United States of America* **2008,** 105, (47), 18120-18125.

69. Hillenkamp, F.; Unsöld, E.; Kaufmann, R.; Nitsche, R., A high-sensitivity laser microprobe mass analyzer. *Applied Physics A: Materials Science & Processing* **1975,** 8, (4), 341-348.
70. Struyf, H., van Roy, W., van Vaeck, L., van Grieken, R., Gijbels, R., Laser microprobe Fourier transform mass spectrometer with external ion source for organic and inorganic microanalysis. *Analytica Chimica Acta* **1993,** 283, 139-151.
71. van Vaeck, L., Struyf, H., van Roy, W., Adams, F., Organic and inorganic analysis with laser microprobe mass spectrometry. Part I: Instrumentation and methodology. *Mass Spectrometry Reviews* **1994,** 13, (3).
72. van Vaeck, L., Struyf, H., van Roy, W., Adams, F., Organic and inorganic analysis with laser microprobe mass spectrometry. Part II: Applications. *Mass Spectrometry Reviews* **1994,** 13, (3).
73. Vogt, H., Heinen, H. J., Meier, S., Wechsung, R., LAMMA 500 principle and technical description of the instrument. *Fresenius' Journal of Analytical Chemistry* **1981,** 308, (3), 195-200.
74. Heinen, H. J.; Meier, S.; Vogt, H.; Wechsung, R., LAMMA 1000, a new laser microprobe mass analyzer for bulk samples. *International Journal of Mass Spectrometry and Ion Physics* **1983,** 47, 19-22.
75. *ToF-SIMS: Surface analysis by mass spectrometry*. IM Publications and Surface Spectra Limited: Chichester, Manchester, **2001**.
76. Koestler, M.; Kirsch, D.; Hester, A.; Leisner, A.; Guenther, S.; Spengler, B., A high-resolution scanning microprobe matrix-assisted laser desorption/ionization ion source for imaging analysis on an ion trap/Fourier transform ion cyclotron resonance mass spectrometer. *Rapid Communications in Mass Spectrometry* **2008,** 22, (20), 3275-3285.
77. Amstalden van Hove, E. R.; Smith, D. F.; Fornai, L.; Glunde, K.; Heeren, R. M. A., An alternative paper based tissue washing method for Mass Spectrometry Imaging: Localized Washing and Fragile Tissue Analysis. *Journal of the American Society for Mass Spectrometry* **2011**, 22, (10), 1885-1890.
78. Monroe, E. B.; Jurchen, J. C.; Koszczuk, B. A.; Losh, J. L.; Rubakhin, S. S.; Sweedler, J. V., Massively parallel sample preparation for the MALDI MS analyses of tissues. *Analytical Chemistry* **2006,** 78, (19), 6826-6832.
79. Puolitaival, S. M.; Burnum, K. E.; Cornett, D. S.; Caprioli, R. M., Solvent-Free Matrix Dry-Coating for MALDI Imaging of Phospholipids. *Journal of the American Society for Mass Spectrometry* **2008,** 19, (6), 882-886.
80. Adriaens, A.; van Ham, R.; van Vaeck, L., Fundamental Aspects of Inorganic SIMS. In *ToF-SIMS: Surface analysis by mass spectrometry*, C., V. J.; D., B., Eds. IM Publications and Surface Spectra Limited: Chichester, Manchester, **2001**; pp 195-222.
81. Delcorte, A., Fundamental Aspects of Organic SIMS. In *ToF-SIMS: Surface analysis by mass spectrometry.* , C., V. J.; D., B., Eds. IM Publications and Surface Spectra Limited: Chichester, Manchester, 2001; pp 161-194.
82. Urbassek, H. M., Status of Cascade Theory. *In: Vickerman JC, Briggs D, editors. ToF-SIMS: Surface analysis by mass spectrometry. Chichester: IM Publications.* **2001**, 139-159.

83. Colliver, T. L.; Brummel, C. L.; Pacholski, M. L.; Swanek, F. D.; Ewing, A. G.; Winograd, N., Atomic and molecular imaging at the single-cell level with TOF-SIMS. *Analytical Chemistry* **1997,** 69, (13), 2225-2231.
84. Pacholski, M. L.; Cannon, D. M.; Ewing, A. G.; Winograd, N., Static time-of-flight secondary ion mass spectrometry imaging of freeze-fractured, frozen-hydrated biological membranes. *Rapid Communications in Mass Spectrometry* **1998,** 12, (18), 1232-1235.
85. Todd, P. J.; Schaaff, T. G.; Chaurand, P.; Caprioli, R. M., Organic ion imaging of biological tissue with secondary ion mass spectrometry and matrix-assisted laser desorption/ionization. *Journal of Mass Spectrometry* **2001,** 36, (4), 355-69.
86. Eijkel, G. B.; Kaletas, B. K.; van der Wiel, I. M.; Kros, J. M.; Luider, T. M.; Heeren, R. M. A., Correlating MALDI and SIMS imaging mass spectrometric datasets of biological tissue surfaces. *Surface and Interface Analysis* **2009,** 41, (8), 675-685.
87. Chandra, S.; Morrison, G. H., Imaging ion and molecular transport at subcellular resolution by secondary ion mass spectrometry. *International Journal of Mass Spectrometry and Ion Processes* **1995,** 143, 161-176.
88. Chandra, S.; Smith, D. R.; Morrison, G. H., Peer Reviewed: A Subcellular Imaging by Dynamic SIMS Ion Microscopy. *Analytical Chemistry* **2000,** 72, (3), 104 A-114 A.
89. Strick, R.; Strissel, P. L.; Gavrilov, K.; Levi-Setti, R., Cation-chromatin binding as shown by ion microscopy is essential for the structural integrity of chromosomes. *Journal of Cell Biology* **2001,** 155, (6), 899-910.
90. Knochenmuss, R., Ion formation mechanisms in UV-MALDI. *Analyst* **2006,** 131, (9), 966-86.
91. Dreisewerd, K., The Desorption Process in MALDI. *Chemical Reviews* **2003,** 103, (2), 395-426.
92. Takats, Z.; Wiseman, J. M.; Gologan, B.; Cooks, R. G., Mass Spectrometry Sampling Under Ambient Conditions with Desorption Electrospray Ionization. *Science* **2004,** 306, (5695), 471-473.
93. Cooks, R. G.; Ouyang, Z.; Takats, Z.; Wiseman, J. M., Ambient Mass Spectrometry. *Science* **2006,** 311, (5767), 1566-1570.
94. Wiseman, J. M.; Ifa, D. R.; Song, Q.; Cooks, R. G., Tissue Imaging at Atmospheric Pressure Using Desorption Electrospray Ionization (DESI) Mass Spectrometry13. *Angewandte Chemie International Edition* **2006,** 45, (43), 7188-7192.
95. Wiseman, J. M.; Ifa, D. R.; Venter, A.; Cooks, R. G., Ambient molecular imaging by desorption electrospray ionization mass spectrometry. *Nature Protocols* **2008,** 3, (3), 517-524.
96. Kertesz, V.; Van Berkel, G. J.; Vavrek, M.; Koeplinger, K. A.; Schneider, B. B.; Covey, T. R., Comparison of Drug Distribution Images from Whole-Body Thin Tissue Sections Obtained Using Desorption Electrospray Ionization Tandem Mass Spectrometry and Autoradiography. *Analytical Chemistry* **2008,** 80, (13), 5168-5177.
97. Pol, J.; Vidova, V.; Kruppa, G.; Kobliha, V.; Novak, P.; Lemr, K.; Kotiaho, T.; Kostiainen, R.; Havlicek, V.; Volny, M., Automated Ambient Desorption-Ionization Platform for Surface Imaging Integrated with a Commercial Fourier Transform Ion Cyclotron Resonance Mass Spectrometer. *Analytical Chemistry* **2009,** 81, (20), 8479-8487.

98. Volny, M.; Venter, A.; Smith, S. A.; Pazzi, M.; Cooks, R. G., Surface effects and electrochemical cell capacitance in desorption electrospray ionization. *Analyst* **2008,** 133, (4), 525-531.
99. McDonnell, L. A.; van Remoortere, A.; van Zeijl, R. J. M.; Dalebout, H.; Bladergroen, M. R.; Deelder, A. M., Automated imaging MS: Toward high throughput imaging mass spectrometry. *Journal of Proteomics* **2009,** In Press, Corrected Proof.
100. Vestal, C.; Parker, K.; Hayden, K.; Mills, G.; Vestal, M.; Cornett, S.; Caprioli, R. M., Tissue Imaging by 5 kHz High-performance MALDI-TOF In *57th American Society for Mass Spectrometry Conference on Mass Spectrometry and Allied Topics*
Philadelphia, PA, USA, 2009.
101. McLean, J. A.; Ridenour, W. B.; Caprioli, R. M., Profiling and imaging of tissues by imaging ion mobility-mass spectrometry. *Journal of Mass Spectrometry* **2007,** 42, (8), 1099-1105.
102. Jackson, S. N.; Ugarov, M.; Egan, T.; Post, J. D.; Langlais, D.; Schultz, J. A.; Woods, A. S., MALDI-ion mobility-TOFMS imaging of lipids in rat brain tissue. *Journal of Mass Spectrometry* **2007,** 42, (8), 1093-1098.
103. Cornett, D. S.; Frappier, S. L.; Caprioli, R. M., MALDI-FTICR imaging mass spectrometry of drugs and metabolites in tissue. *Analytical Chemistry* **2008,** 80, (14), 5648-5653.
104. Taban, I. M.; Altelaar, A. F. M.; Van der Burgt, Y. E. M.; McDonnell, L. A.; Heeren, R. M. A.; Fuchser, J.; Baykut, G., Imaging of peptides in the rat brain using MALDI-FTICR mass spectrometry. *Journal of the American Society for Mass Spectrometry* **2007,** 18, (1), 145-151.
105. Stemmler, E. A.; Cashman, C. R.; Messinger, D. I.; Gardner, N. P.; Dickinson, P. S.; Christie, A. E., High-mass-resolution direct-tissue MALDI-FTMS reveals broad conservation of three neuropeptides (APSGFLGMRamide, GYRKPPFNGSIFamide and pQDLDHVFLRFamide) across members of seven decapod crustaean infraorders. *Peptides* **2007,** 28, (11), 2104-2115.
106. Jones, E. A.; Fletcher, J. S.; Thompson, C. E.; Jackson, D. A.; Lockyer, N. P.; Vickerman, J. C., ToF-SIMS analysis of bio-systems: Are polyatomic primary ions the solution? *Applied Surface Science* **2006,** 252, (19), 6844-6854.
107. Carado, A.; Passarelli, M. K.; Kozole, J.; Wingate, J. E.; Winograd, N.; Loboda, A. V., C-60 Secondary Ion Mass Spectrometry with a Hybrid-Quadrupole Orthogonal Time-of-Flight Mass Spectrometer. *Analytical Chemistry* **2008,** 80, (21), 7921-7929.
108. Fletcher, J. S.; Rabbani, S.; Henderson, A.; Blenkinsopp, P.; Thompson, S. P.; Lockyer, N. P.; Vickerman, J. C., A new dynamic in mass spectral imaging of single biological cells. *Analytical Chemistry* **2008,** 80, (23), 9058-64.
109. Klerk, L. A.; Kharchenko, A.; Dankers, P. Y. W.; Popa, E. R.; Vickerman, J. C.; Heeren, R. M. A.; Lockyer, N. P., C60 high resolution secondary ion MS microscopy using a delay line detector. *Analytical Chemistry* **2010**, Submitted.
110. Zimmerman, T. A.; Monroe, E. B.; Sweedler, J. V., Adapting the stretched sample method from tissue profiling to imaging. *Proteomics* **2008,** 8, (18), 3809-3815.
111. Schwartz, S. A.; Weil, R. J.; Johnson, M. D.; Toms, S. A.; Caprioli, R. M., Protein Profiling in Brain Tumors Using Mass Spectrometry: Feasibility of a New Technique for the Analysis of Protein Expression. *Clinical Cancer Research* **2004,** 10, (3), 981-987.

112. Troendle, F. J.; Reddick, C. D.; Yost, R. A., Detection of pharmaceutical compounds in tissue by matrix-assisted laser desorption/ionization and laser desorption/chemical ionization tandem mass spectrometry with a quadrupole ion trap. *Journal of the American Society for Mass Spectrometry* **1999,** 10, (12), 1315-1321.
113. Stoeckli, M.; Staab, D.; Capretta, S., Automated Matrix Deposition for MALDI MSI In *54th American Society for Mass Spectrometry Conference on Mass Spectrometry and Allied Topics*, Seattle, WA, USA, 2006.
114. Adams, R. L.; Roy, J., A One-Dimensional Numerical Model of a Drop-On-Demand Ink Jet. *Journal of Applied Mechanics* **1986,** 53, (1), 193-197.
115. Nakanishi, T., Ohtsu, I., Furuta, M., Ando, E., Nishimura, O., Direct MS/MS analysis of proteins blotted on membranes by a matrix-assisted laser desorption/ionization-quadrupole ion trap-time-of-flight tandem mass spectrometer. *Journal of Proteome Research* **2005,** 4, 743-747.
116. Aerni, H.-R.; Cornett, D. S.; Caprioli, R. M., Automated Acoustic Matrix Deposition for MALDI Sample Preparation. *Analytical Chemistry* **2005,** 78, (3), 827-834.
117. Baluya, D. L.; Garrett, T. J.; Yost, R. A., Automated MALDI Matrix Deposition Method with Inkjet Printing for Imaging Mass Spectrometry. *Analytical Chemistry* **2007,** 79, (17), 6862-6867.
118. Hankin, J. A.; Barkley, R. M.; Murphy, R. C., Sublimation as a method of matrix application for mass spectrometric imaging. *Journal of the American Society for Mass Spectrometry* **2007,** 18, (9), 1646-1652.
119. Chou, Y.-L., *Analysis, with business and economical applications*. New York 1975; Vol. 17.9.
120. Wall, M. E., Rechtsteiner, A., Rocha, L.M., *A practical approach to microarray data analysis*. Kluwer Academic Publishers: 2003; p 91-109.
121. Hanselmann, M.; Kirchner, M.; Renard, B. Y.; Amstalden, E. R.; Glunde, K.; Heeren, R. M. A.; Hamprecht, F. A., Concise Representation of Mass Spectrometry Images by Probabilistic Latent Semantic Analysis. *Analytical Chemistry* **2008,** 80, (24), 9649-9658.
122. Hanselmann, M.; KoÌˆthe, U.; Kirchner, M.; Renard, B. Y.; Amstalden, E. R.; Glunde, K.; Heeren, R. M. A.; Hamprecht, F. A., Toward Digital Staining using Imaging Mass Spectrometry and Random Forests. *Journal of Proteome Research* **2009,** 8, (7), 3558-3567.
123. McDonnell, L. A.; van Remoortere, A.; van Zeijl, R. J. M.; Deelder, A. M., Mass Spectrometry Image Correlation: Quantifying Colocalization. *Journal of Proteome Research* **2008,** 7, (8), 3619-3627.
124. Chaurand, P.; Schwartz, S. A.; Caprioli, R. M., Imaging mass spectrometry: a new tool to investigate the spatial organization of peptides and proteins in mammalian tissue sections. *Current Opinion in Chemical Biology* **2002,** 6, (5), 676-681.
125. Chaurand, P.; Stoeckli, M.; Caprioli, R. M., Direct Profiling of Proteins in Biological Tissue Sections by MALDI Mass Spectrometry. *Analytical Chemistry* **1999,** 71, (23), 5263-5270.
126. Muller, M.; Gras, R.; Appel, R. D.; Bienvenut, W. V.; Hochstrasser, D. F., Visualization and analysis of molecular scanner peptide mass spectra. *Journal of the American Society for Mass Spectrometry* **2002,** 13, (3), 221-231.

127. Luxembourg, S. L.; Vaezaddeh, A. R.; Amstalden, E. R.; Zimmermann-Ivol, C. G.; Hochstrasser, D. F.; Heeren, R. M. A., The molecular scanner in microscope mode. *Rapid Communications in Mass Spectrometry* **2006,** 20, (22), 3435-3442.
128. Altelaar, A. F. M., Taban, I.M., McDonnell, L.A., Verhaert, P.D.E.M., de Lange, R.P.J., Adan, R.A.H., Mooi, W.J., Heeren, R.M.A., Piersma, S.R., High-resolution MALDI imaging mass spectrometry allows localization of peptide distributions at cellular length scales in pituitary tissue sections. *International Journal of Mass Spectrometry* **2007,** 260, 203-211.
129. Li, C.; Greenwood, T. R.; Glunde, K., Glucosamine-bound near-infrared fluorescent probes with lysosomal specificity for breast tumor imaging. *Neoplasia* **2008,** 10, (4), 389-398.
130. Lagarrigue, M.; Becker, M.; Lavigne, R.; Deininger, S.-O.; Walch, A.; Aubry, F.; Suckau, D.; Pineau, C., Revisiting rat spermatogenesis with MALDI imaging at 20 Âµm resolution. *Molecular & Cellular Proteomics*.
131. Amstalden van Hove, E. R.; Smith, D. F.; Heeren, R. M. A., A concise review of mass spectrometry imaging. *Journal of Chromatography A* **2010,** 1217, (25), 3946-54.
132. Chughtai, K.; Heeren, R. M. A., Mass spectrometric imaging for biomedical tissue analysis. *Chemical Reviews* **2010,** 110, (5), 3237-77.
133. Teunissen, S. F.; Rosing, H.; Schinkel, A. H.; Schellens, J. H. M.; Beijnen, J. H., Bioanalytical methods for determination of tamoxifen and its phase I metabolites: A review. *Analytica Chimica Acta* **2010,** 683, (1), 21-37.
134. Hopfgartner, G.; Varesio, E.; Stoeckli, M., Matrix-assisted laser desorption/ionization mass spectrometric imaging of complete rat sections using a triple quadrupole linear ion trap. *Rapid Communications in Mass Spectrometry* **2009,** 23, (6), 733-736.
135. Reich, R. F.; Cudzilo, K.; Levisky, J. A.; Yost, R. A., Quantitative MALDI-MSn Analysis of Cocaine in the Autopsied Brain of a Human Cocaine User Employing a Wide Isolation Window and Internal Standards. *Journal of the American Society for Mass Spectrometry* **2010,** 21, (4), 564-571.
136. Nilsson, A.; Fehniger, T. E.; Gustavsson, L.; Andersson, M.; Kenne, K.; Marko-Varga, G.; Andren, P. E., Fine Mapping the Spatial Distribution and Concentration of Unlabeled Drugs within Tissue Micro-Compartments Using Imaging Mass Spectrometry. *Plos One* **2010,** 5, (7), 8.
137. Koeniger, S. L.; Talaty, N.; Luo, Y. P.; Ready, D.; Voorbach, M.; Seifert, T.; Cepa, S.; Fagerland, J. A.; Bouska, J.; Buck, W.; Johnson, R. W.; Spanton, S., A quantitation method for mass spectrometry imaging. *Rapid Communications in Mass Spectrometry* **2011,** 25, (4), 503-510.
138. Amstalden van Hove, E. R.; Smith, D. F.; Fornai, L.; Glunde, K.; Heeren, R. M. A., An alternative paper based tissue washing method for Mass Spectrometry Imaging: Localized Washing and Fragile Tissue Analysis. *Journal of The American Society for Mass Spectrometry* **2011,** 22, (10), 1885-1890.
139. Luxembourg, S. L.; Heeren, R. M. A., Fragmentation at and above surfaces in SIMS: Effects of biomolecular yield enhancing surface modifications. *International Journal of Mass Spectrometry* **2006,** 253, (3), 181-192.

140. Amstalden van Hove, E. R.; Smith, D. F.; Dillen, L.; Cuyckens, F.; Anciaux, K.; Heeren, R. M. A. In *SIMS and MALDI Mass Spectrometry Imaging of Drugs and Metabolites in Whole-Body Mouse Sections*, 58th ASMS Conference on Mass Spectrometry, Salt Lake City, 2010; Salt Lake City, 2010.
141. Hills, B. A., An alternative view of the role(s) of surfactant and the alveolar model. *Journal of Applied Physiology* **1999,** 87, (5), 1567-1583.
142. Delcorte, A.; Bour, J.; Aubriet, F.; Muller, J. F.; Bertrand, P., Sample Metallization for Performance Improvement in Desorption/Ionization of Kilodalton Molecules: Quantitative Evaluation, Imaging Secondary Ion MS, and Laser Ablation. *Analytical Chemistry* **2003,** 75, (24), 6875-6885.
143. Linton, R. W.; Mawn, M. P.; Belu, A. M.; DeSimone, J. M.; Hunt, M. O.; Menceloglu, Y. Z.; Cramer, H. G.; Benninghoven, A., Time-of-flight secondary ion mass spectrometric analysis of polymer surfaces and additives. *Surface and Interface Analysis* **1993,** 20, (12), 991-999.
144. Delcorte, A.; Bertrand, P.; Garrison, B. J.; Hamraoui, K.; Mouhib, T.; Restrepo, O. A.; Santos, C. N.; Yunus, S., Probing soft materials with energetic ions and molecules: from microscopic models to the real world. *Surface and Interface Analysis* **2010,** 42, (8), 1380-1386.
145. Restrepo, O.; Prabhakaran, A.; Hamraoui, K.; Wehbe, N.; Yunus, S.; Bertrand, P.; Delcorte, A., Mechanisms of metal-assisted secondary ion mass spectrometry: a mixed theoretical and experimental study. *Surface and Interface Analysis* **2010,** 42, (6-7), 1030-1034.
146. Restrepo, O. A.; Delcorte, A., Molecular dynamics study of metal-organic samples bombarded by kiloelectronvolt projectiles. *Surface and Interface Analysis* **2010,** 43, (1-2), 70-73.
147. McDonnell, L. A.; Heeren, R. M. A.; de Lange, R. P. J.; Fletcher, I. W., Higher Sensitivity Secondary Ion Mass Spectrometry of Biological Molecules for High Resolution, Chemically Specific Imaging. *Journal of the American Society for Mass Spectrometry* **2006,** 17, (9), 1195-1202.
148. Kurhanewicz, J.; Vigneron, D. B.; Nelson, S. J., Three-dimensional magnetic resonance spectroscopic imaging of brain and prostate cancer. *Neoplasia* **2000,** 2, (1-2), 166-189.
149. Glunde, K.; Shah, T.; Winnard, P. T.; Raman, V.; Takagi, T.; Vesuna, F.; Artemov, D.; Bhujwalla, Z. M., Hypoxia regulates choline kinase expression through hypoxia-inducible factor-lot signaling in a human prostate cancer model. *Cancer Research* **2008,** 68, (1), 172-180.
150. Bathen, T. F.; Holmgren, K.; Lundemo, A. G.; Hjelstuen, M. H.; Krokan, H. E.; Gribbestad, I. S.; Schonberg, S. A., Omega-3 fatty acids suppress growth of SW620 human colon cancer xenografts in nude mice. *Anticancer Research* **2008,** 28, (6A), 3717-3723.
151. de Molina, A. R.; Sormentero-Estrada, J.; Beldo-Iniesta, C.; Taron, M.; de Molina, V. R.; Cejas, P.; Skrzypski, M.; Gallego-Ortega, D.; de Castro, J.; Casado, E.; Garcia-Cabezas, M. A.; Sanchez, J. J.; Nistal, M.; Rosell, R.; Gonzalez-Baron, M.; Lacal, J. C., Expression of choline kinase alpha to predict outcome in patients with early-stage non-small-cell lung cancer: a retrospective study. *Lancet Oncology* **2007,** 8, 889-897.

152. Mori, N.; Delsite, R.; Natarajan, K.; Kulawiec, M.; Bhujwalla, Z. M.; Singh, K. K., Loss of p53 function in colon cancer cells results in increased phosphocholine and total choline. *Molecular Imaging* **2004,** 3, (4), 319-23.
153. Hara, T.; Bansal, A.; DeGrado, T. R., Choline transporter as a novel target for molecular imaging of cancer. *Molecular Imaging* **2006,** 5, (4), 498-509.
154. Gabellieri, C.; Beloueche-Babari, M.; Jamin, Y.; Payne, G. S.; Leach, M. O.; Eykyn, T. R., Modulation of choline kinase activity in human cancer cells observed by dynamic P-31 NMR. *NMR in biomedicine* **2009,** 22, (4), 456-461.
155. Spadaro, F.; Ramoni, C.; Mezzanzanica, D.; Miotti, S.; Alberti, P.; Cecchetti, S.; Iorio, E.; Dolo, V.; Canevari, S.; Podo, F., Phosphatidylcholine-specific phospholipase C activation in epithelial ovarian cancer cells. *Cancer Research* **2008,** 68, (16), 6541-9.
156. Al-Saeedi, F.; Smith, T.; Welch, A., [Methyl-H-3]-choline incorporation into MCF-7 cells: Correlation with proliferation, choline kinase and phospholipase D assay. *Anticancer Research* **2007,** 27, (2), 901-906.
157. Glunde, K.; Jie, C. F.; Bhujwalla, Z. M., Mechanisms of indomethacin-induced alterations in the choline phospholipid metabolism of breast cancer cells. *Neoplasia* **2006,** 8, (9), 758-771.
158. Baykal, A. T.; Jain, M. R.; Li, H., Aberrant regulation of choline metabolism by mitochondrial electron transport system inhibition in neuroblastoma cells. *Metabolomics* **2008,** 4, (4), 347-356.
159. Schaeffer, E. L.; Gattaz, W. F., Cholinergic and glutamatergic alterations beginning at the early stages of Alzheimer disease: participation of the phospholipase A(2) enzyme. *Psychopharmacology* **2008,** 198, (1), 1-27.
160. Inglese, M.; Li, B. S. Y.; Rusinek, H.; Babb, J. S.; Grossman, R. I.; Gonen, O., Diffusely elevated cerebral choline and creatine in relapsing-remitting multiple sclerosis. *Magnetic Resonance in Medicine* **2003,** 50, (1), 190-195.
161. Mori, N.; Natarajan, K.; Chacko, V. P.; Artemov, D.; Bhujwalla, Z. M., Choline phospholipid metabolites of human vascular endothelial cells altered by cyclooxygenase inhibition, growth factor depletion, and paracrine factors secreted by cancer cells. *Molecular Imaging* **2003,** 2, (2), 124-30.
162. Li, X. J.; Lu, Y.; Pirzkall, A.; McKnight, T.; Nelson, S. J., Analysis of the spatial characteristics of metabolic abnormalities in newly diagnosed glioma patients. *Journal of Magnetic Resonance Imaging* **2002,** 16, (3), 229-237.
163. Katz-Brull, R.; Lavin, P. T.; Lenkinski, R. E., Clinical utility of proton magnetic resonance spectroscopy in characterizing breast lesions. *Journal of the National Cancer Institute* **2002,** 94, (16), 1197-1203.
164. Leach, M. O.; Verrill, M.; Glaholm, J.; Smith, T. A. D.; Collins, D. J.; Payne, G. S.; Sharp, J. C.; Ronen, S. M.; McCready, V. R.; Powles, T. J.; Smith, I. E., Measurements of human breast cancer using magnetic resonance spectroscopy: a review of clinical measurements and a report of localized P-31 measurements of response to treatment. *NMR in biomedicine* **1998,** 11, (7), 314-340.
165. Nimmagadda, S.; Glunde, K.; Pomper, M. G.; Bhujwalla, Z. M., Pharmacodynamic markers for choline kinase down-regulation in breast cancer cells. *Neoplasia* **2009,** 11, (5), 477-484.

166. Glunde, K.; Jacobs, M. A.; Bhujwalla, Z. M., Choline metabolism in cancer: implications for diagnosis and therapy. *Expert Review of Molecular Diagnostics* **2006,** 6, (6), 821-829.
167. Herring, K. D.; Oppenheimer, S. R.; Caprioli, R. M., Direct tissue analysis by matrix-assisted laser desorption ionization mass spectrometry: Application to kidney biology. *Seminars in Nephrology* **2007,** 27, (6), 597-608.
168. Glunde, K.; Guggino, S. E.; Solaiyappan, M.; Pathak, A. P.; Ichikawa, Y.; Bhujwalla, Z. M., Extracellular acidification alters lysosomal trafficking in human breast cancer cells. *Neoplasia* **2003,** 5, (6), 533-545.
169. Glunde, K.; Raman, V.; Mori, N.; Bhujwalla, Z. M., RNA interference-mediated choline kinase suppression in breast cancer cells induces differentiation and reduces proliferation. *Cancer Research* **2005,** 65, (23), 11034-43.
170. Glunde, K.; Jie, C.; Bhujwalla, Z. M., Molecular causes of the aberrant choline phospholipid metabolism in breast cancer. *Cancer Research* **2004,** 64, (12), 4270-6.
171. Klinkert, I.; McDonnell, L. A.; Luxembourg, S. L.; Altelaar, A. F. M.; Amstalden, E. R.; Piersma, S. R.; Heeren, R. M. A., Tools and strategies for visualization of large image data sets in high-resolution imaging mass spectrometry. *Review of Scientific Instruments* **2007,** 78, (5).
172. Bhujwalla, Z. M.; Aboagye, E. O.; Gillies, R. J.; Chacko, V. P.; Mendola, C. E.; Backer, J. M., Nm23-transfected MDA-MB-435 human breast carcinoma cells form tumors with altered phospholipid metabolism and pH: A P-31 nuclear magnetic resonance study in vivo and in vitro. *Magnetic Resonance in Medicine* **1999,** 41, (5), 897-903.
173. Iorio, E.; Mezzanzanica, D.; Alberti, P.; Spadaro, F.; Ramoni, C.; D'Ascenzo, S.; Millimaggi, D.; Pavan, A.; Dolo, V.; Canevari, S.; Podo, F., Alterations of choline phospholipid metabolism in ovarian tumor progression. *Cancer Research* **2005,** 65, (20), 9369-9376.
174. Eliyahu, G.; Kreizman, T.; Degani, H., Phosphocholine as a biomarker of breast cancer: Molecular and biochemical studies. *International Journal of Cancer* **2007,** 120, (8), 1721-1730.
175. Summers, R. M.; Joseph, P. M.; Kundel, H. L., Sodium nuclear magnetic resonance imaging of neuroblastoma in the nude mouse. *Investigative Radiology* **1991,** 26, (3), 233-241.
176. Jang, S. H.; Kang, K. S.; Ryu, P. D.; Lee, S. Y., Kv1.3 voltage-gated K+ channel subunit as a potential diagnostic marker and therapeutic target for breast cancer. *Bmb Reports* **2009,** 42, (8), 535-539.
177. Szabò, I.; Zoratti, M.; Gulbins, E., Contribution of voltage-gated potassium channels to the regulation of apoptosis. *FEBS Letters* **2010,** 584, (10), 2049-2056.

Publications

This thesis is based on the following publications

Erika R. Amstalden van Hove, Donald F. Smith, Ron M.A. Heeren, A Concise Review of Mass Spectrometry Imaging. *Journal of Chromatography A*, 2010, 1217 (25), 3946-3954. (**Chapter 2**)

Erika R. Amstalden van Hove, Donald F. Smith, Lara Fornai, Kristine Glunde, Ron M.A Heeren, An alternative paper based tissue washing method for Mass Spectrometry Imaging: Localized Washing and Fragile Tissue Analysis, *Journal of The American Society for Mass Spectrometry*, 2011, **22** (10), 1885-1890. (**Chapter 3**)

Erika R. Amstalden van Hove, Donald F. Smith, Gert Eijkel, Lieve Dillen, Hilde De Man, Katelijne Anciaux, Filip Cuyckens, Ron M.A. Heeren, Feasibility study of drug quantitation in tissue homogenates by MS imaging techniques, *Rapid Communications in Mass Spectrometry*, submitted. (**Chapter 4**)

Erika R. Amstalden van Hove, Tiffany R. Blackwell, Ivo Klinkert, Gert Eijkel**,** Ron M. A. Heeren, Kristine Glunde, Multimodal Mass Spectrometric Imaging of Small Molecules Reveals Distinct Spatio-Molecular Signatures in Differentially Metastatic Breast Tumor Models, *Cancer Research* , 2010, **70** (22), 9012-9021. (**Chapter 5**)

Other Publications

1. L. Jiang, T.R. Greenwood, E.R. Amstalden van Hove, K. Chughtai, Z. Bhujwalla, V. Raman, P. Winnard Jr., R.M.A. Heeren, D. Artemov, K. Glunde, Multimodal multi-scale molecular imaging platform for combined magnetic resonance, fluorescence, and histological imaging. *Magnetic Resonance in Medicine,* submitted.
2. K. Chughtai, L. Jiang, T.R. Greenwood, I. Klinkert, E.R. Amstalden van Hove, R.M.A. Heeren, Kristine Glunde, Multimodal Imaging Platform for Three-dimensional Mass Spectrometric and Optical Imaging. *Nature Methods*, to be submitted.
3. L. Fornai, A. Angelini, I. Klinkert, F. Giskes, L.A. Klerk, E.R. Amstalden van Hove, M. Fedrigo, M. Valente, G. Thiene, R.M.A. Heeren, 3-D (three-dimensional) molecular reconstruction of the heart from Imaging mass spectrometry, *Circulation Research*, submitted.
4. M. Hanselmann, U. Kothe, M. Kirchner, B. Renard, E.R. Amstalden van Hove, K. Glunde, R.M.A. Heeren and F.A. Hamprecht, Toward Digital Staining using Imaging Mass Spectrometry and Random Forests. *Journal of Proteome Research* 8 (7), 3558 (2009).
5. M. Hanselmann, M. Kirchner, B. Renard, E.R. Amstalden van Hove, K. Glunde, R.M.A. Heeren, F.A. Hamprecht, Concise Representation of Mass Spectrometry Images by Probabilistic Latent Semantic Analysis. *Analytical Chemistry* 80 (24), 9649 (2008).
6. I. Klinkert, L.A. McDonnell, S.L. Luxembourg, A.F.M. Altelaar; E.R. Amstalden van Hove, S. Piersma, R.M.A. Heeren, Tools and strategies for visualization of large image data sets in high-resolution imaging mass spectrometry. *Review of Scientific Instruments* 78 (5) (2007).
7. R.M.A. Heeren, L.A. McDonnell, E.R. Amstalden van Hove, S.L. Luxembourg, A.F.M. Altelaar; Sander Piersma, Why don't biologists use SIMS? A critical evaluation of imaging MS. *Applied Surface Science* 252 (19), 6827 (2006).
8. S.L. Luxembourg, A.R. Vaezaddeh, E.R. Amstalden, C.G. Zimmermann-Ivol, D.F. Hochstrasser, R.M.A. Heeren, The molecular scanner in microscope mode. *Rapid Communications in Mass Spectrometry* 20 (22), 3435 (2006).
9. M. Przybylski, E.R. Amstalden, A. Marquardt, X. Tian, R. Stefanescu, E.N. Damoc, Identification of antibody-paratope peptides by affinity-proteomics using high resolution FT-ICR mass spectrometry. *Biopolymers* 80 (4), 603 (2005).
10. R. Stefanescu, R.E Iacob, E.N. Damoc, A. Marquardt, E.R. Amstalden, M. Manea, I. Perdivara, M. Maftei, G. Paraschiv, M. Przybylski, Mass spectrometric approaches for elucidation of antigen-anti body recognition structures in molecular immunology. *European Journal of Mass Spectrometry* 13 (1), 69 (2007).
11. M. Przybylski, X. Tian, R.E. Cecal, A. Marquardt, M. Manea, E.R. Amstalden, G. Mezo, F.Hudecz, J. McLaurin, P. St George-Hyslop, Affinity Proteomics and Mass Spectrometric epitope analysis: powerfull tools for identification of vaccine lead structures against Alzheimer's disease. *Journal of Peptide Science* 10, 294 (2004).
12. M. Przybylski, X. Tian, R. Iacob, E.R. Amstalden, A. Marquardt, M. Manea, R. Stefanescu, G. Mezo, F. Hudecz, Affinity- and antibody-proteomics using high resolution FTICR-MS: powerful tools for elucidation of vaccine lead structures and molecular diagnostics. *Molecular & Cellular Proteomics* 3 (10), S45 (2004).

Dankwoord

Er zijn heel veel mensen die mij op een of andere manier hebben geholpen tijdens mijn promotie. Ik heb ook heel veel vrienden gemaakt, en ontzettend veel geleerd.

Jaren geleden, tijdens een gespreek met Ron Heeren in Konstanz, tijdens een kofffiepauze, heeft hij me verteld over zijn werk op AMOLF. Het maakte op mij een zo sterke indruk dat ik weer in Nederland meteen een afspraak maakte om zijn groep en de (vele) onderzoeken die daar gedaan werden te kunnen zien. Ik was meteen weg van de groep, van de sfeer en van het soort onderzoek dat daar plaats vond, en wilde meteen daar gaan promoveren. Gelukkig kon dat ook, en zo kwam ik terecht bij AMOLF.

Daar kon ik mijn promotor, Ron Heeren, nog beter leren kenen en hij bleef mij positief verrassen. Als begeleider heeft hij mij vrijheid gegeven om nieuwe onderzoeksmethoden te ontwikkelen, om iets te ontwerpen om onderzoek te verbeteren en hij gaf ook leiding waar dat nodig was. Maar ik heb ook Ron als vriend gekregen, en zonder zijn steun tijdens een bijzonder moeilijke tijd was deze promotie niet zo afgerond. Ook zijn familie, Mariska, Jasper en Suzanne zijn geweldig, en ik ben blij dat ik hen heb leren kenen.

Toen ik met mijn promotie ben begonnen, had ik ook hulp van Sander Piersma, die naast Ron ook direct betroken was bij mijn onderzoek. En ook van mijn collega's Liam, Maarten en Stefan, die mij alles hebben geleerd over imaging. In het laatste deel van mijn promotie heb ik ook veel met Piet Kistemaker kunnen praten en over mijn werk kunnen discussiëren, tot groot plezier. Met Jaap Boon had ik leuke discussies en hij gaf me dat extra duwtje voor het doorzetten van mijn paperblot experimenten. Bedankt daarvoor.

I had the opportunity to collaborate with Kristine Glunde, whom acted as a mentor in many ways, even if from far away. Therefore my special thanks for all your input during the past years, and most important, for your friendship.

Een onderzoek kan vaak niet door een enkel persoon gedaan worden, en er zijn allerlei soorten hulp die je graag wil hebben tijdens een promotie. Gelukkig ik had steun van alle kanten. Iliya heeft heel veel ontwerpen voor mij gedaan, en ook Dirk-Jan, en het verbaasde mij steeds hoe snel zij mijn idee op papier kregen, precies zoals ik had bedacht of nog beter. En ook de workshop, die alle ontwerpen heeft uitgevoerd met bijzonder hoge kwaliteit.

Ik heb ook heel veel gigabites data geproduceerd (eigenlijk, terrabites), en om deze data optimaal te analyseren en interpreteren heb ik onbetaalbare hulp van Ivo gekregen, met al zijn superhandige software die mijn data van vele verschillende machines kon converteren naar (meestal) prachtige beelden, en ook van Gert met al zijn PCA en matlab truukjes. Ik wil ook de hele E&I afdeling (nu ICT en software engineering) bedanken voor alle hulp tijdens mijn promotie, en in het bijzonder Marco, Lars, Wiebe, Rutger en Richard.

Wouter heeft altijd geholpen met allerlei soorten papierwerk (IND, contracten, etc), Michiel en Tatiana met het sturen van pakketten, de receptionisten met een leuke "goede morgen" en vaak nog en leuk gesprek daarbij (Trees, Magda, Marjan, Marjo, Betty, Caroline, Myrte). Ik vond het ook heel leuke contact te hebben met de secretaresses, speciaal met Karelia en Wenda, met Silvia en Grace, Willem, Ed, Tarik en de hele support staf van AMOLF, die altijd zo attent en vriendelijk zijn.

There is one special person that has been involved in almost all my projects and is a co-author in most of my papers. Dear Don, our discussions and all your help in the process of writing this thesis were more than I could ask or hope for. It is just suitable that as one of my dearest friends you are one of my paranymphs.

I made great friends in the past years, my former colleagues (in alphabetic order) Andrey, Andras, Berta, Els, Frans, Iwona, Jerre, Jonathan, Kamila, Lara, Lennaert, Liam, Luke, Maarten, Marc, Martin, Rimco, Stefan, Yuri, Roland, Chris and three very special ones, who deserve a special mention: Başak, Ioana, and Julia.

I also have to thank to my colleagues outside AMOLF: Els, Iwone, Tiffany, Lu, Filip, Lieve, Hilde and Katelijne. It was a pleasure to work with you all.

Buiten AMOLF heb ik ook veel vrienden van wie ik heel veel houd, Braziliaanse, Nederlandse en Duitse vrienden. Ik had ook de hele tijd de speciale steun van mijn Nederlandse en Braziliaanse familie, in het bijzonder mijn lieve (schoon)ouders Corrie en Michiel, maar ook van Oma van Hove en Oma Kraijo, Annechien en Chris en Natalie en Jannes, en de hele Kraijo en van Hove familie. Mijn familie in Brazilië heeft ook elk deel van het hele proces meegemaakt, en gesteund. Mijn ouders en de hele familie waren heel trots toen ik vertelde over mijn (toen toekomstige) werk, en hebben mij heel veel support gegeven. Ook als dit betekende dat mijn tante voor 3 maanden (meerdere keren) naar Nederland moest komen om mij en Jochem te helpen met onze dochter, en familie en huishouden in Brazilië achter moest laten, wat daar altijd een chaos veroorzaakte.

Helaas zijn heel belangrijke mensen niet meer hier, om de afronding van dit werk te zien. Ik had graag mijn moeder Vera, mijn schoonvader Michiel en mijn grootouders Irene en Leonardo kunnen vertellen hoe alles is afgelopen, omdat die altijd mijn grootste voorbeeld waren.

Sem minha familia seria impossivel completar esse trabalho, pois todo o amor e suporte que vocês sempre me deram foi fundamental. One querida, obrigada por tudo que você fez e ainda faz por mim. Pai, obrigada pelo apoio e carinho. Meus irmãos, cunhadas, tios e tias (vai ficar muito comprido escrever todos os nomes) e vó Lurdes, voces são parte tudo que acontece na minha vida, e portanto parte dessa tese tambem. Apesar da minha mãe querida, Vera, do Michiel, do vô Leonardo e da vó Irene não estarem mais aqui, eles foram fundamentais na minha vida e portanto na minha pesquisa, e foram exemplos que eu espero sempre seguir.

Ik moet me extra bedanken bij Vera, mijn lieve dochter, die het kunstwerk heeft gemaakt dat de cover siert. Ik had al iets anders gedaan toen zij met dit prachtige schilderij langs kwam, en ik heb toen gelijk de cover aangepast.

Lieve Jochem, ik heb geen woorden die goed kunnen zeggen hoe je was en bent voor mij, altijd. Jij en Vera zijn de reden van alles wat ik doe en alles wat ik ben. Bedankt. Voor alles.

Curriculum Vitæ

Erika Regina Amstalden van Hove studied chemistry at the University of Campinas, in Brazil, and received her bachelor degree in 2000. In the same year she started to work at the Analytical Chemistry Department of the University of Konstanz, in Germany, on a mass spectrometry based Alzheimer disease research project, until December 2004. In June 2004 she earned her Master in Science degree from the University of Konstanz. In 2005 Erika started her PhD project at the FOM Institute AMOLF in Amsterdam, The Netherlands. She worked at AMOLF as a PhD researcher until 2009 and as junior researcher in 2010. She is working at the VU University of Amsterdam, The Netherlands, since September 2011.